

Figure S1a. Summary map showing location of analyzed channels presented in Figs. S1b and S3. Deep blue catchments contain 1 trunk stream, Lighter blue catchments contain more than 1 major channel.

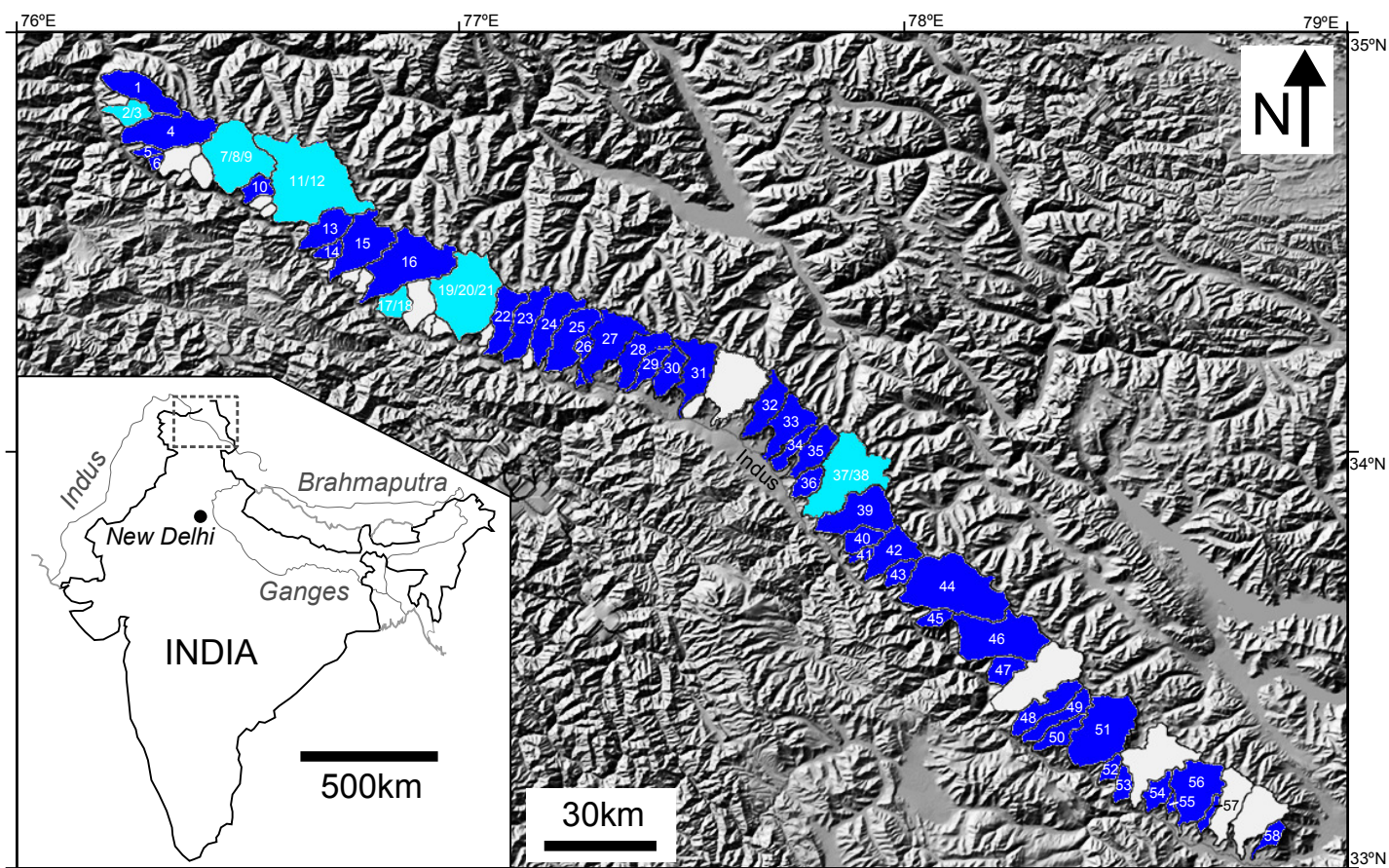
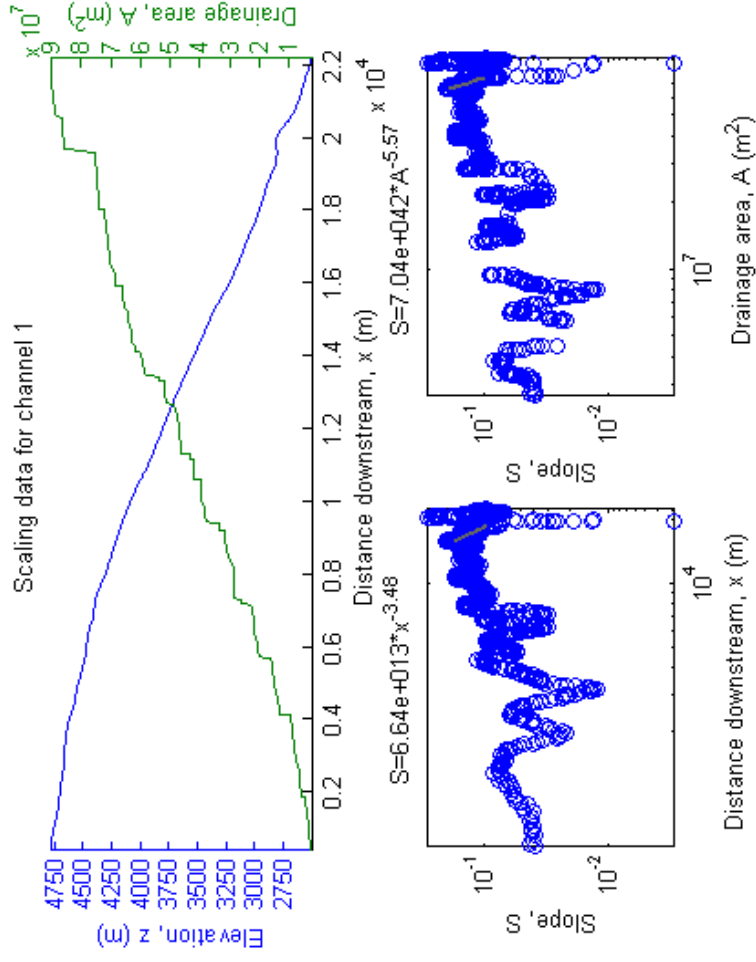


Figure S1b. Plots of long profile ( $z$ - $x$ ) and drainage structure ( $A$ - $x$ ) of each analyzed channel, along with associated slope plots  $S$ - $x$  and  $S$ - $A$ , plotted on logarithmic axes.

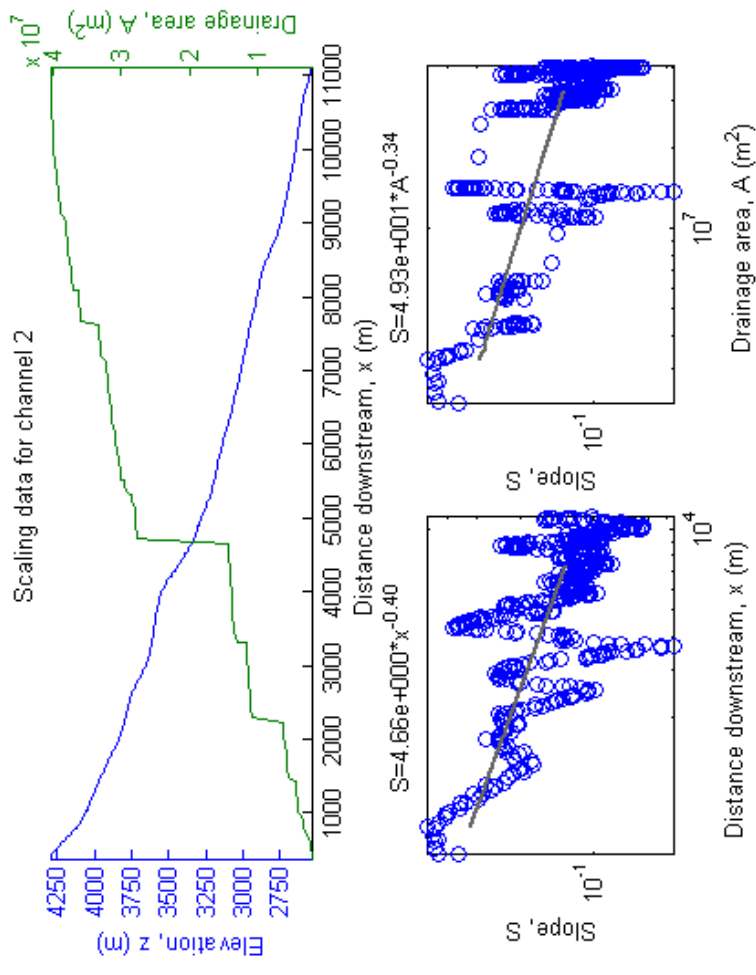
Greyscale lines show slope scaling relations fitted to these latter two plots by the method described in the main text, and the range of values over which the fit is made.

The associated equations are also shown above the figures.

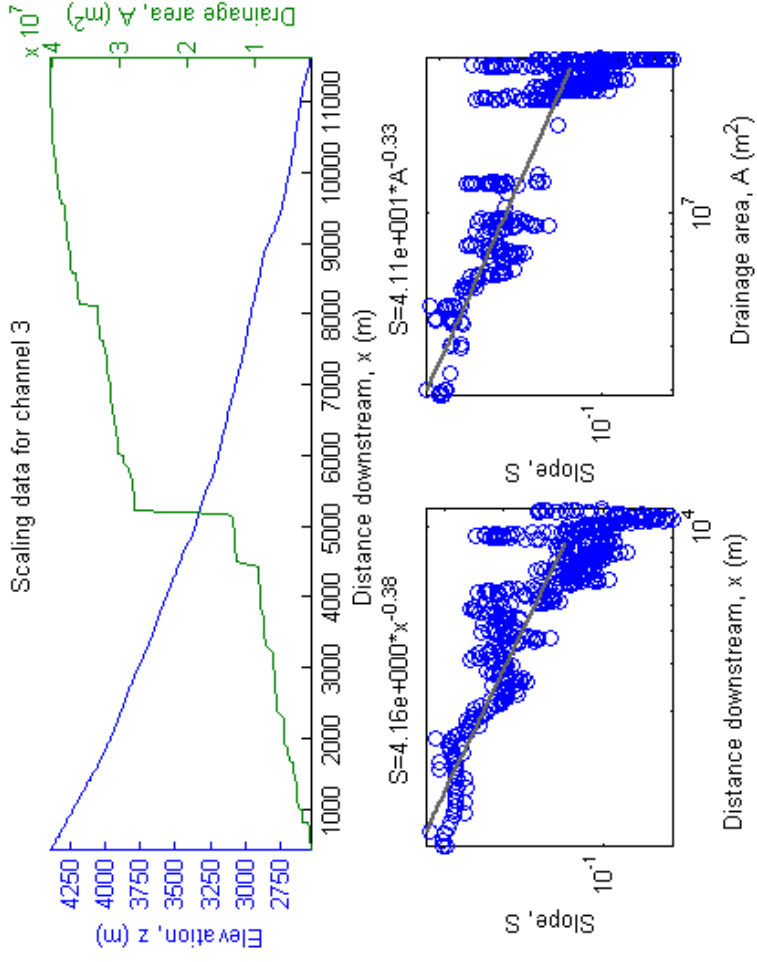
Scaling data for channel 1



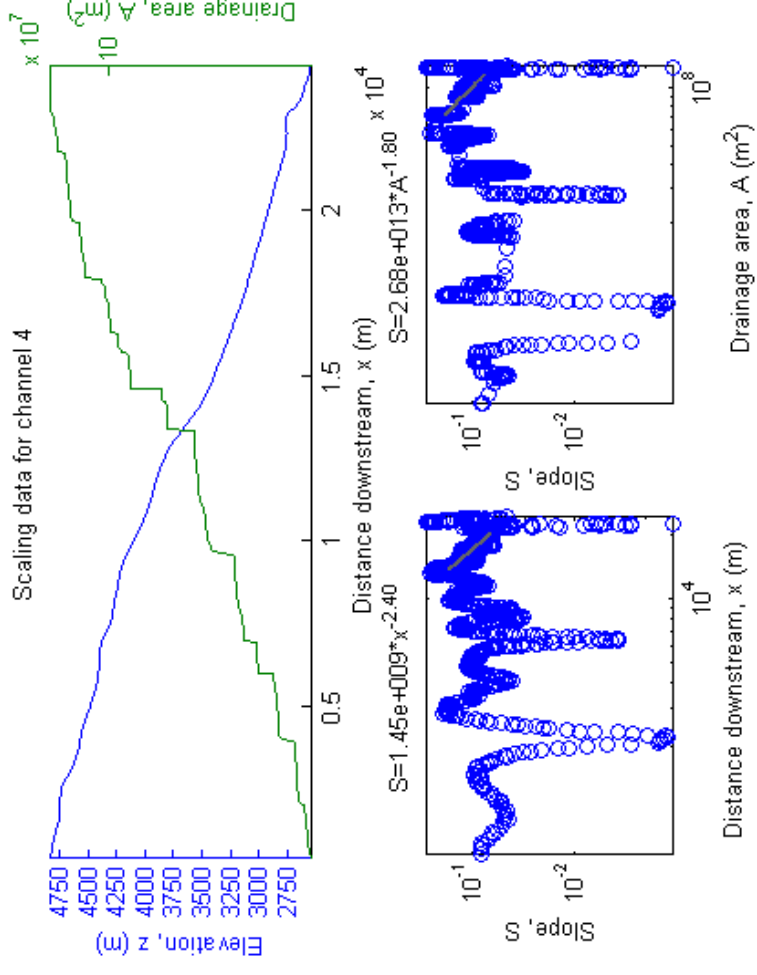
Scaling data for channel 2



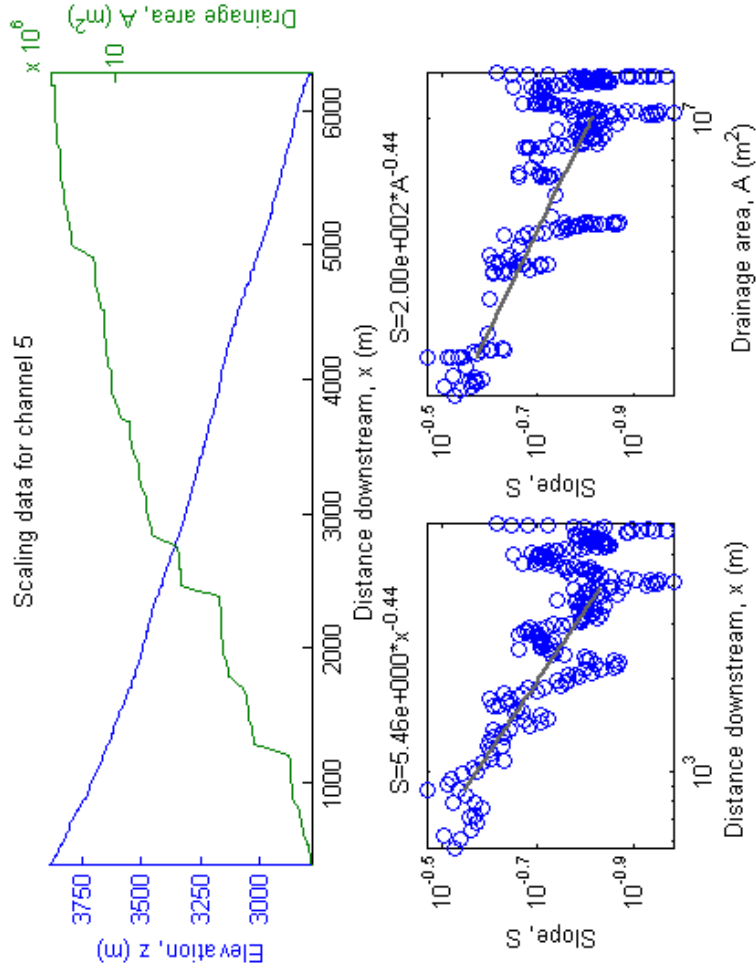
Scaling data for channel 3



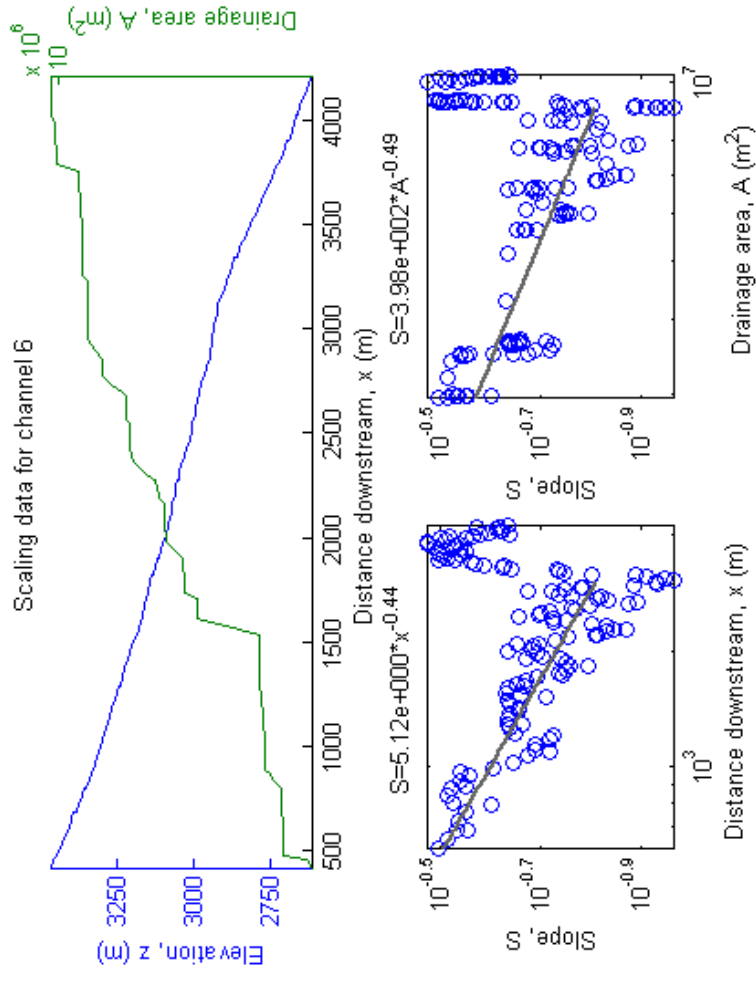
Scaling data for channel 4



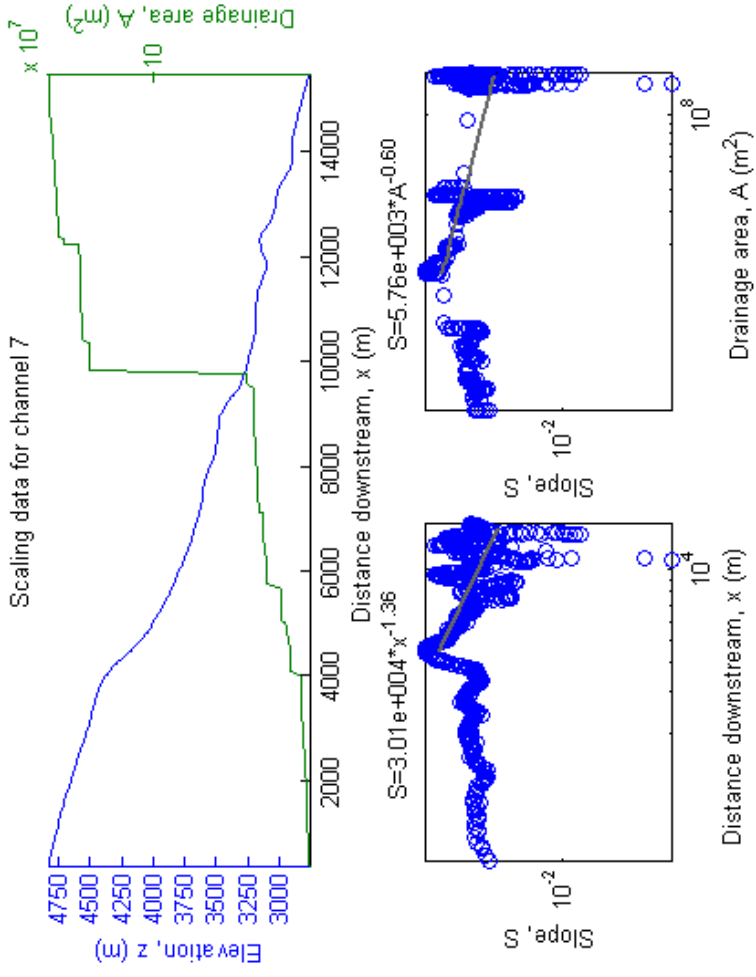
Scaling data for channel 5



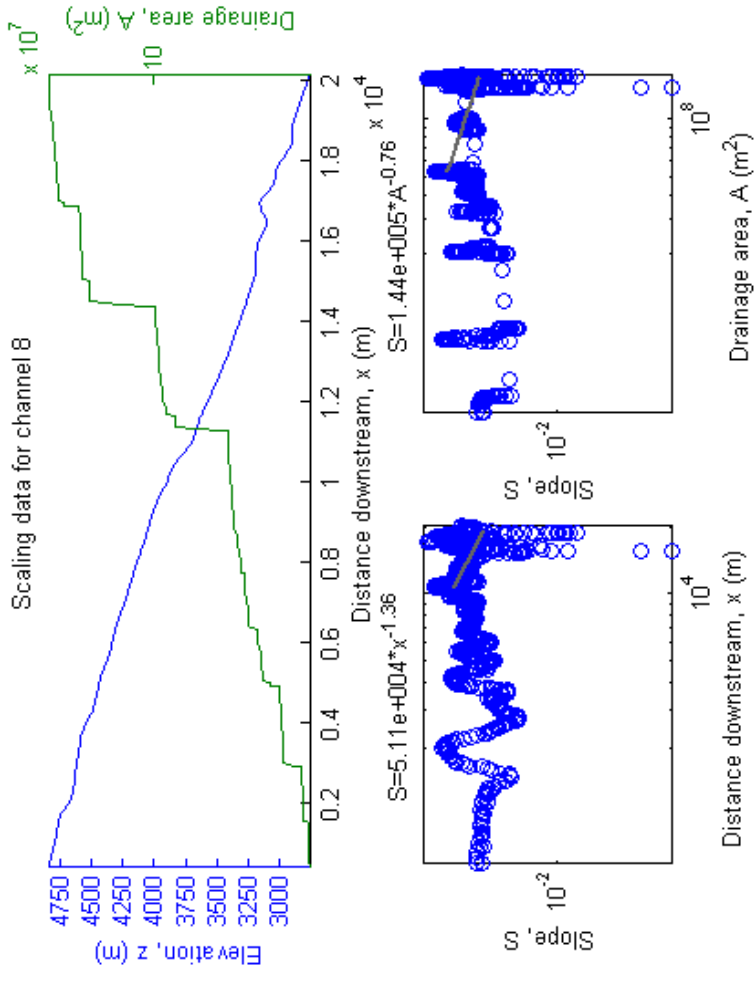
Scaling data for channel 6



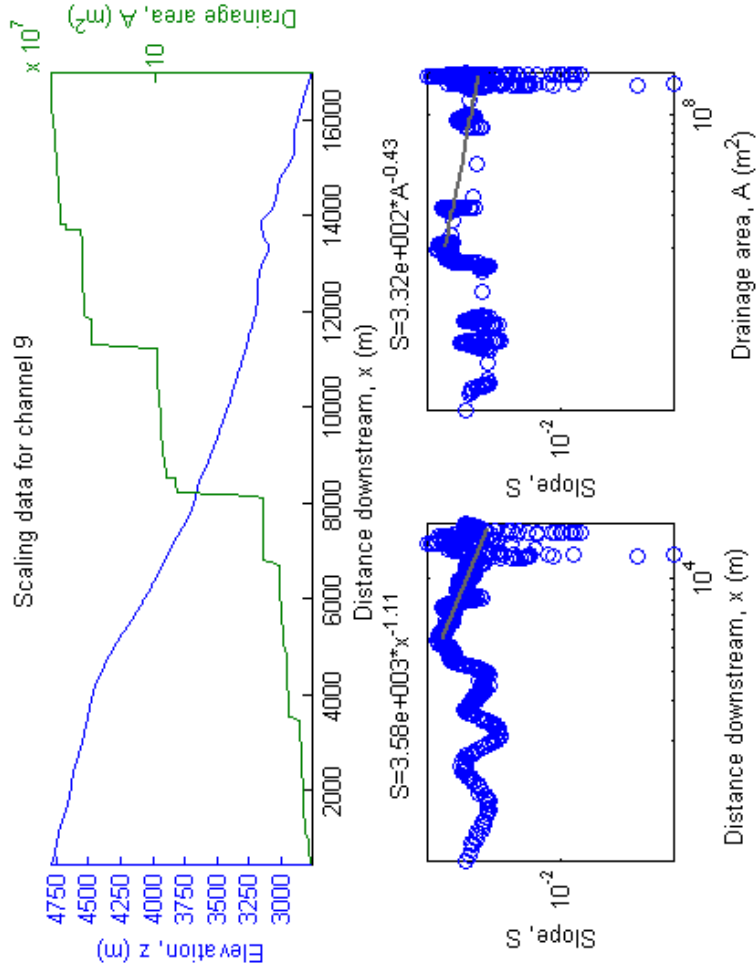
Scaling data for channel 7



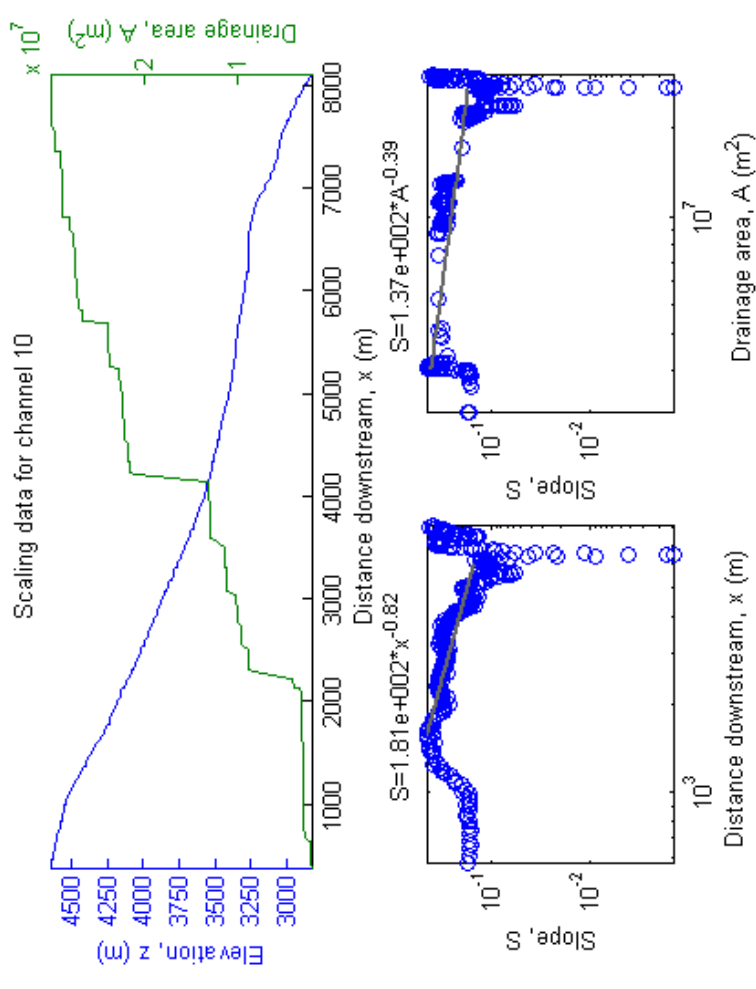
Scaling data for channel 8



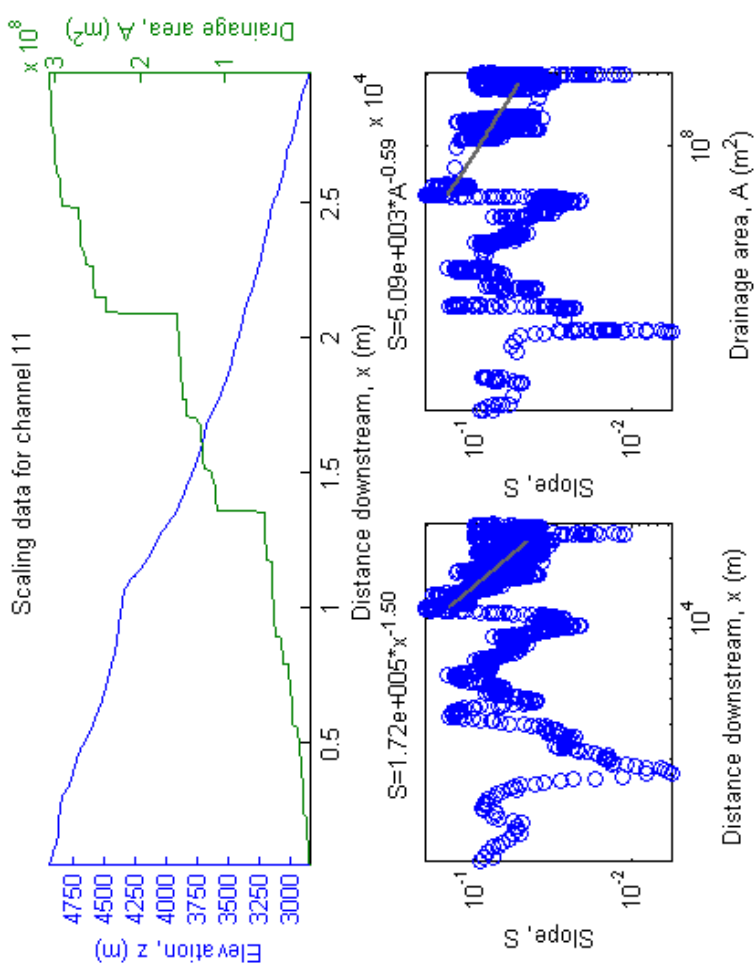
Scaling data for channel 9



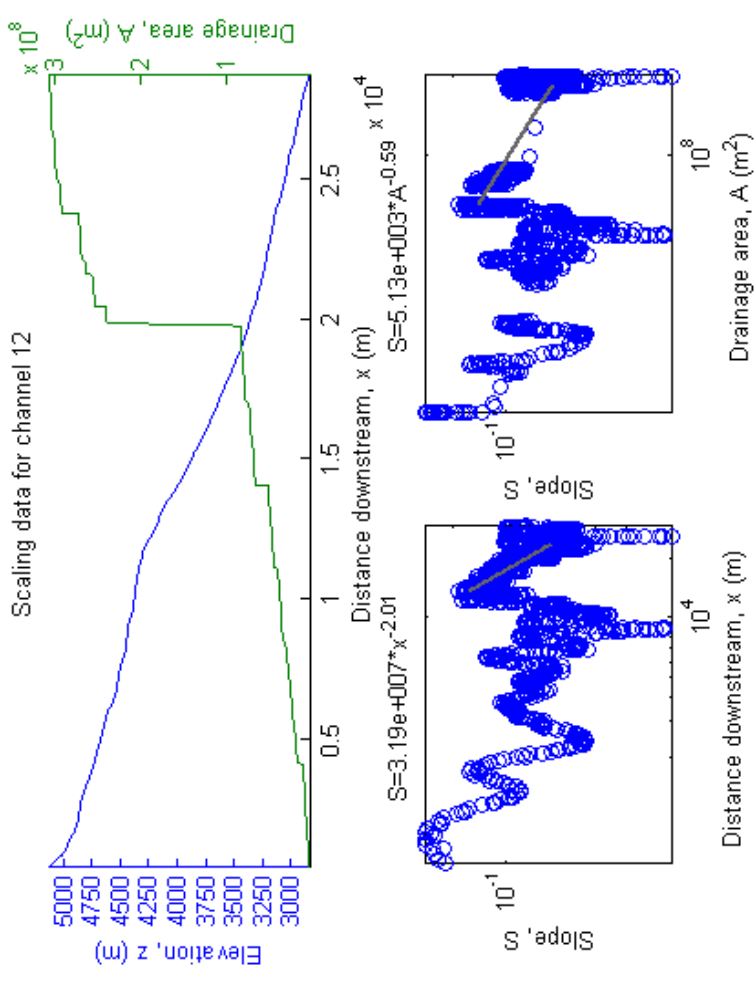
Scaling data for channel 10



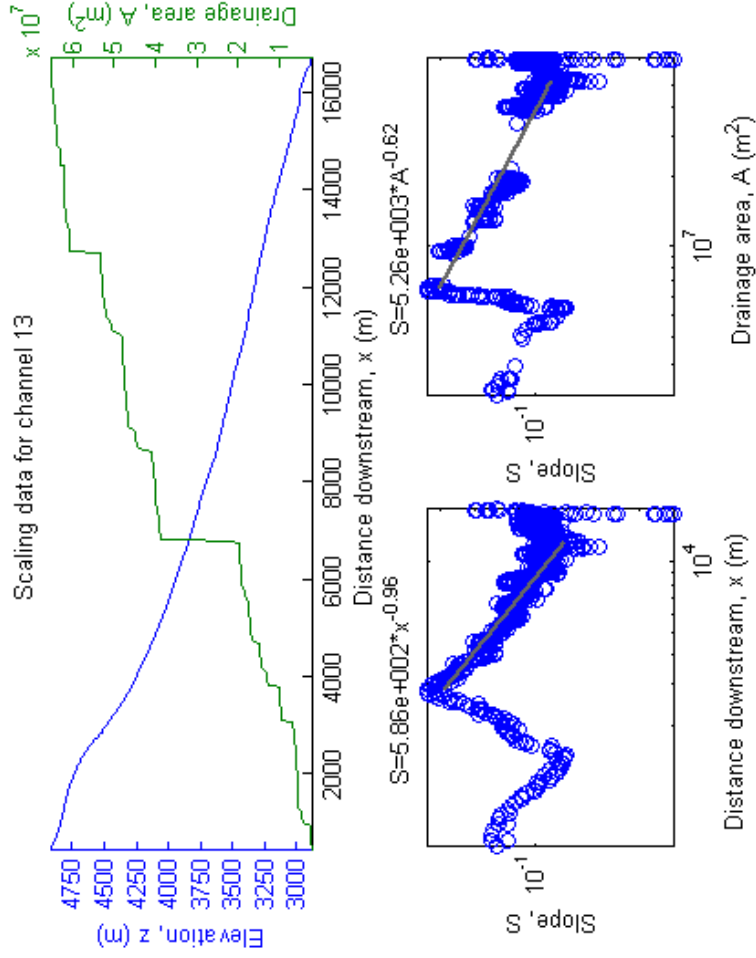
Scaling data for channel 11



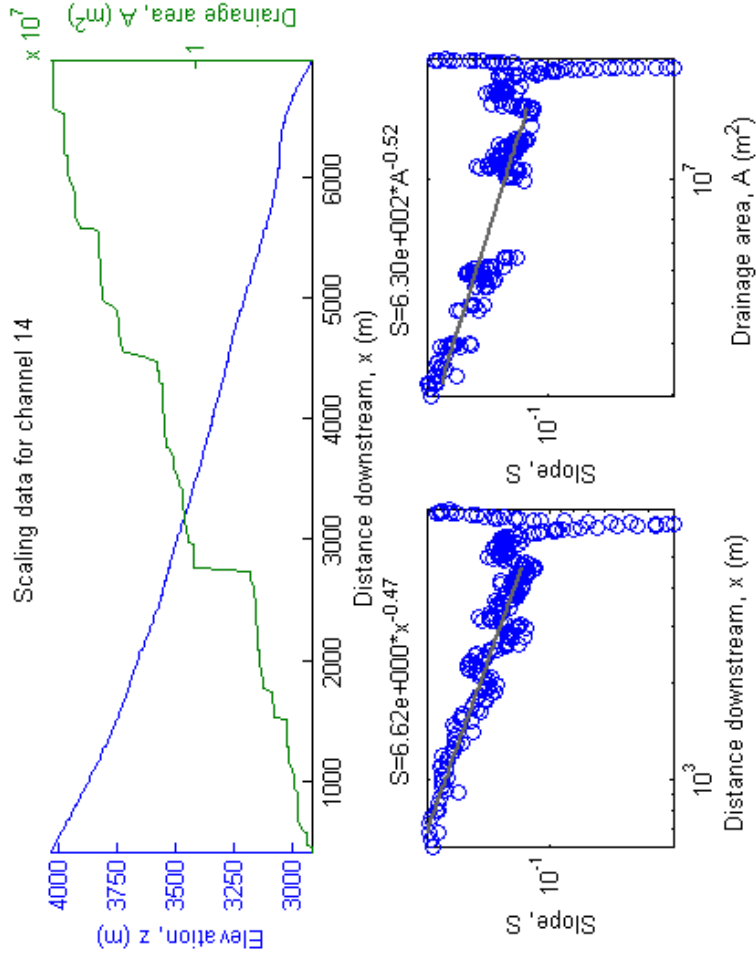
Scaling data for channel 12



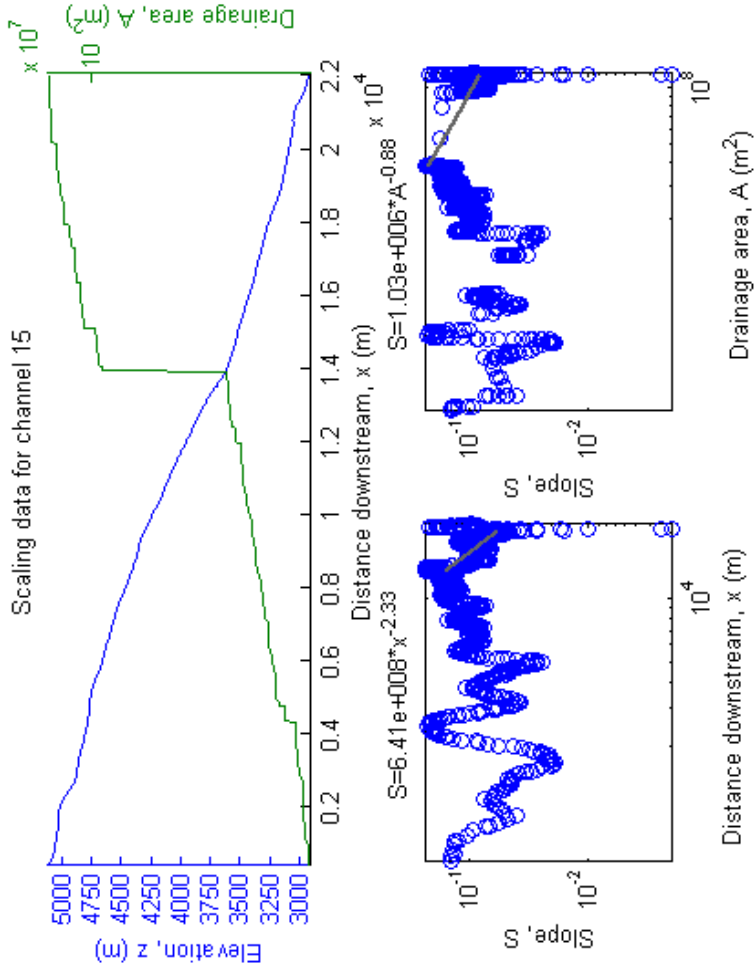
Scaling data for channel 13



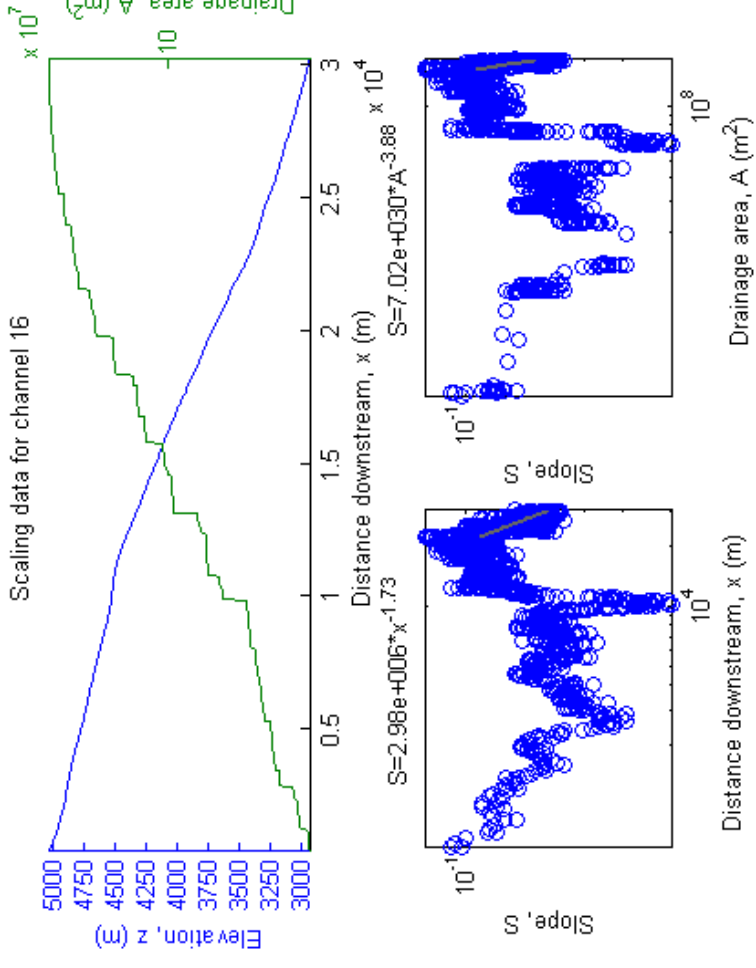
Scaling data for channel 14



Scaling data for channel 15

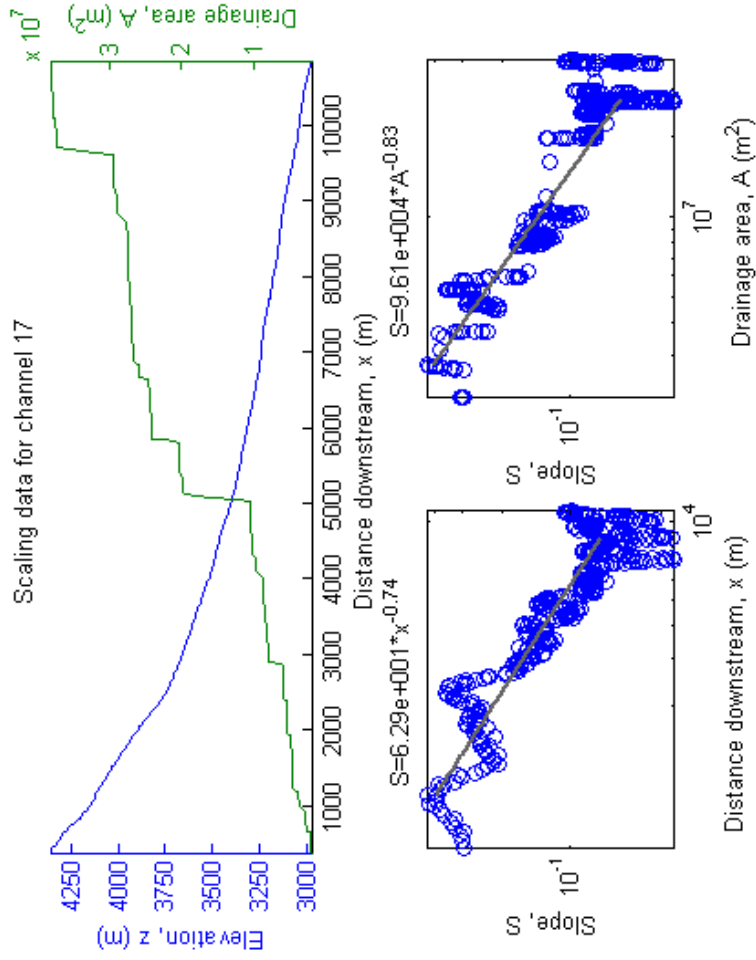


Scaling data for channel 16

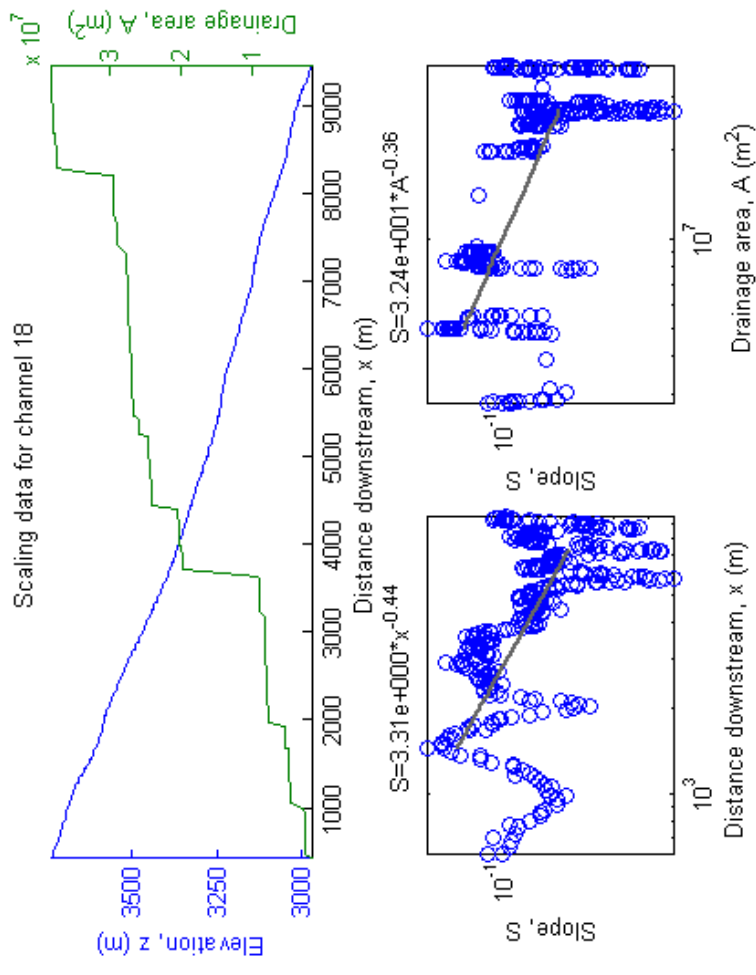




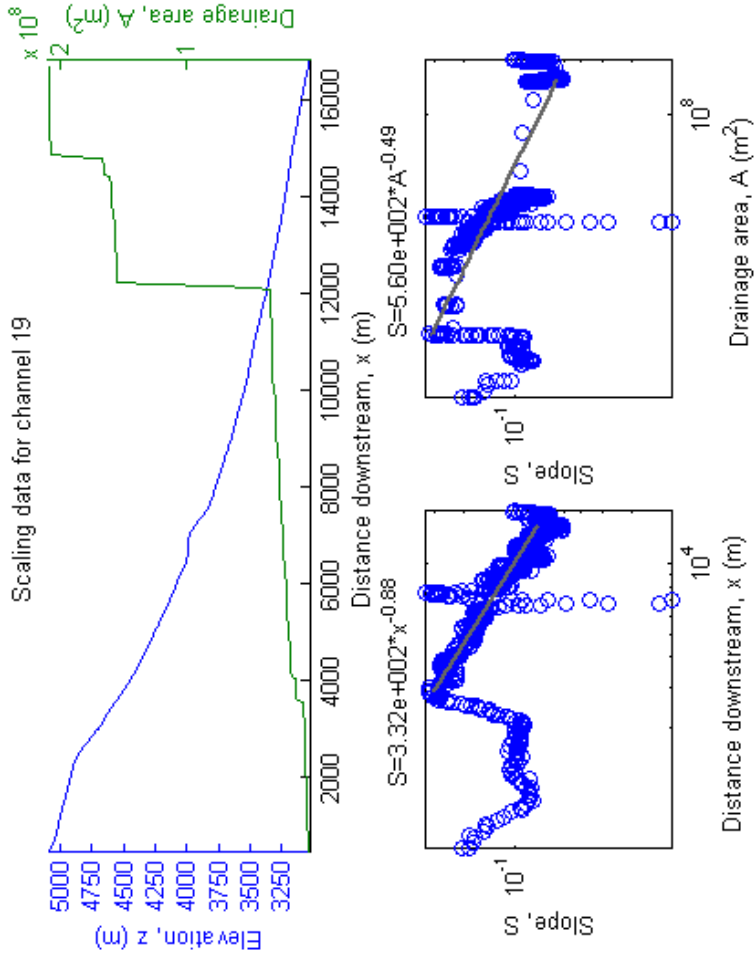
Scaling data for channel 17



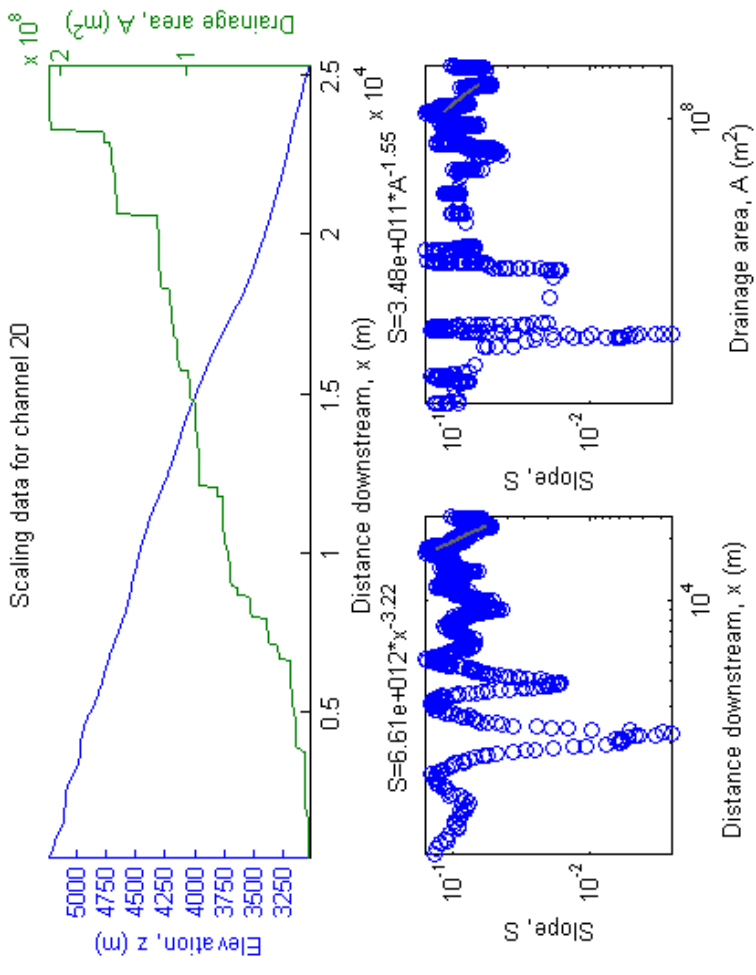
Scaling data for channel 18



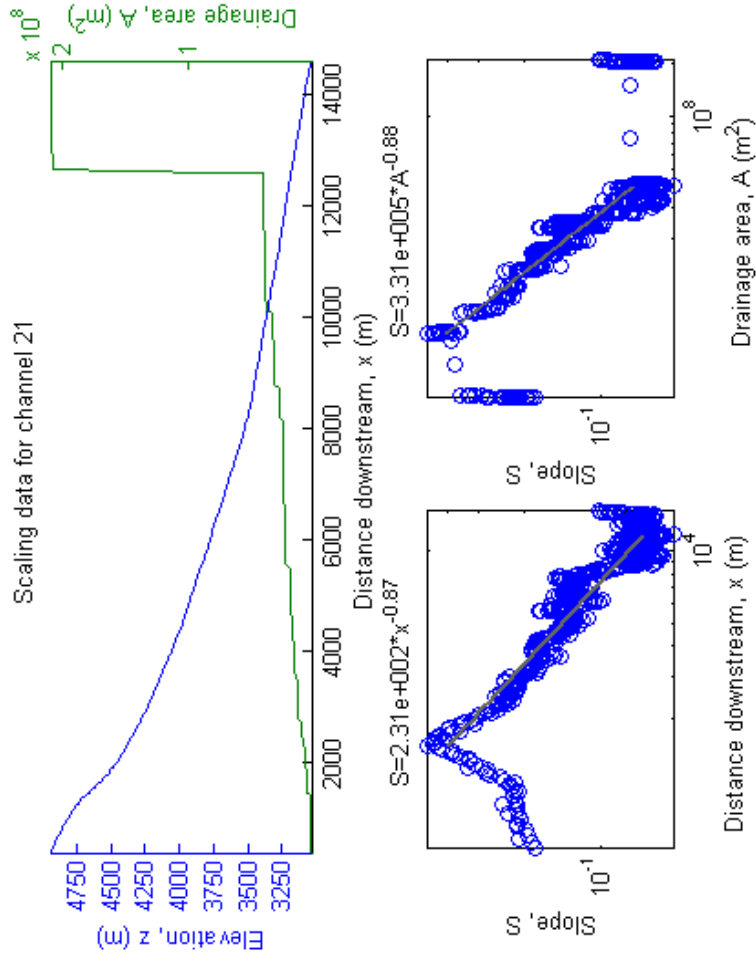
Scaling data for channel 19



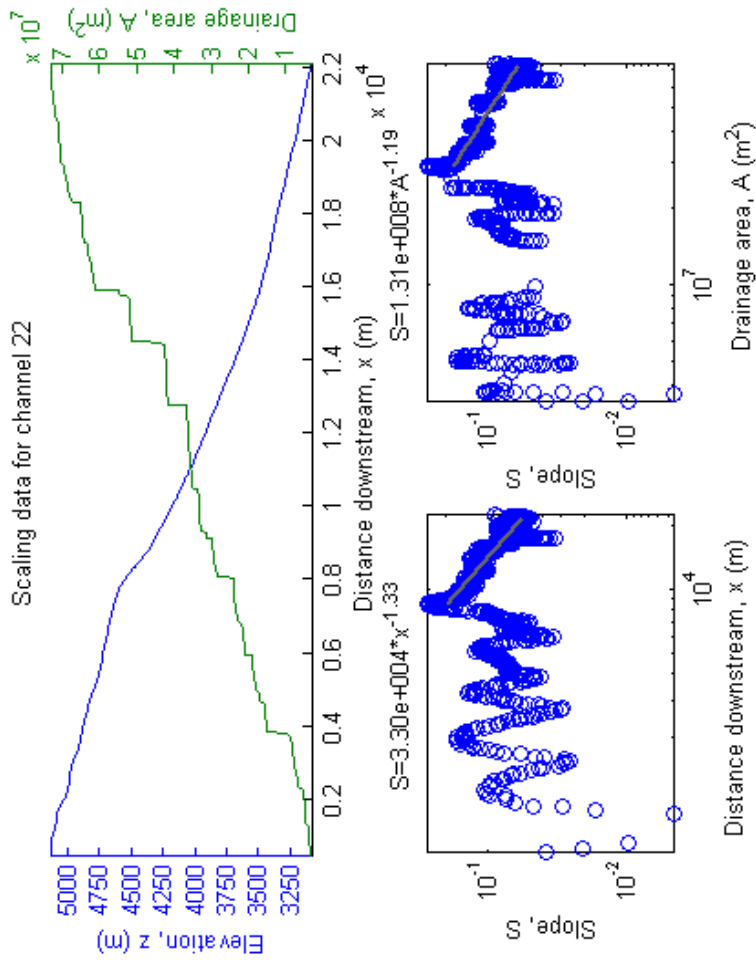
Scaling data for channel 20



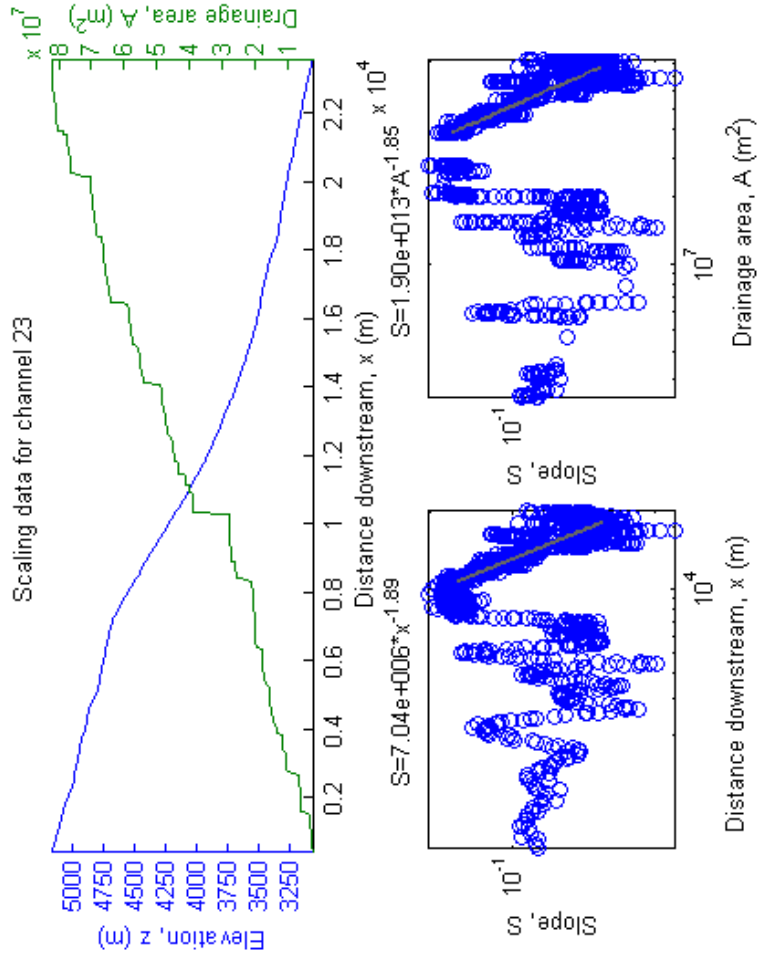
Scaling data for channel 21



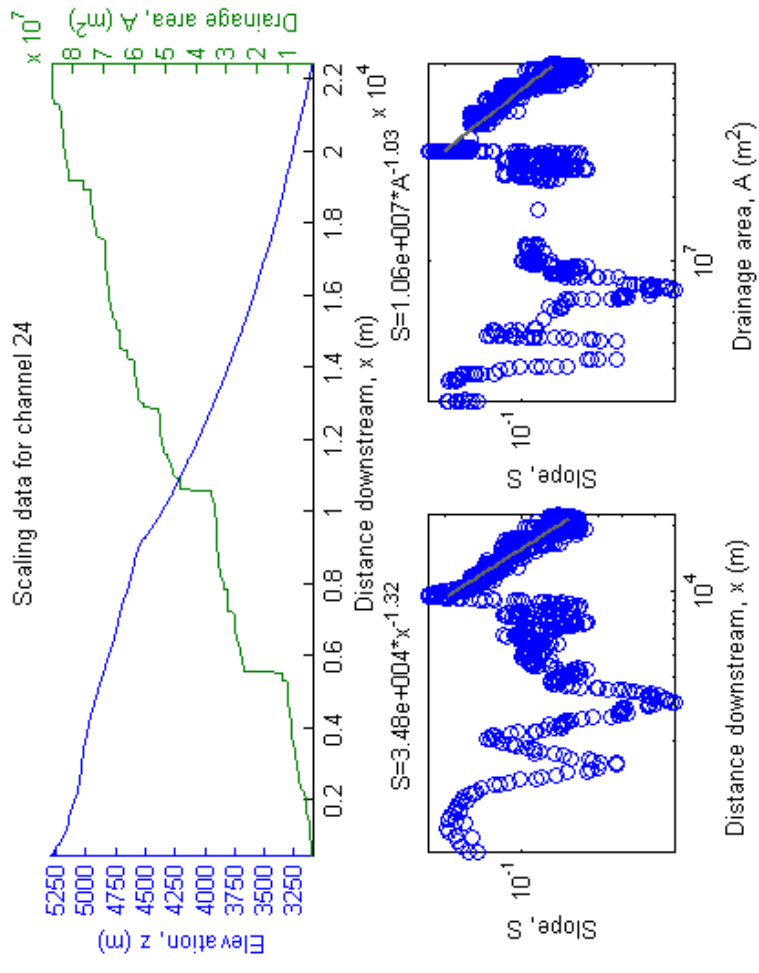
Scaling data for channel 22



Scaling data for channel 23

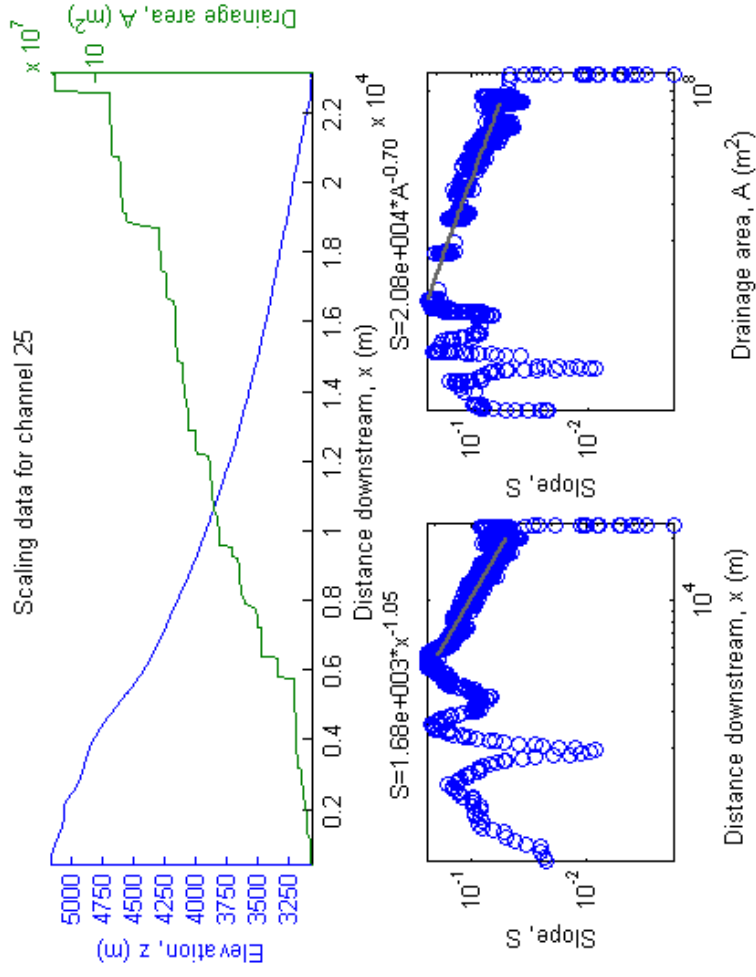


Scaling data for channel 24

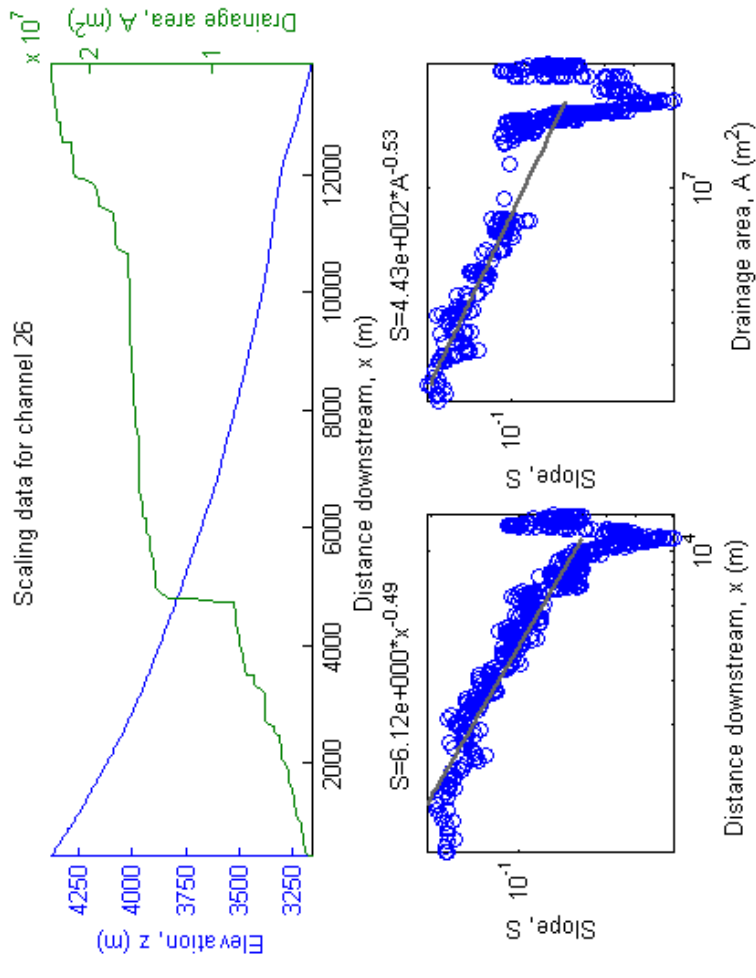




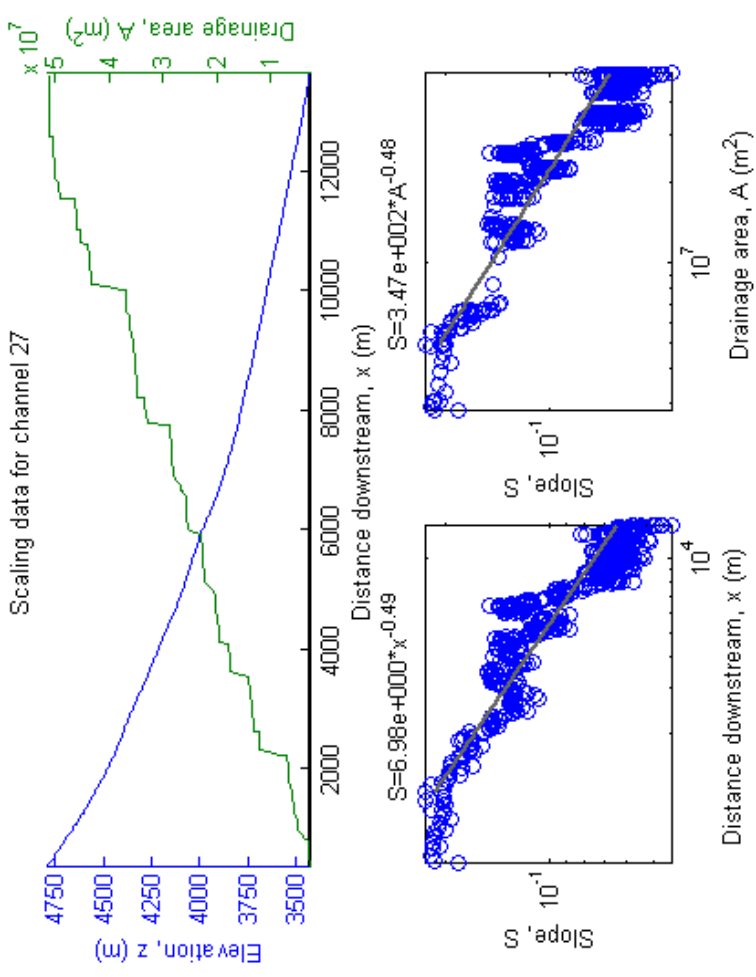
Scaling data for channel 25



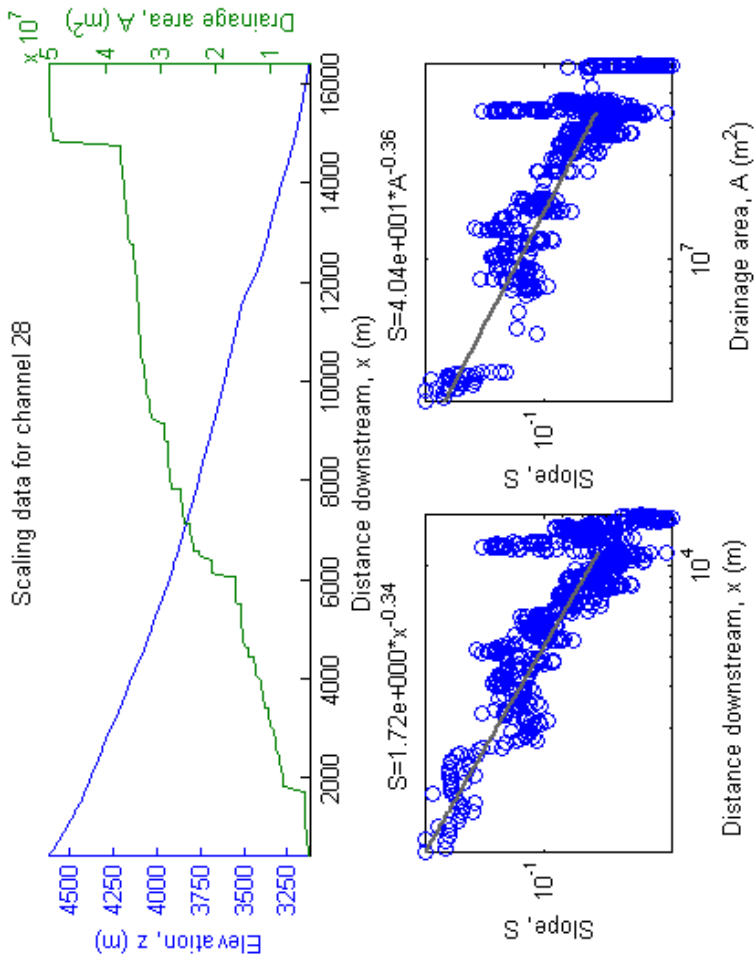
Scaling data for channel 26



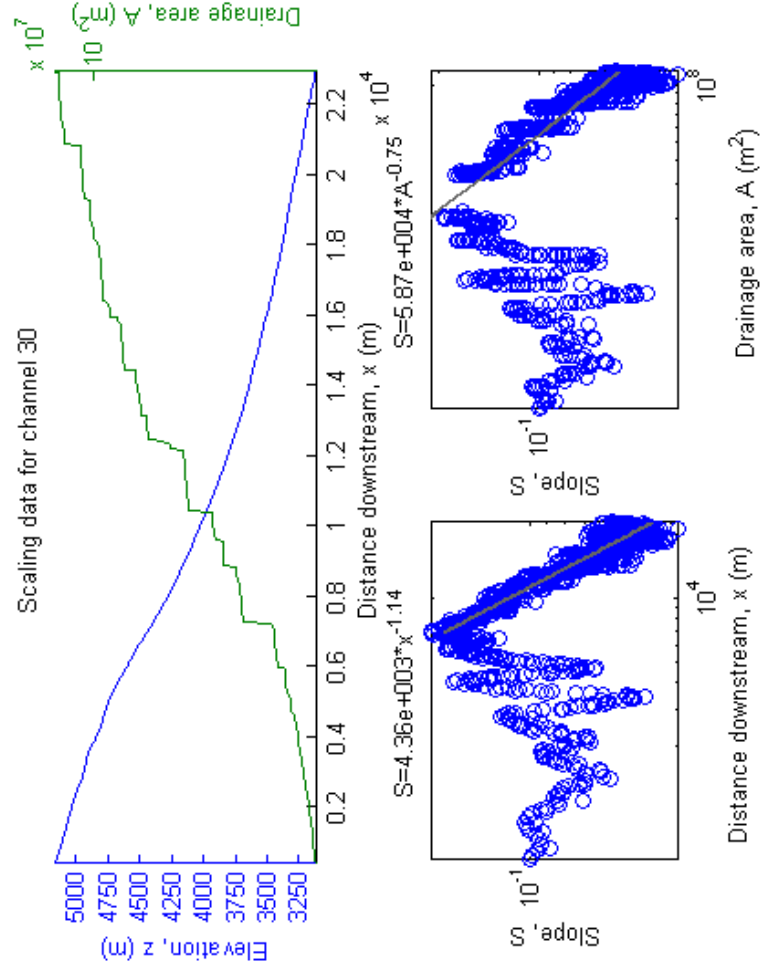
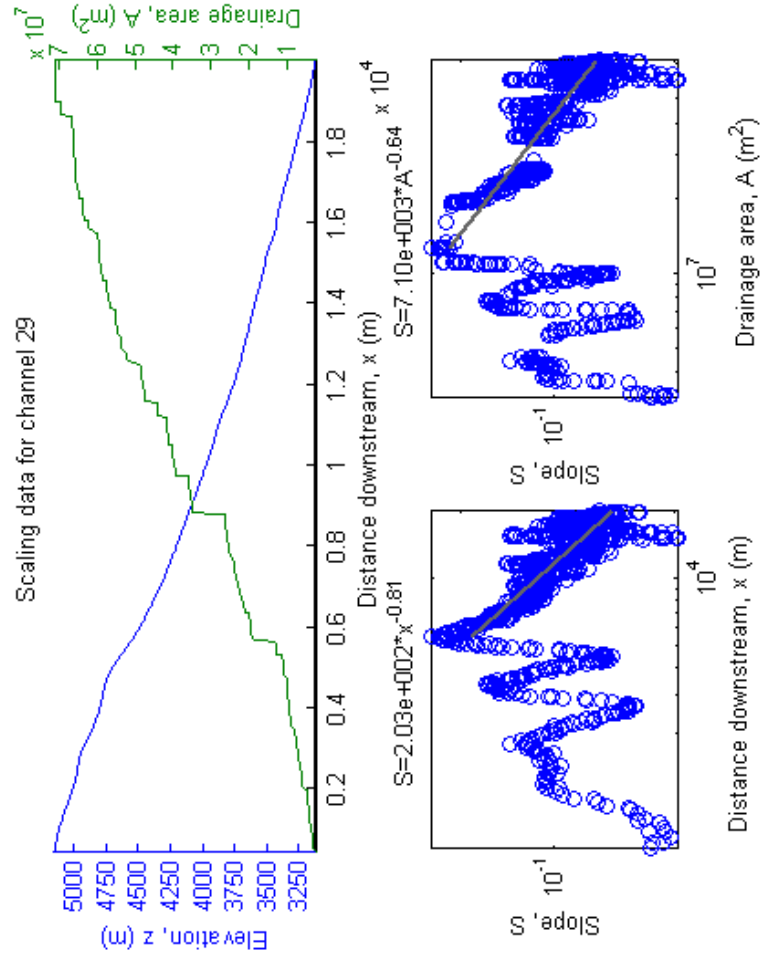
Scaling data for channel 27



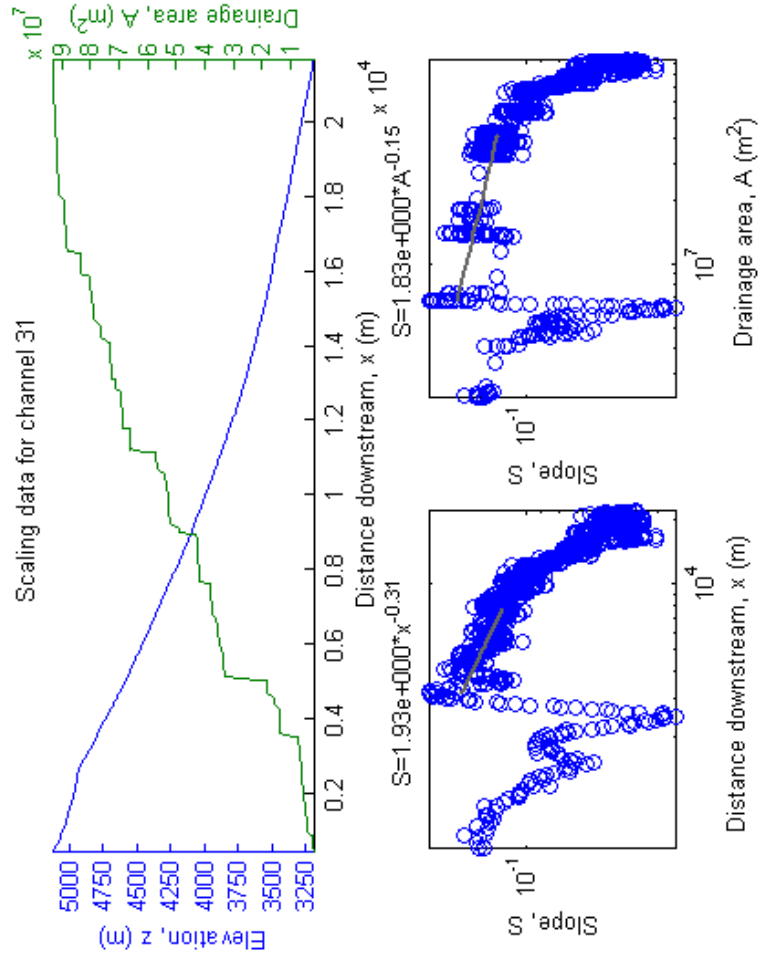
Scaling data for channel 28



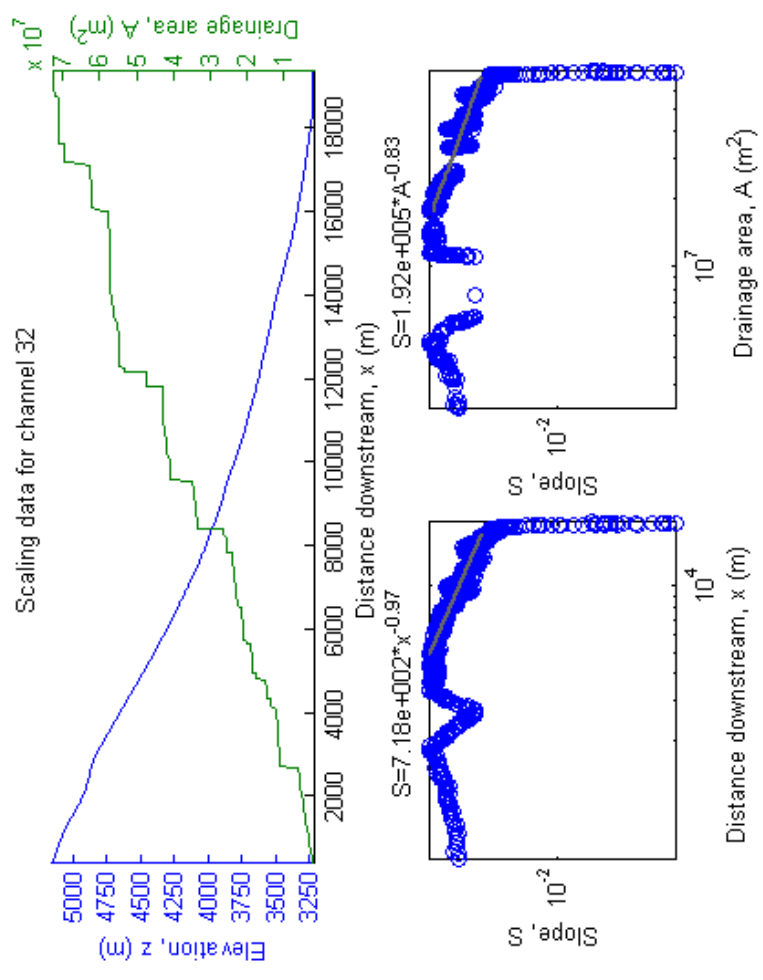
Scaling data for channel 29



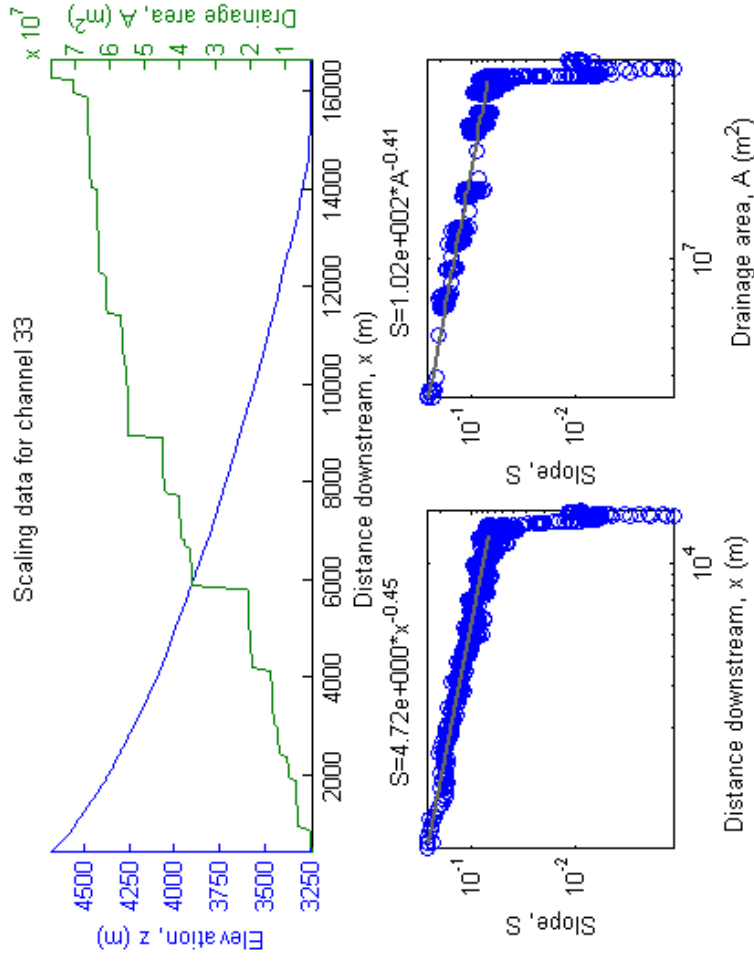
Scaling data for channel 31



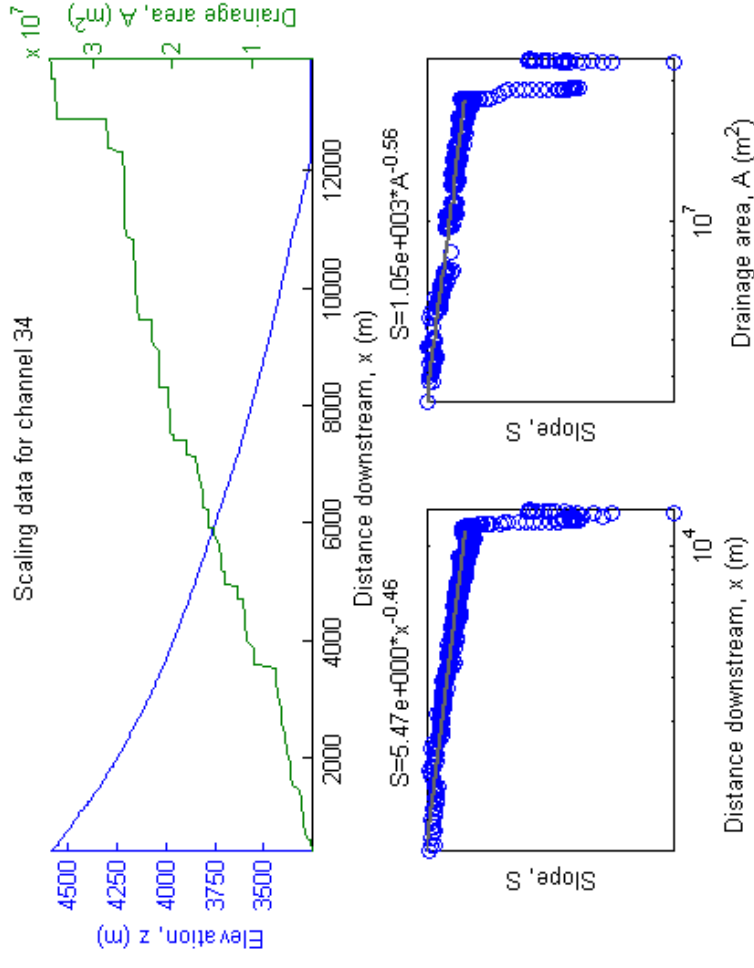
Scaling data for channel 32



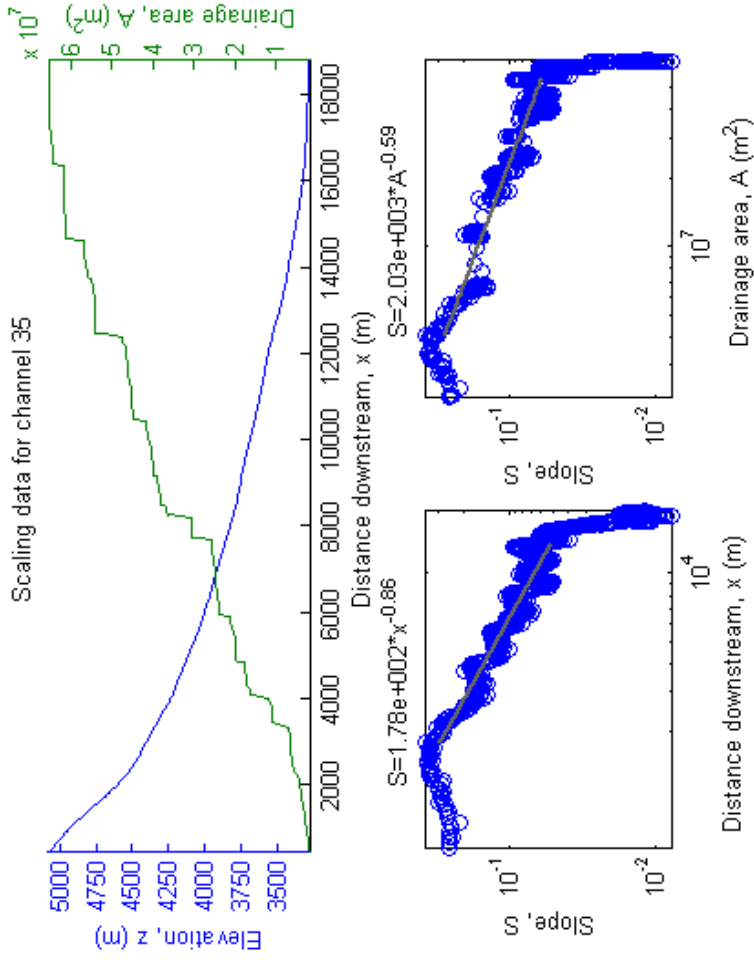
Scaling data for channel 33



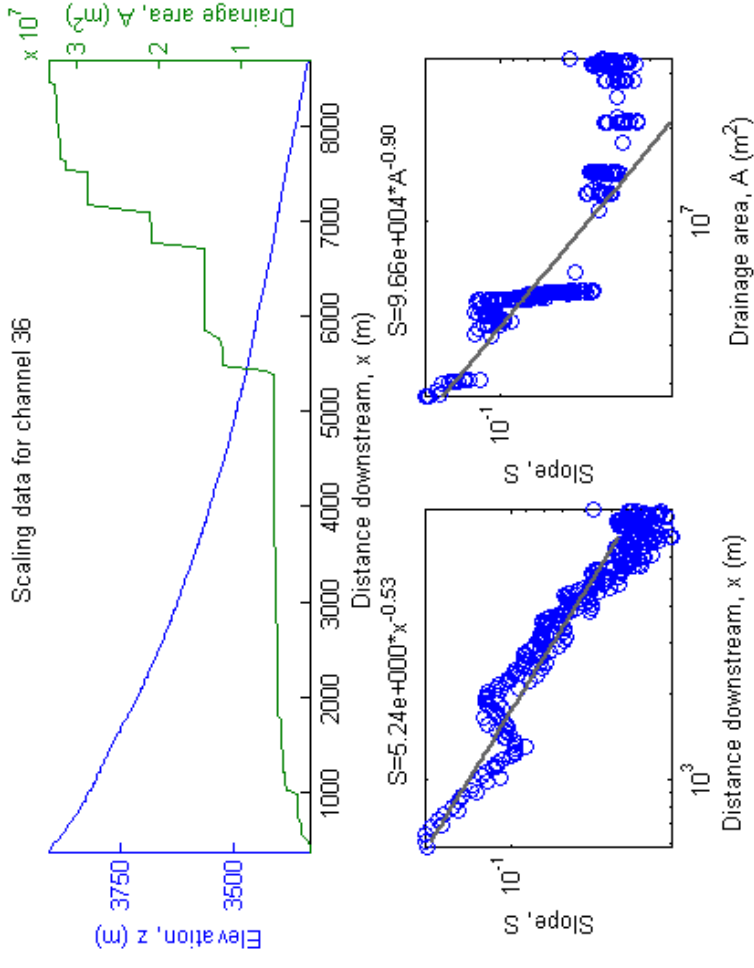
Scaling data for channel 34



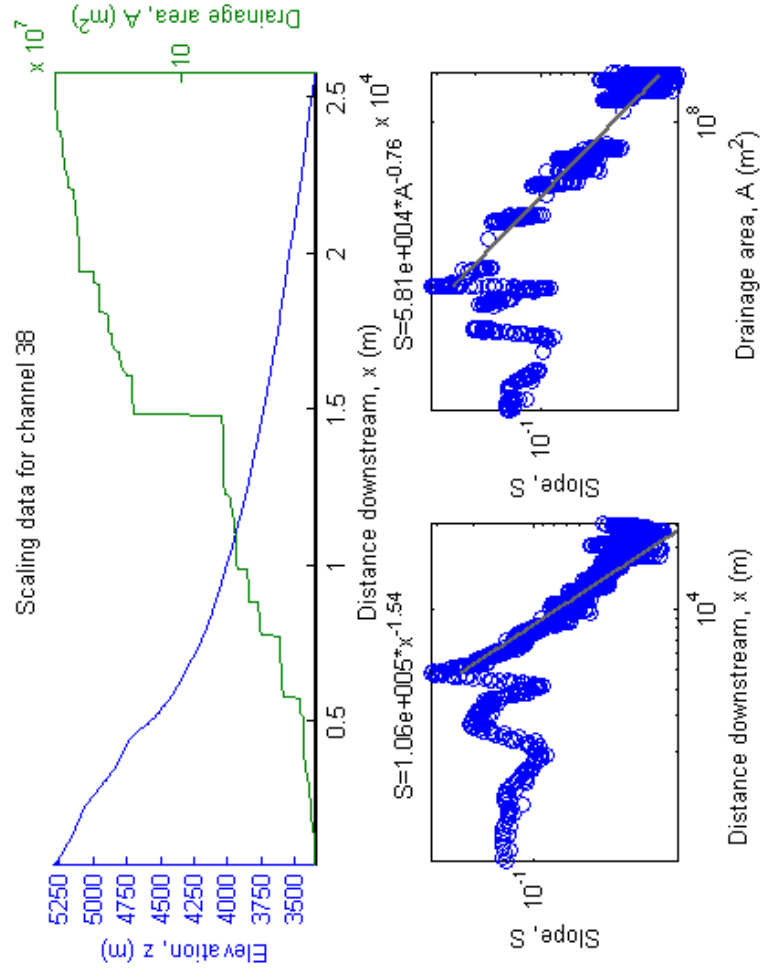
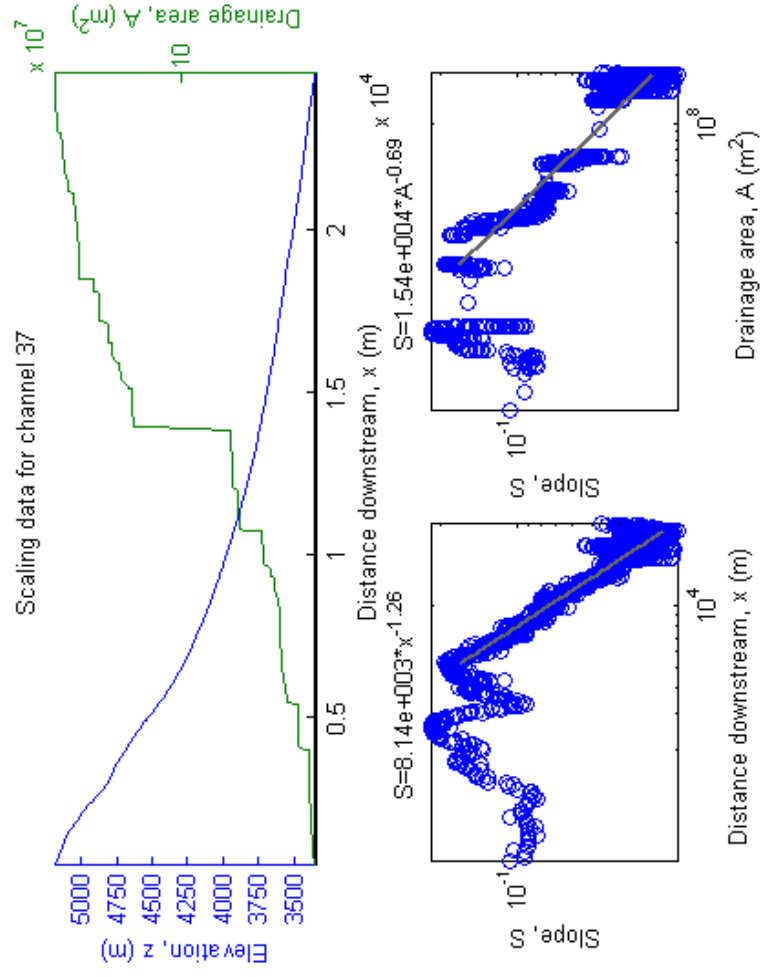
Scaling data for channel 35



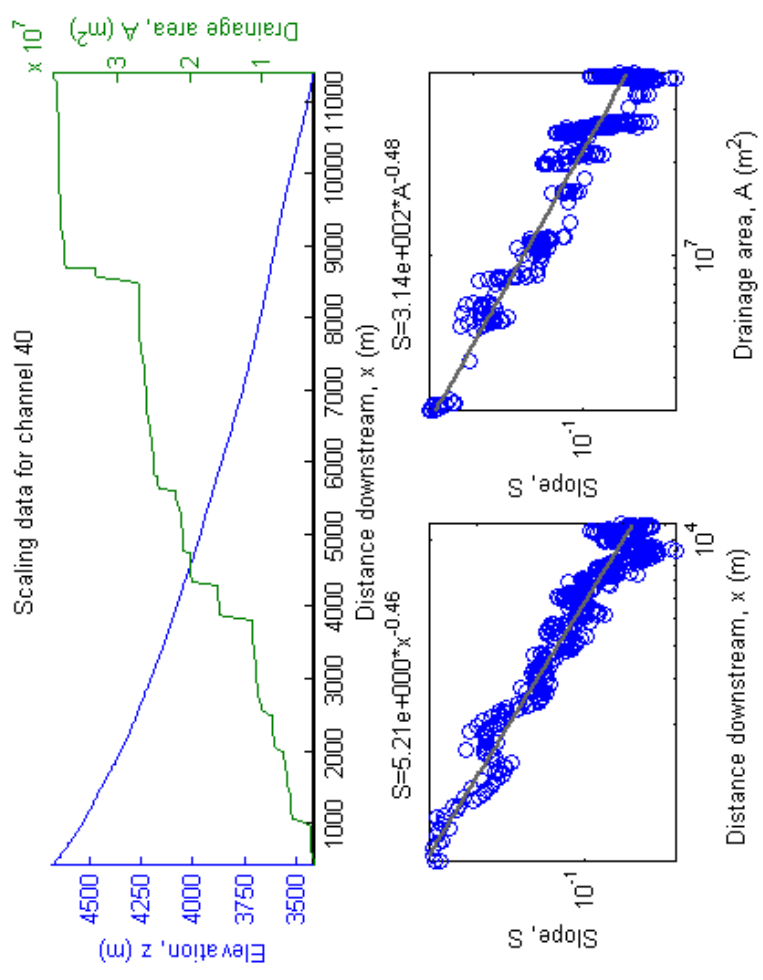
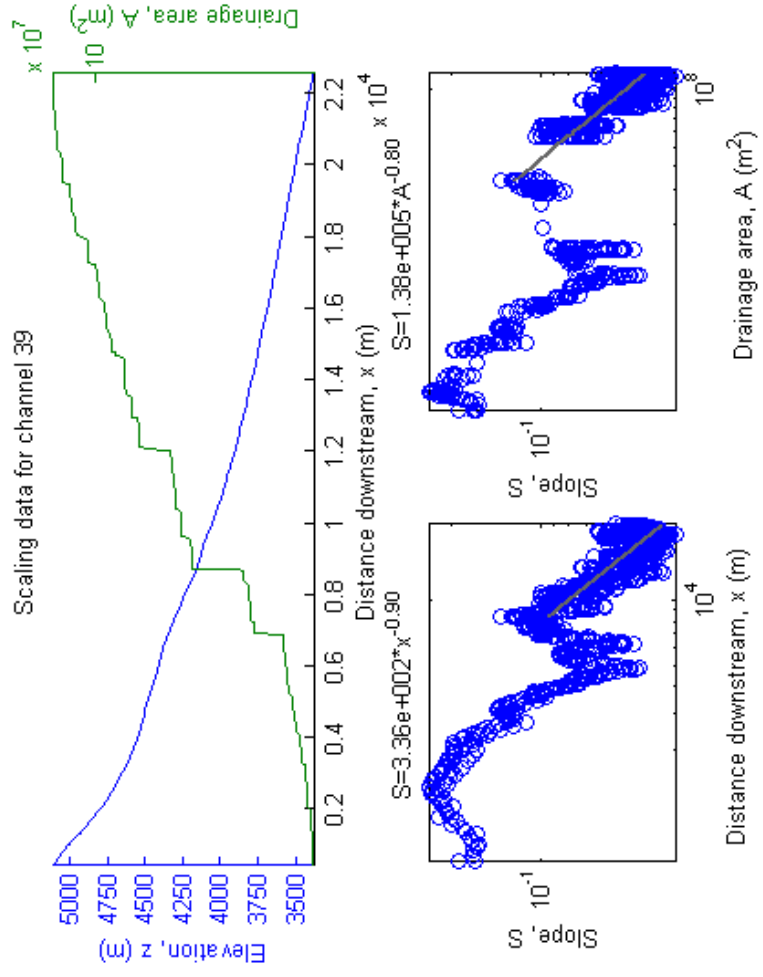
Scaling data for channel 36



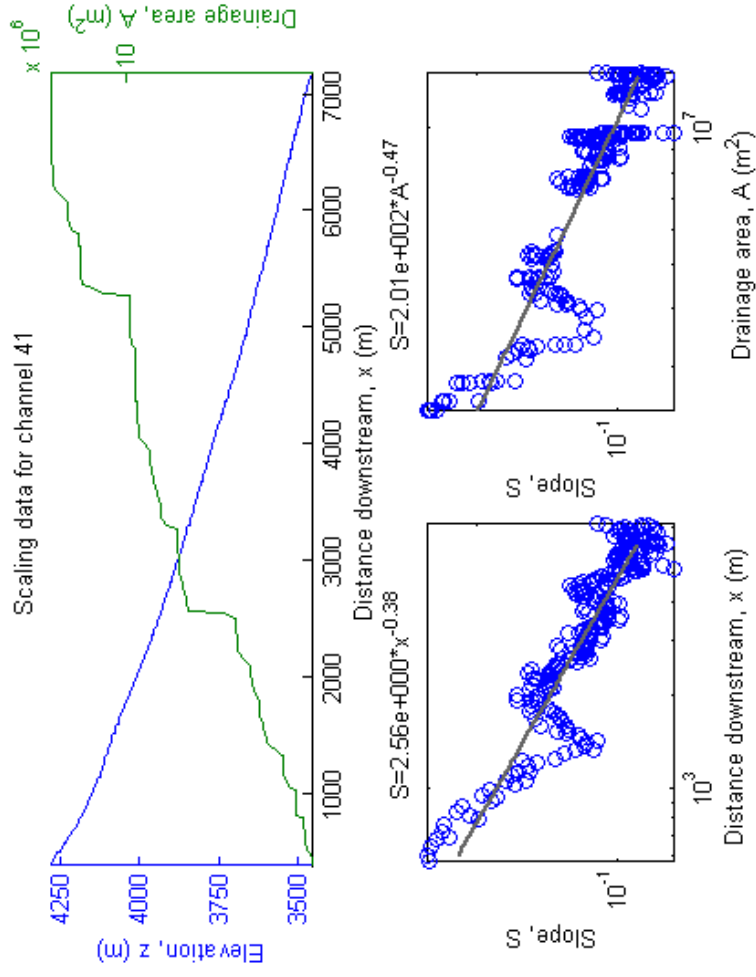
Scaling data for channel 37



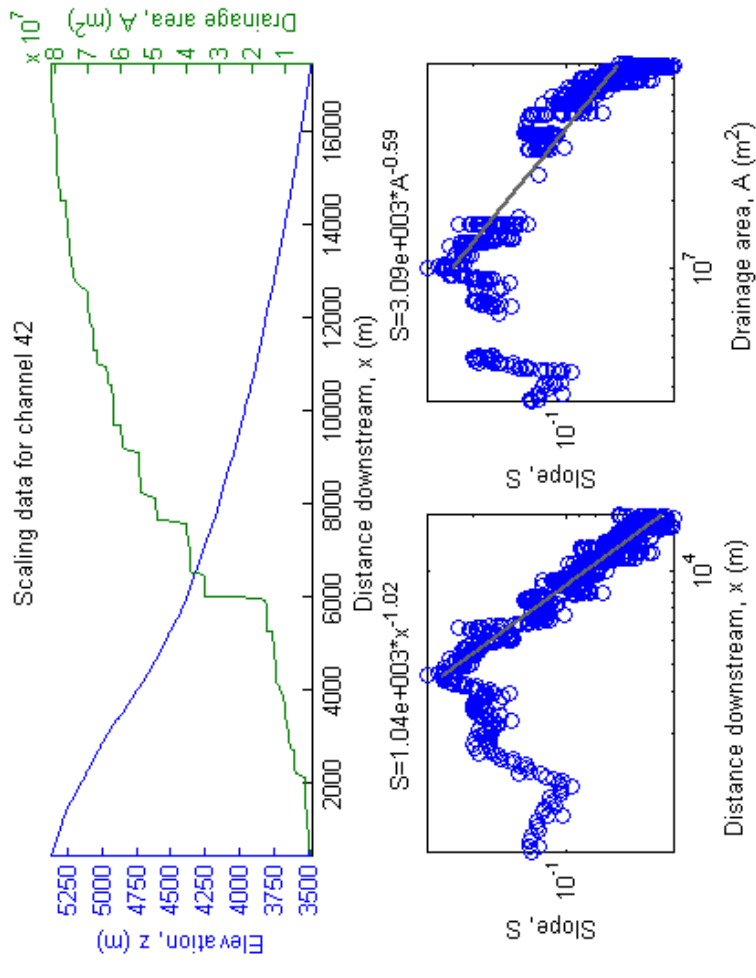
Scaling data for channel 39



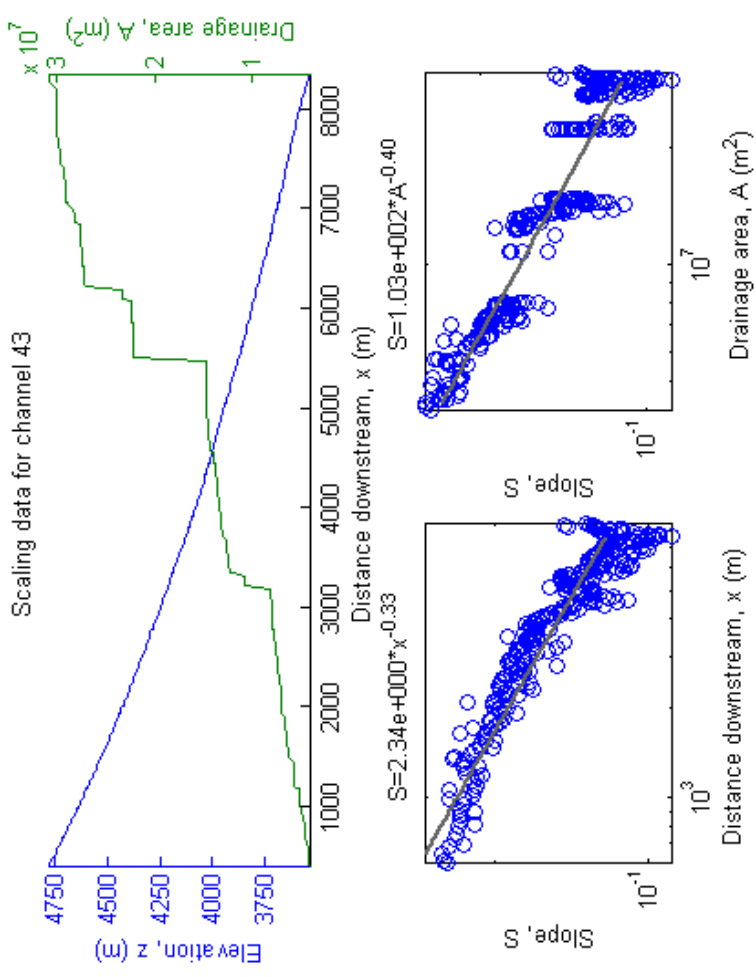
Scaling data for channel 41



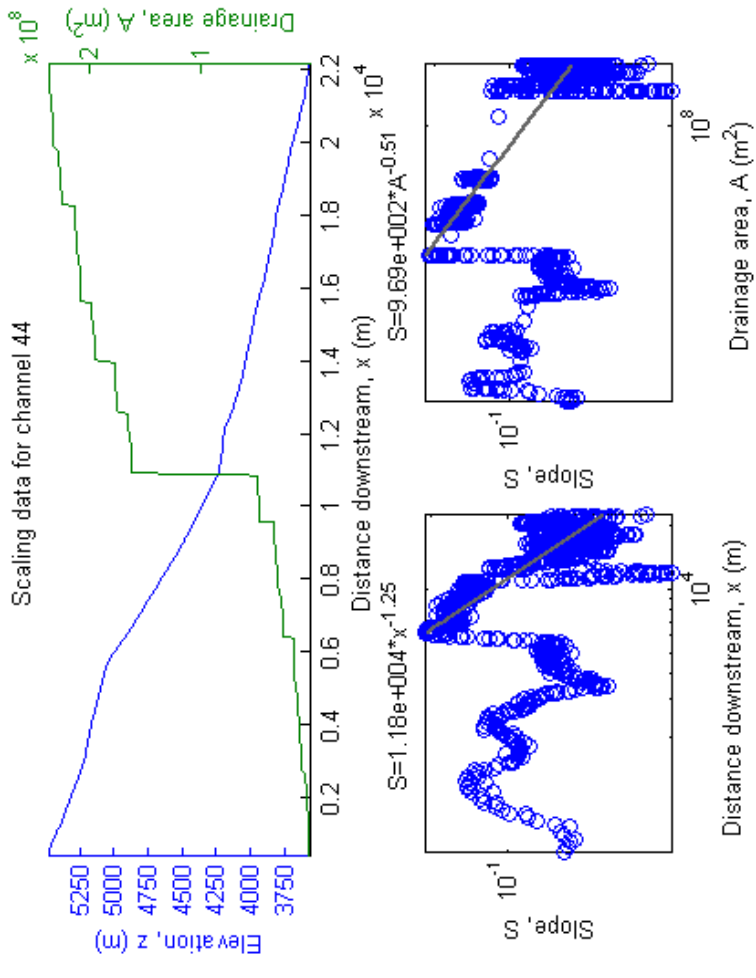
Scaling data for channel 42



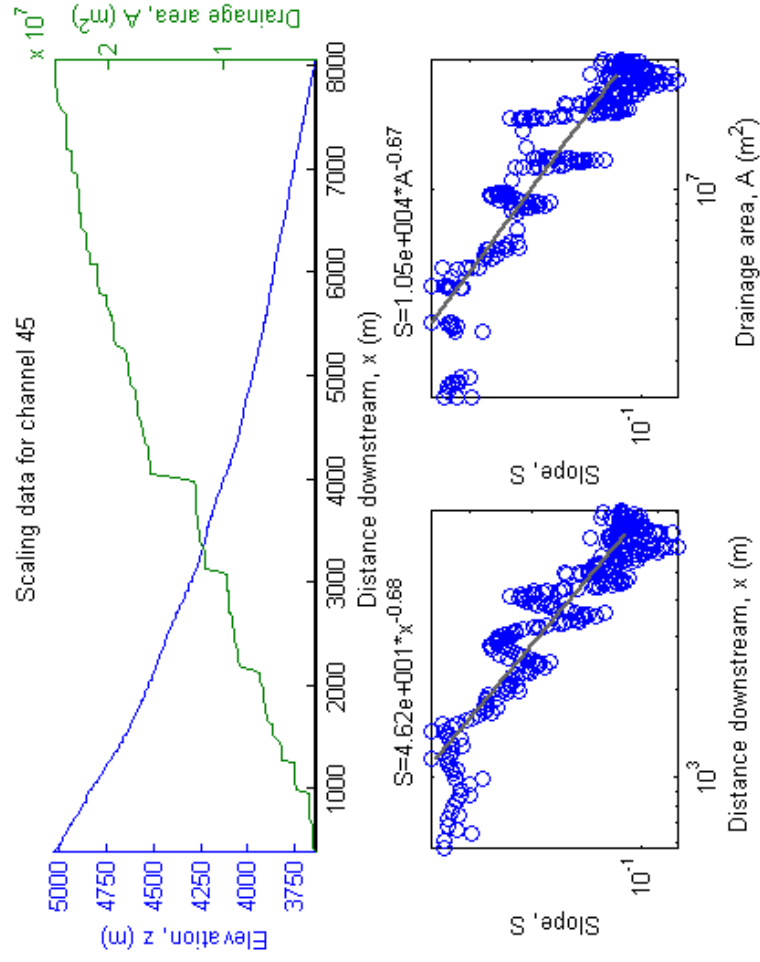
Scaling data for channel 43



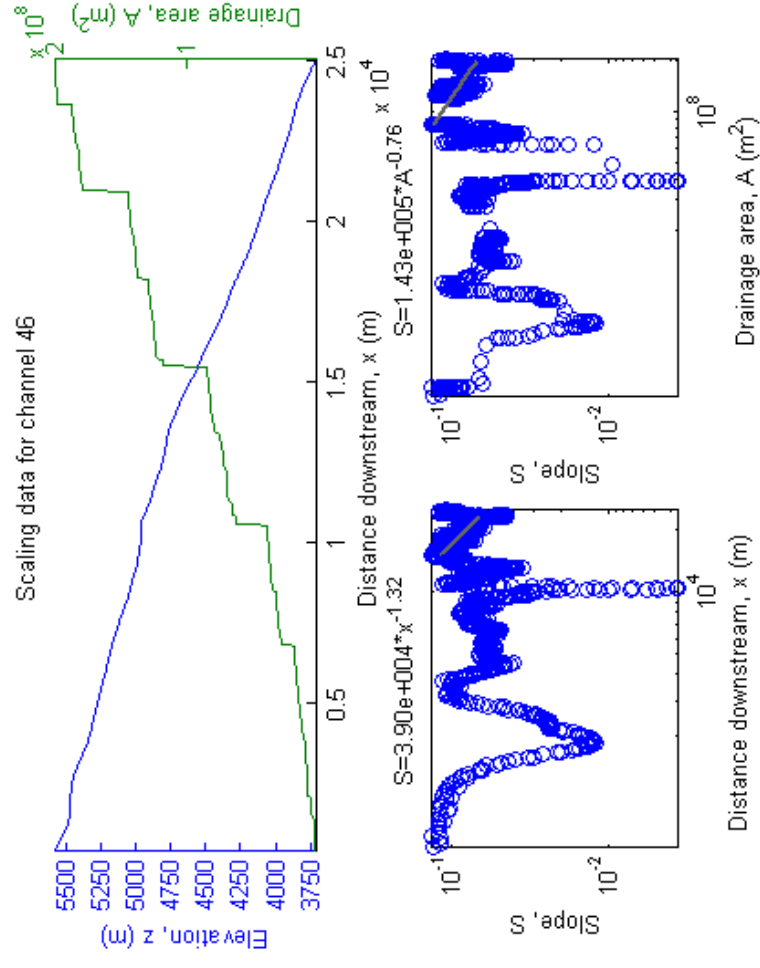
Scaling data for channel 44



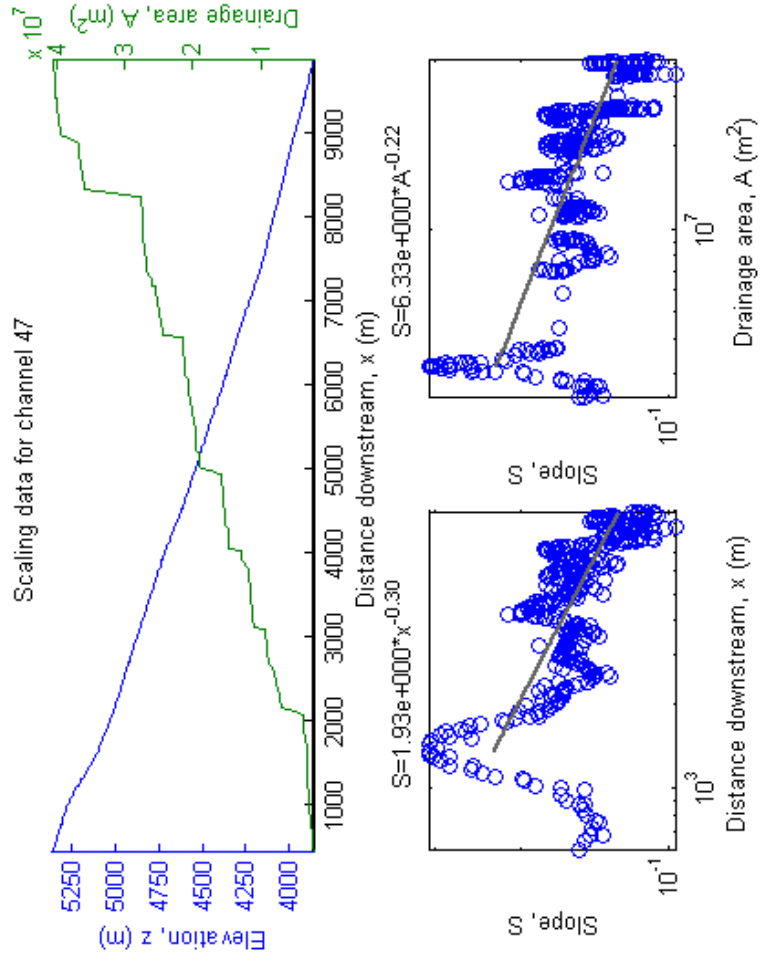
Scaling data for channel 45



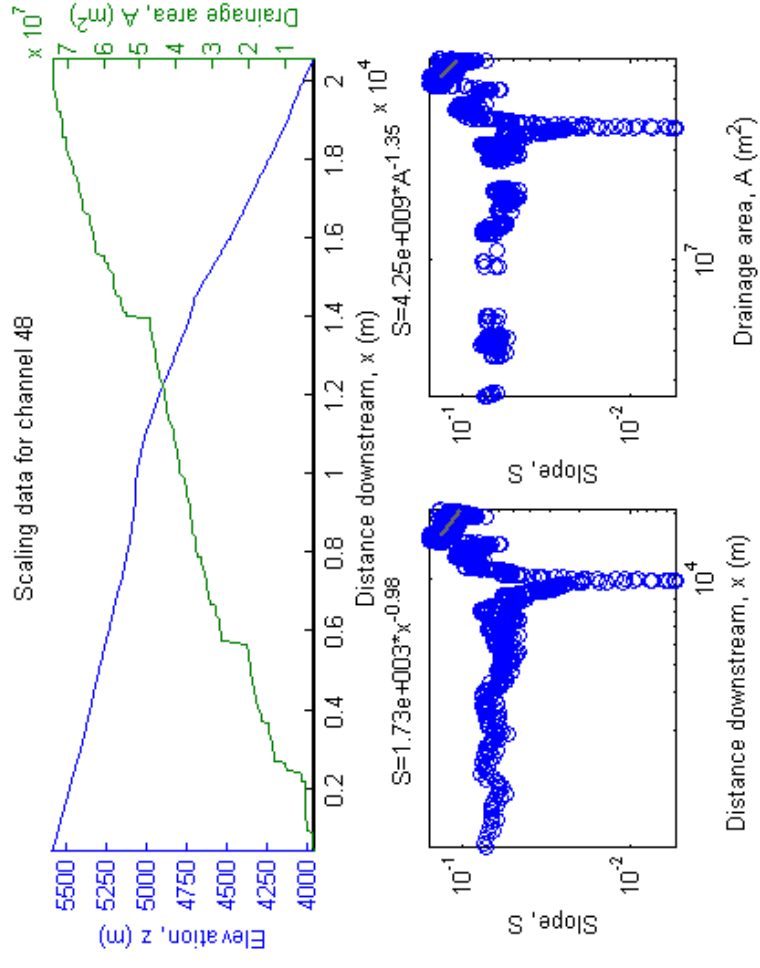
Scaling data for channel 46



Scaling data for channel 47

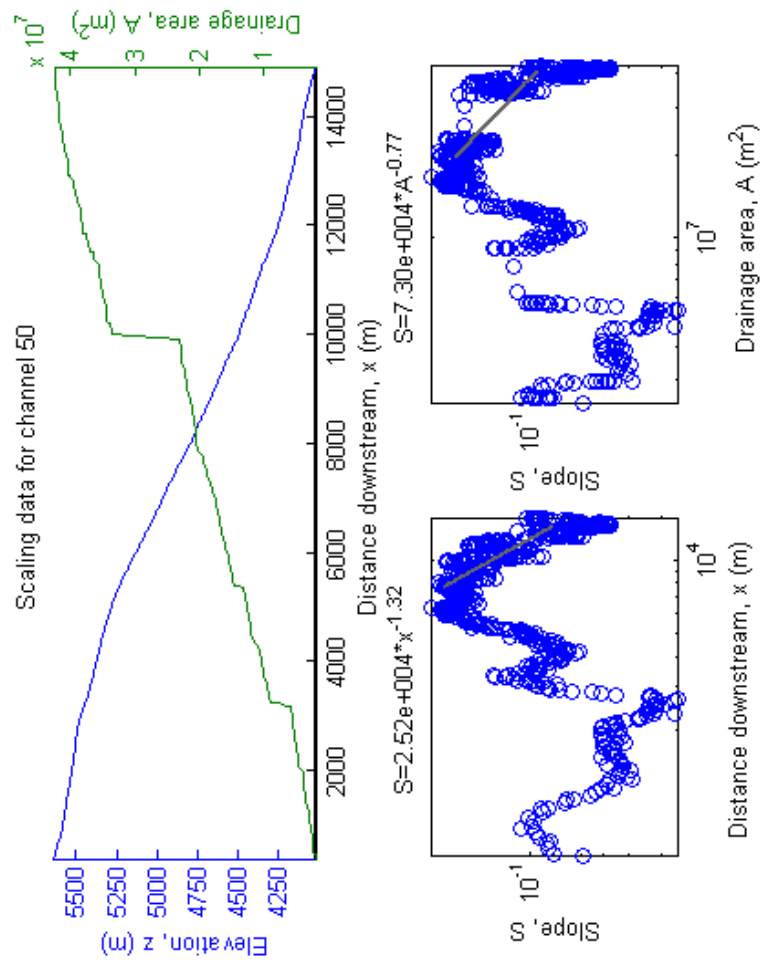
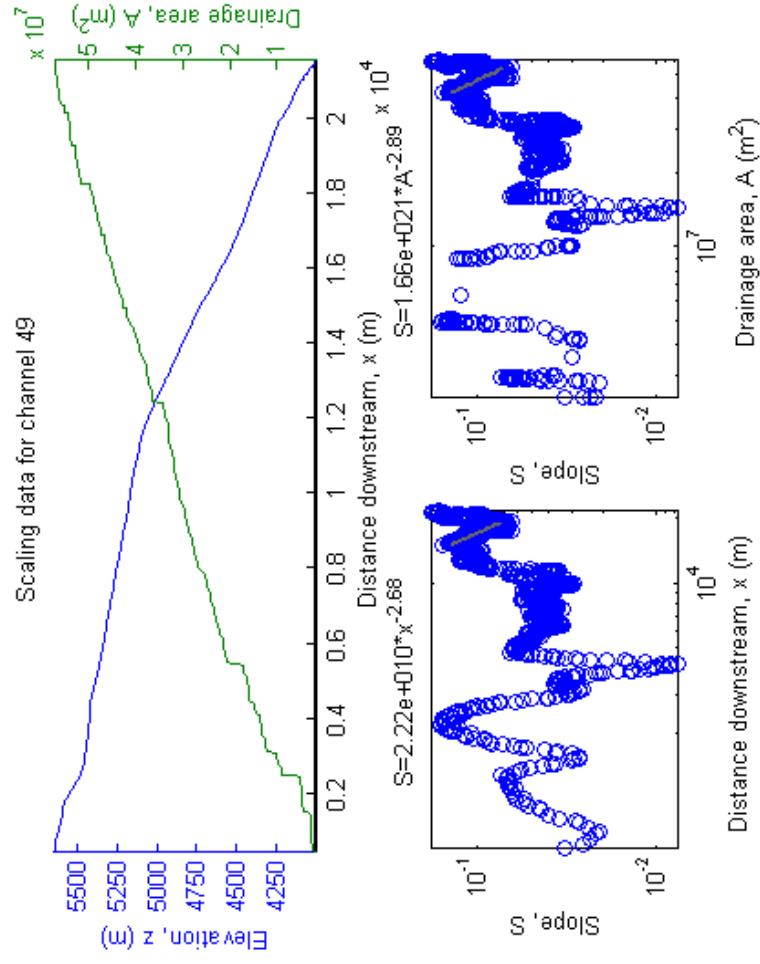


Scaling data for channel 48

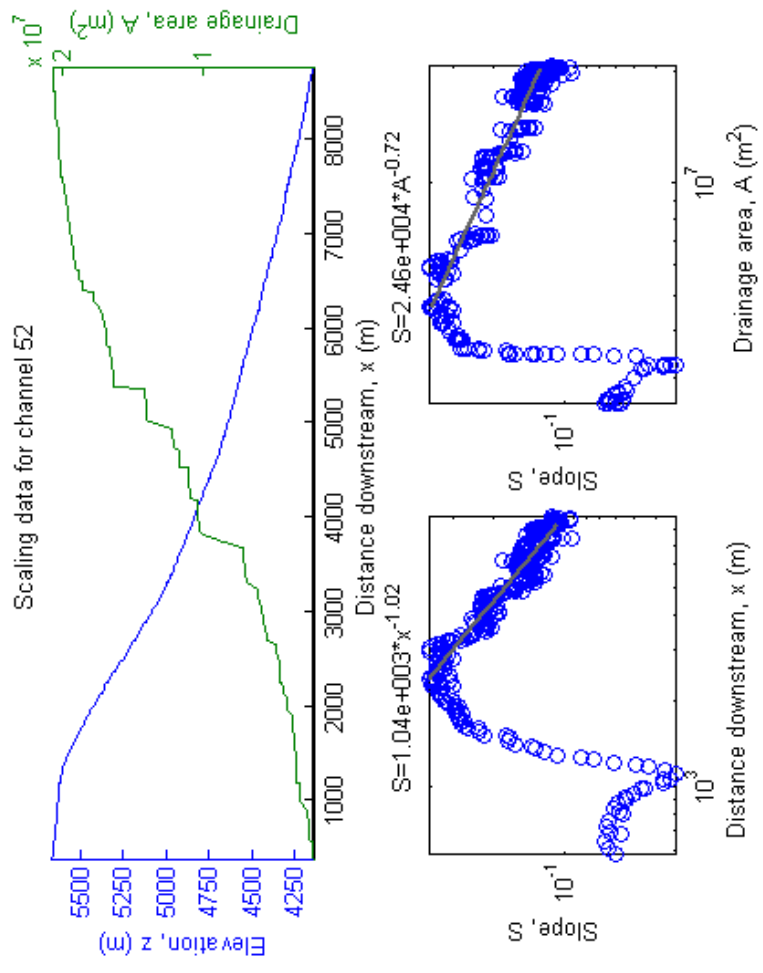
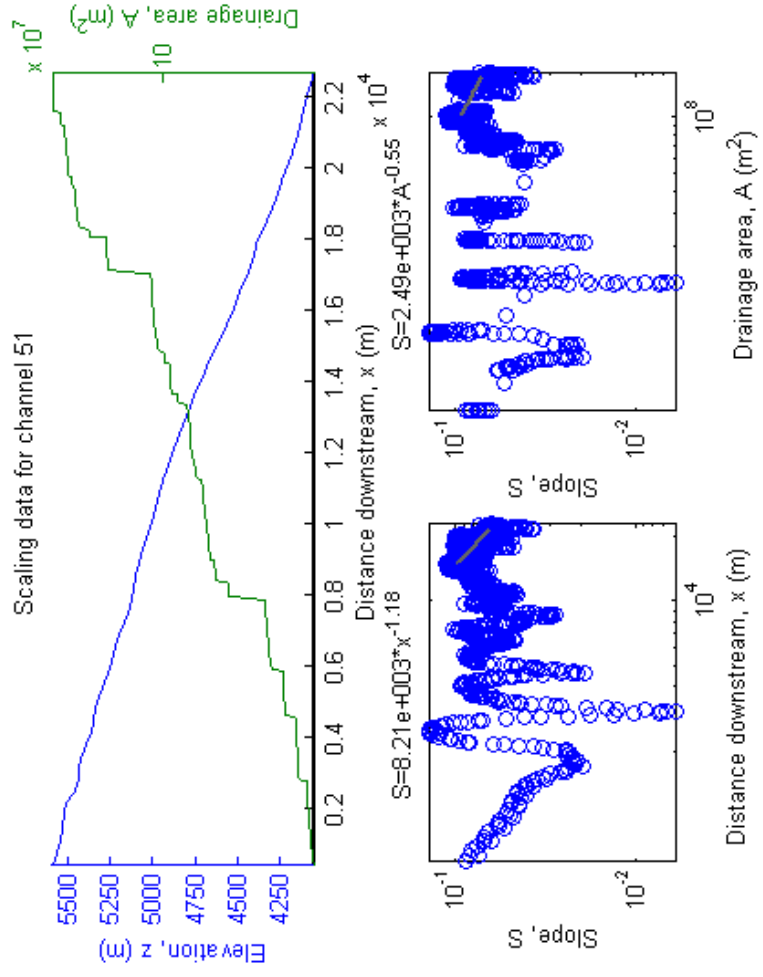




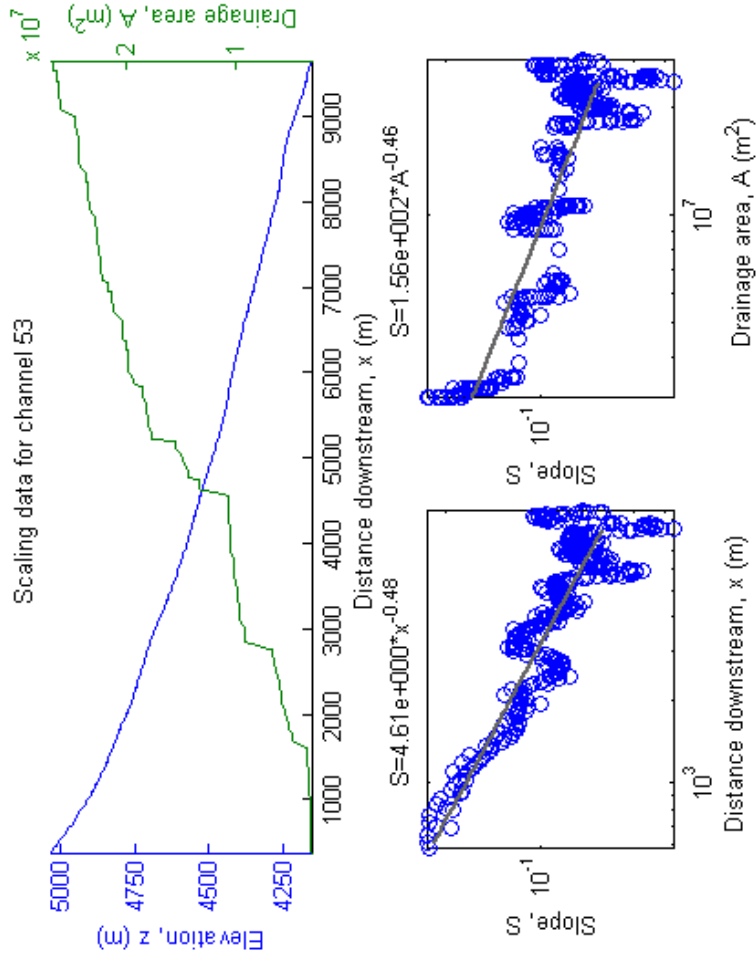
Scaling data for channel 49



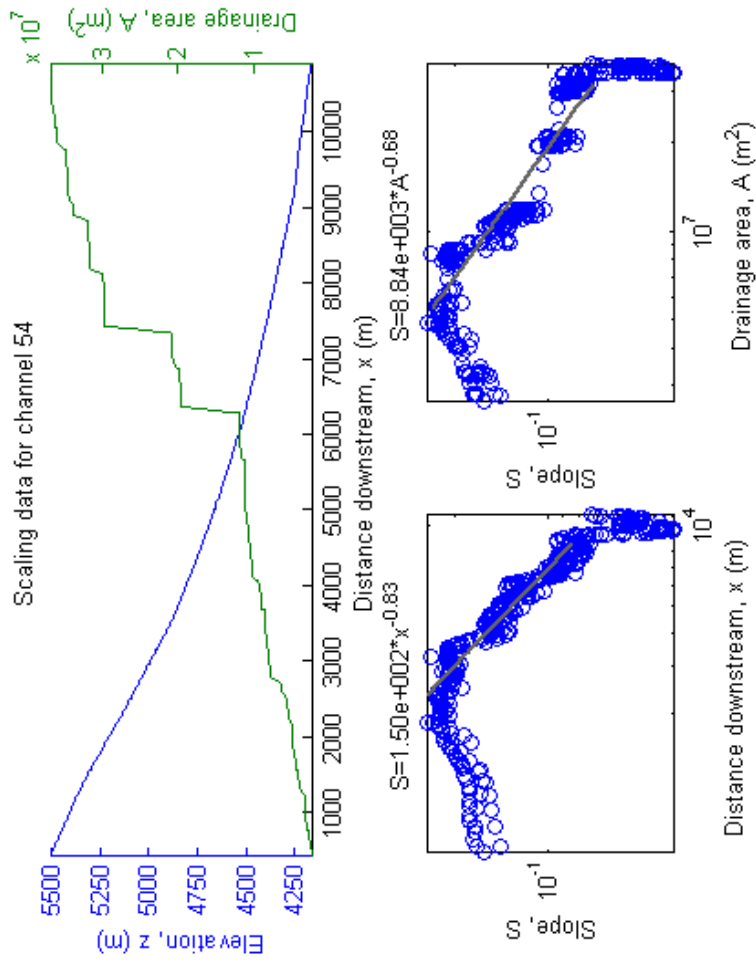
Scaling data for channel 51



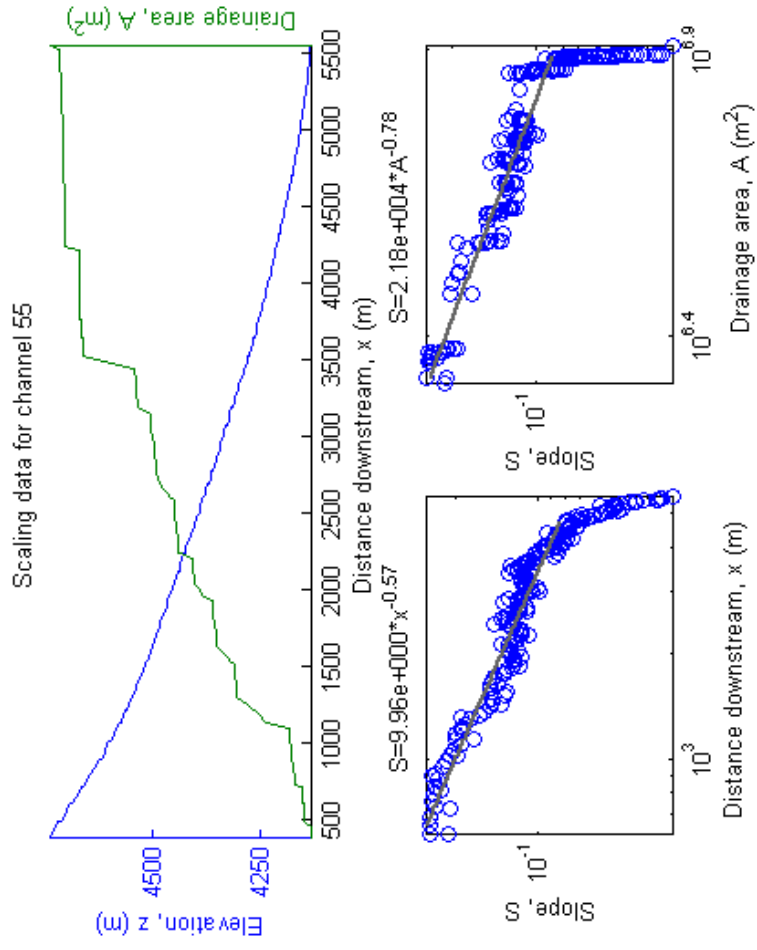
Scaling data for channel 53



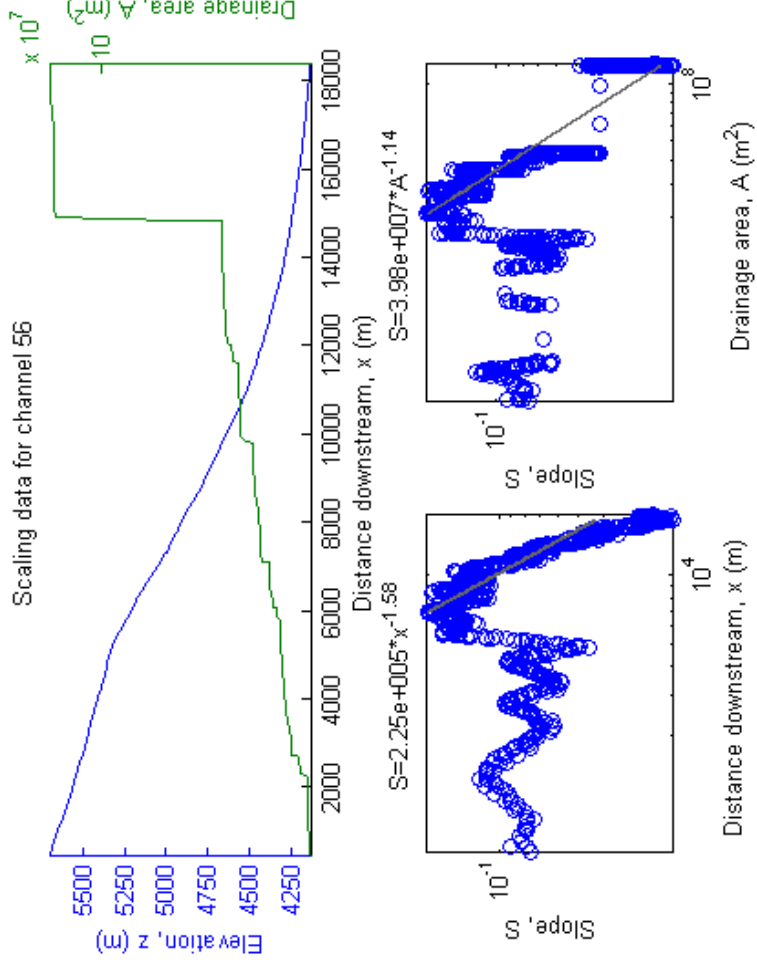
Scaling data for channel 54



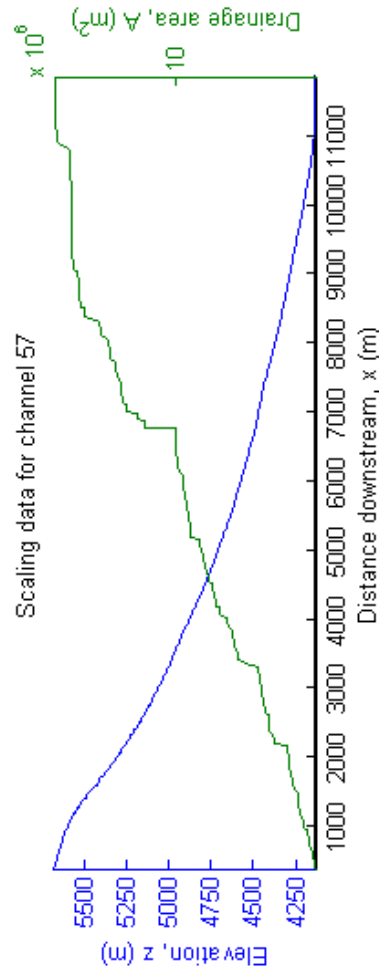
Scaling data for channel 55



Scaling data for channel 56

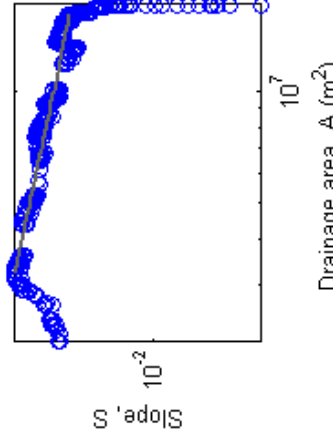
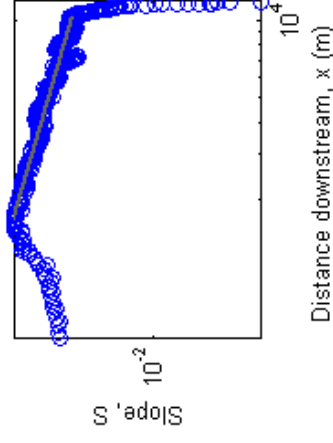


Scaling data for channel 57

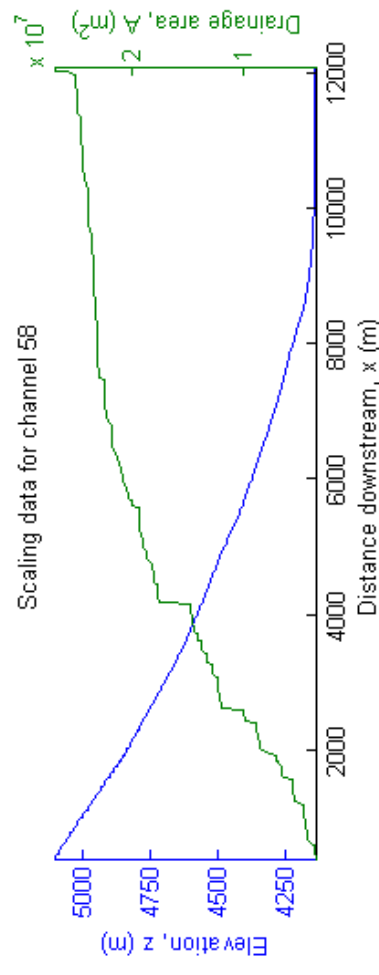


$$S=1.56e+002 \cdot x^{-0.82}$$

$$S=1.54e+005 \cdot A^{-0.87}$$



Scaling data for channel 58



$$S=1.67e+000 \cdot x^{-0.33}$$

$$S=9.72e+001 \cdot A^{-0.41}$$

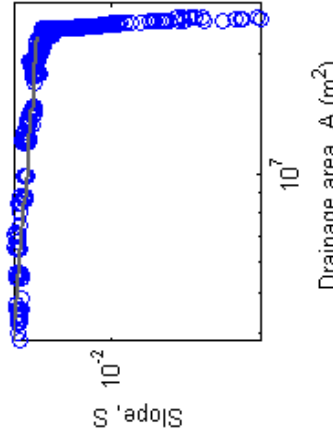
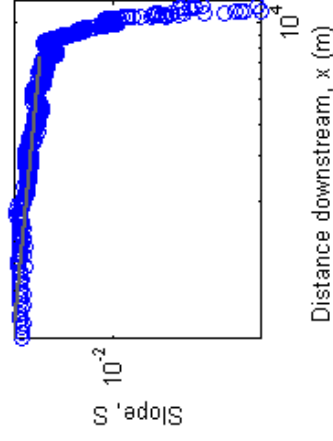


Figure S2a. Comparison of field (black squares) and DEM (grey circles) derived slopes as measured downstream for (i) Basgo valley and (ii) Leh

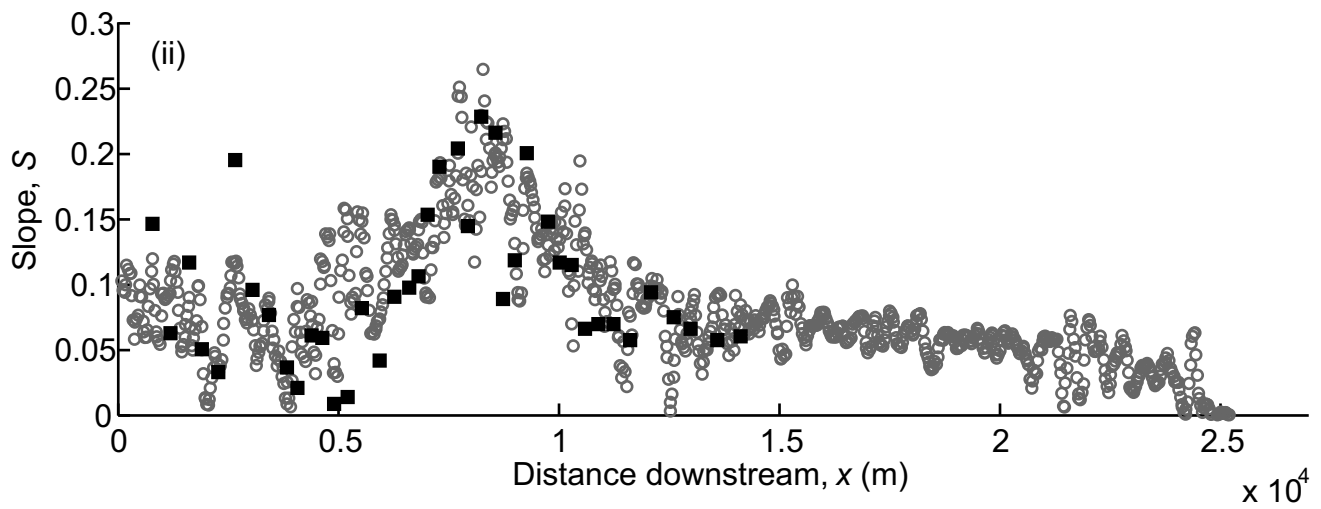
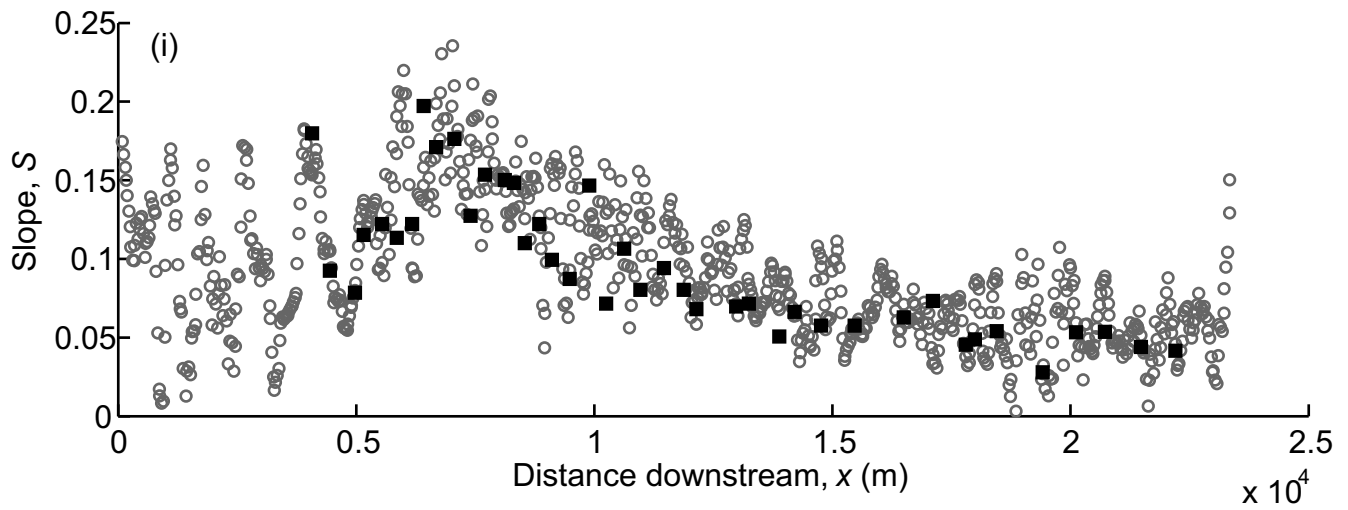


Figure S2b. Field slopes versus DEM slopes for two catchments, (i) Basgo valley, (ii) Leh valley

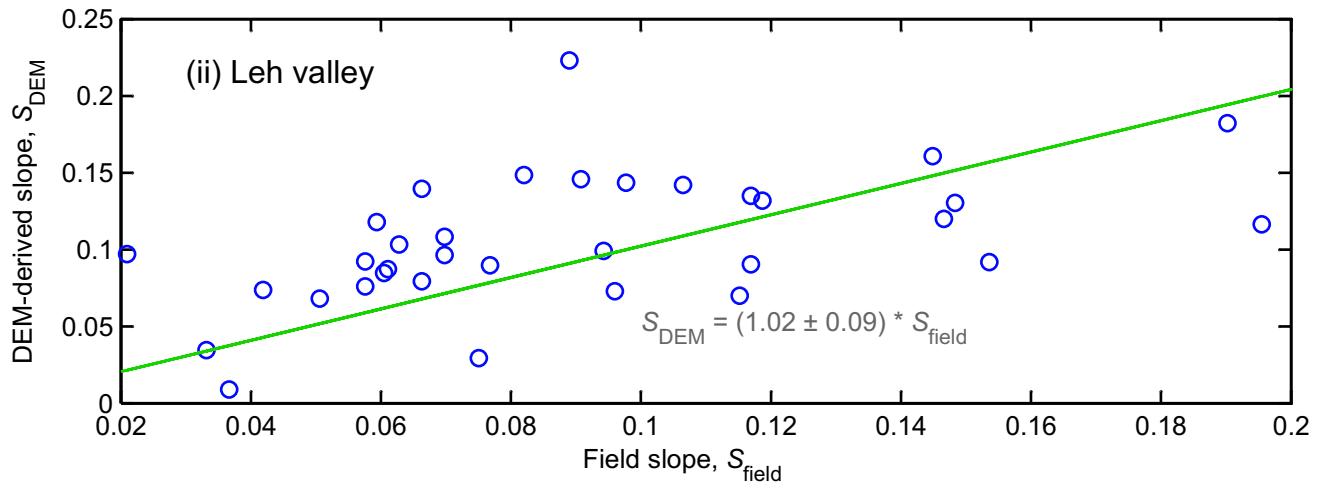
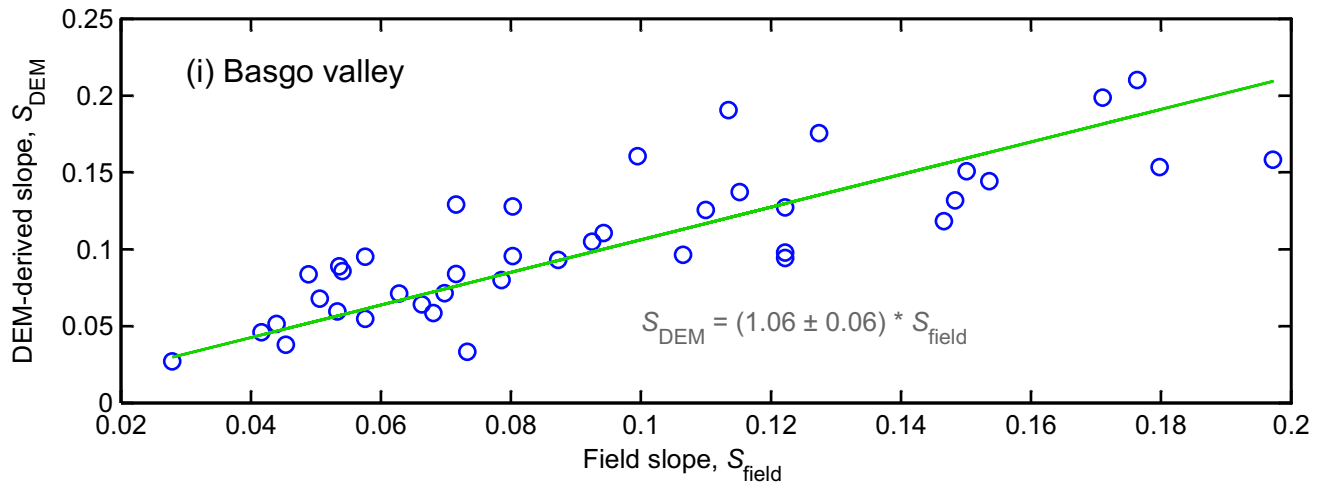
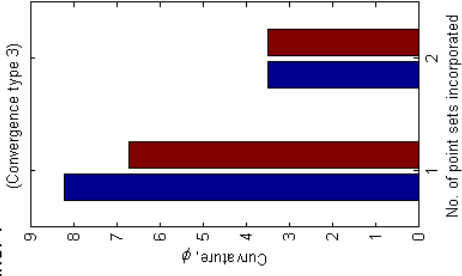
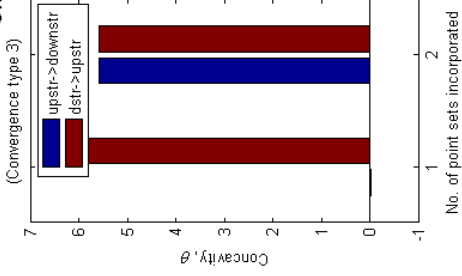


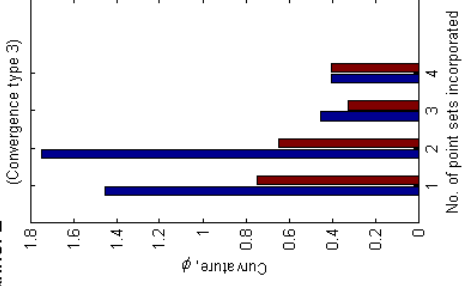
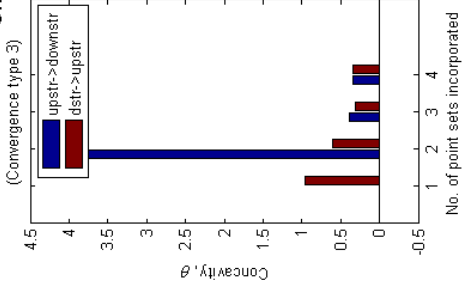
Figure S3. Plots of calculated concavity and curvature values for each catchment, subdividing the data to investigate possible variations in the values downstream. Data is plotted incorporating different numbers of sets of 50 data points, working both from upstream to downstream (blue) and downstream to upstream (red). The pattern of convergence as described in the accompanying supporting text is noted above each graph. See accompanying text for full explanation.



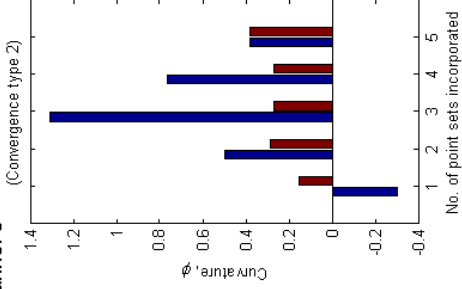
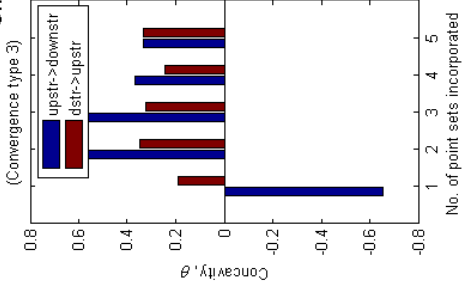
Channel 1



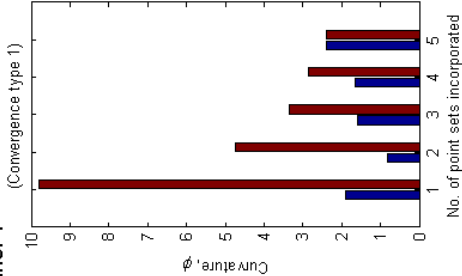
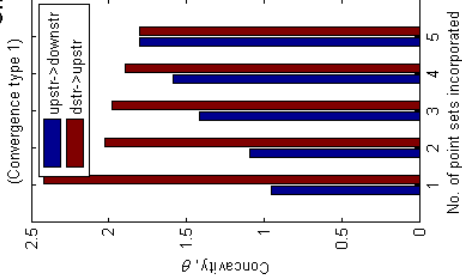
Channel 2



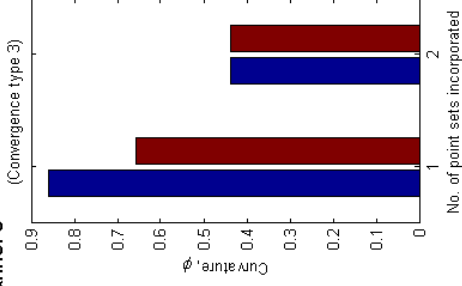
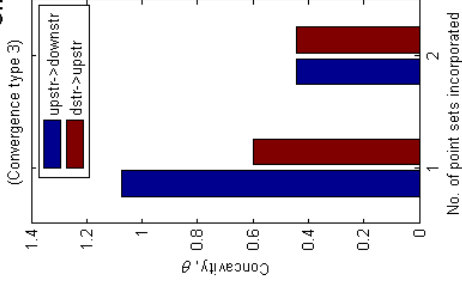
Channel 3



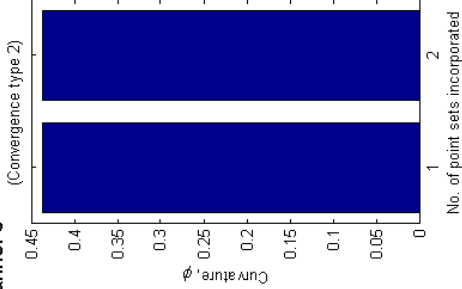
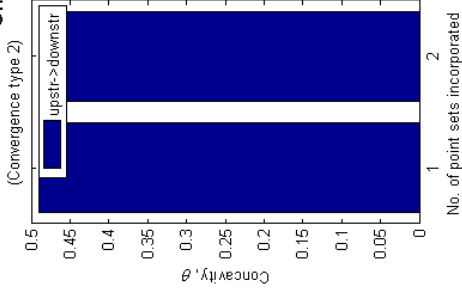
Channel 4



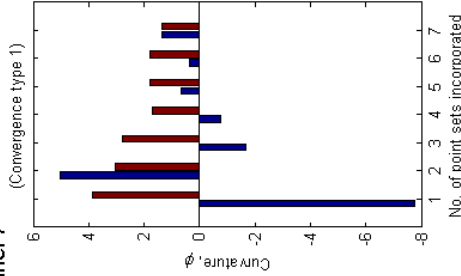
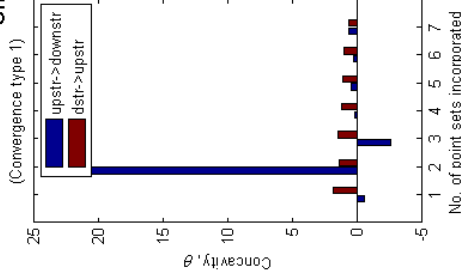
Channel 5



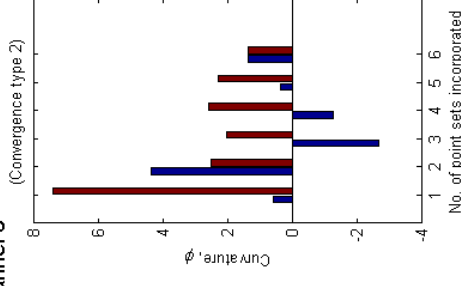
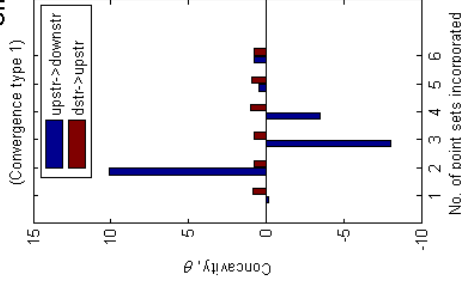
Channel 6



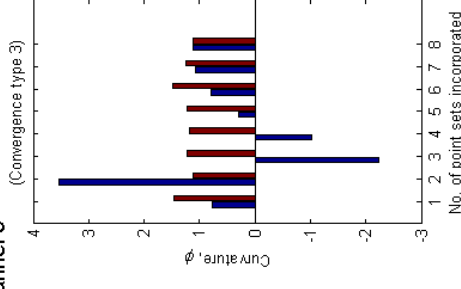
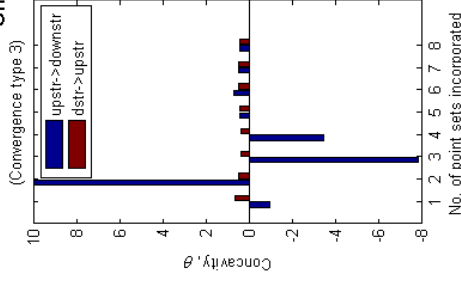
Channel 7



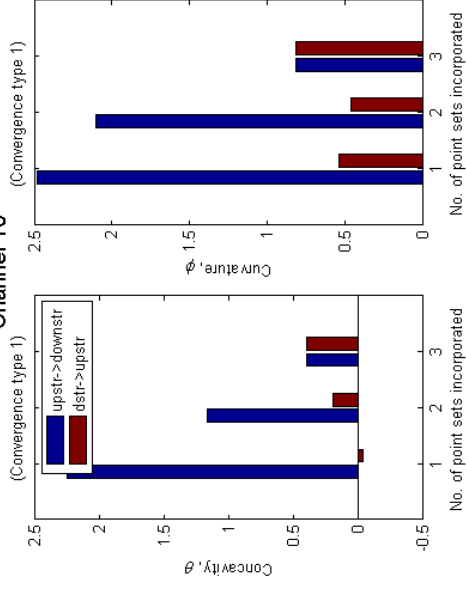
Channel 8



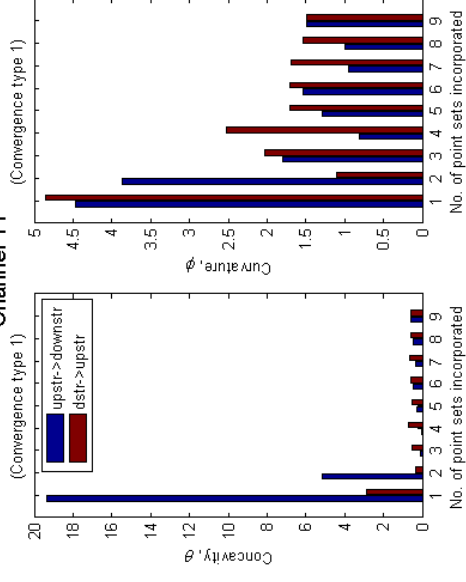
Channel 9



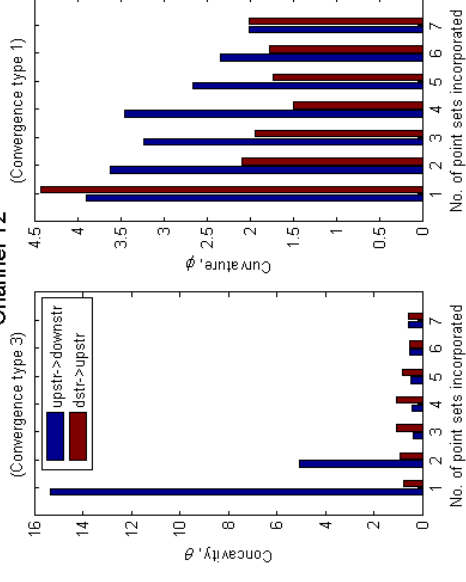
Channel 10



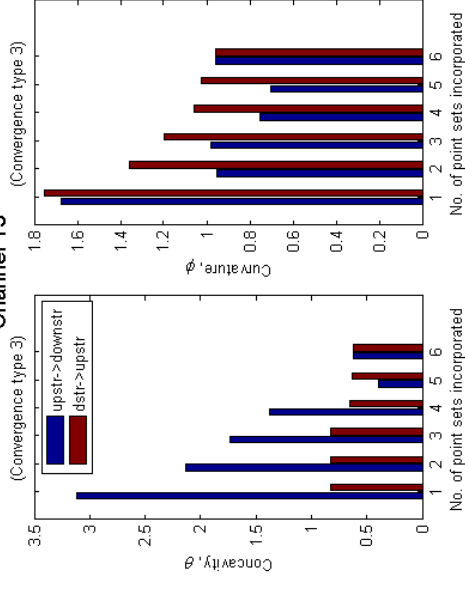
Channel 11



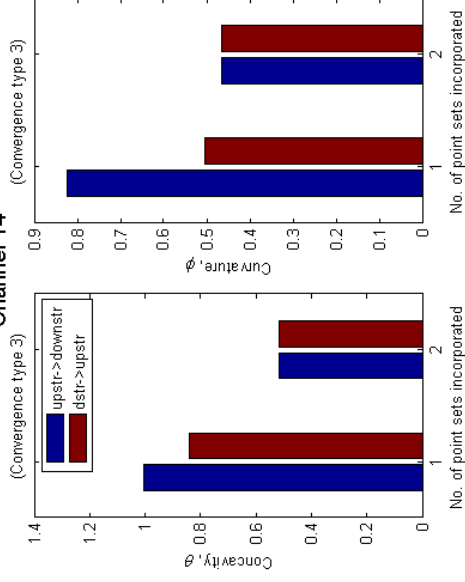
Channel 12



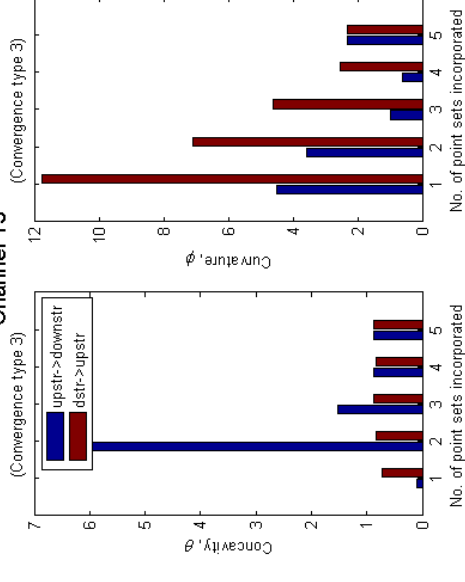
Channel 13



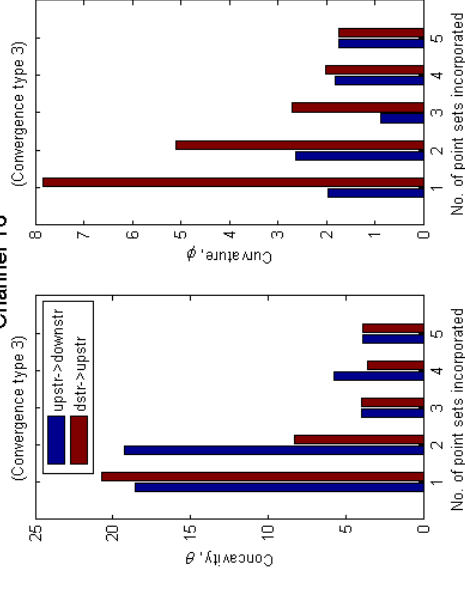
Channel 14



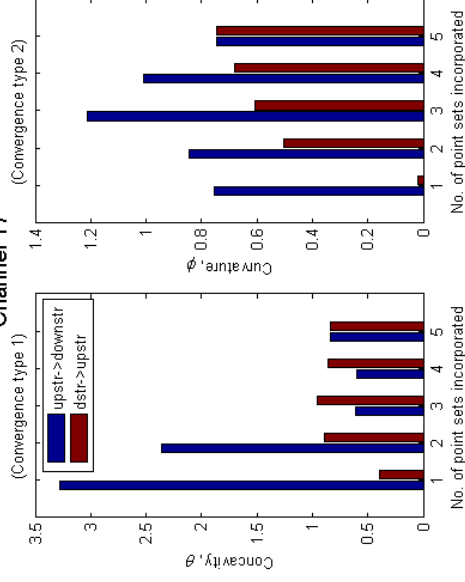
Channel 15



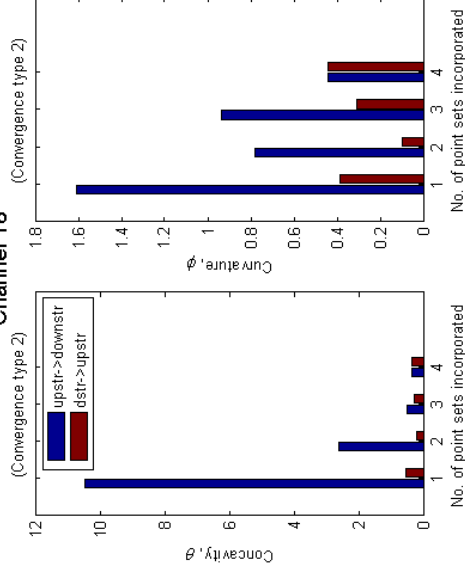
Channel 16



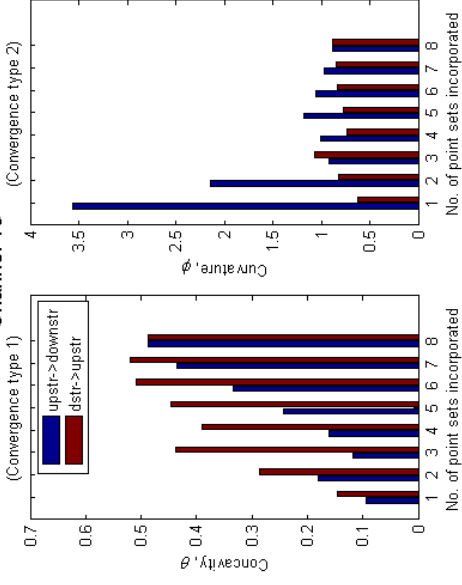
Channel 17



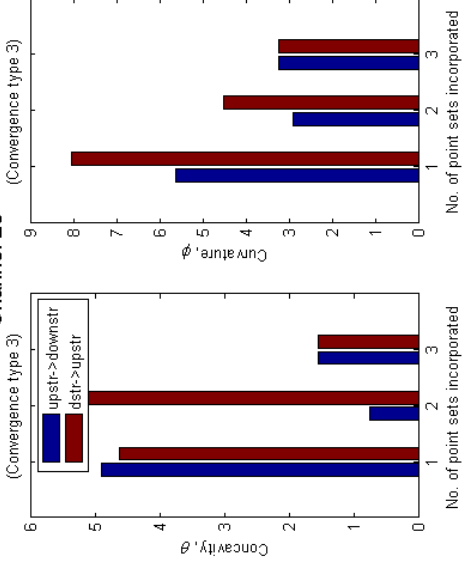
Channel 18



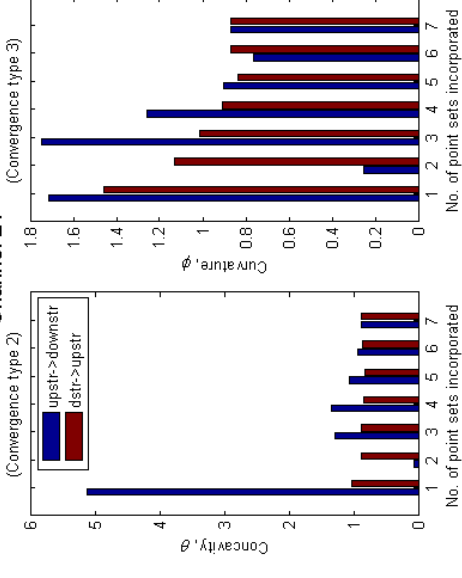
Channel 19



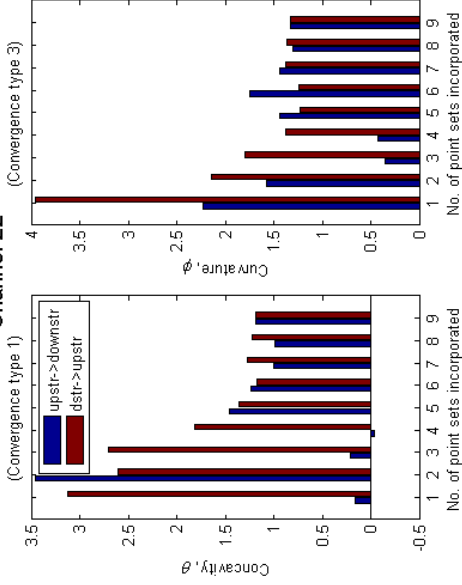
Channel 20



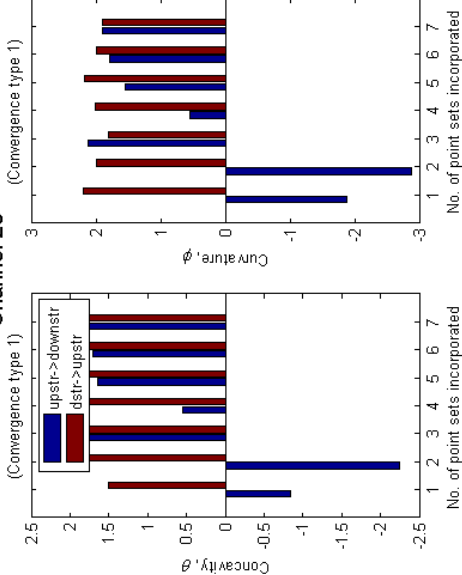
Channel 21



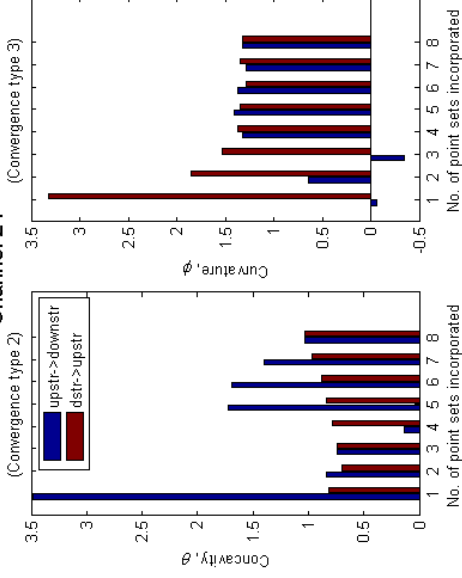
Channel 22



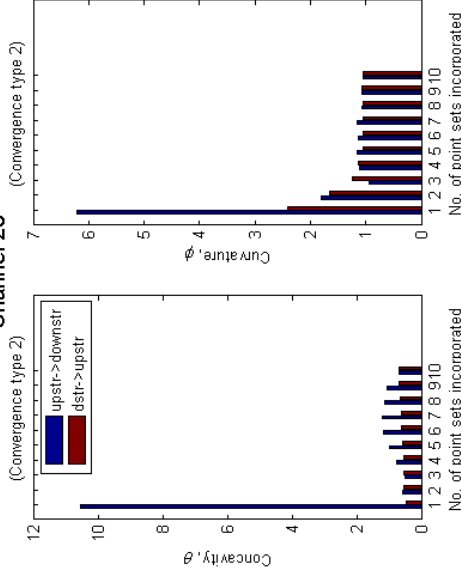
Channel 23



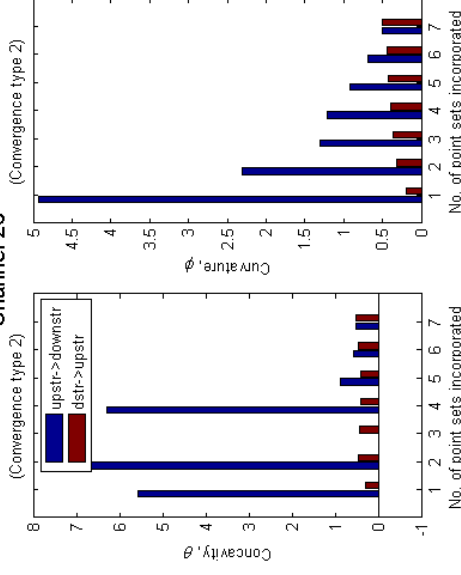
Channel 24



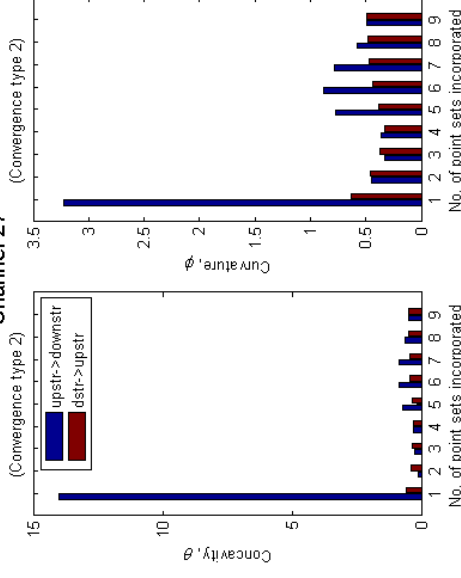
Channel 25



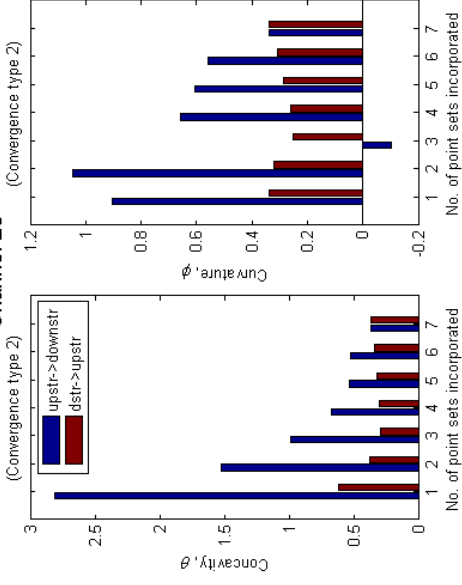
Channel 26



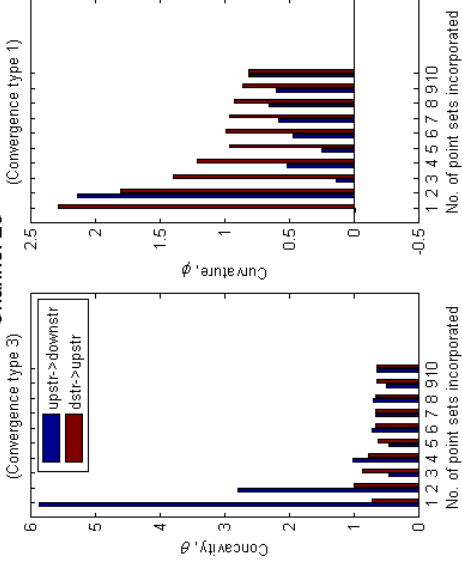
Channel 27



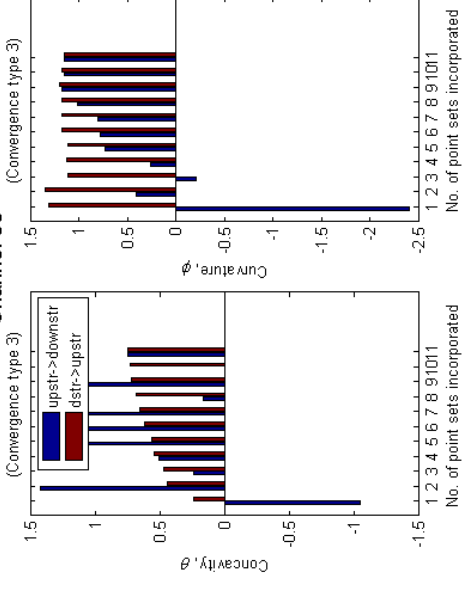
Channel 28



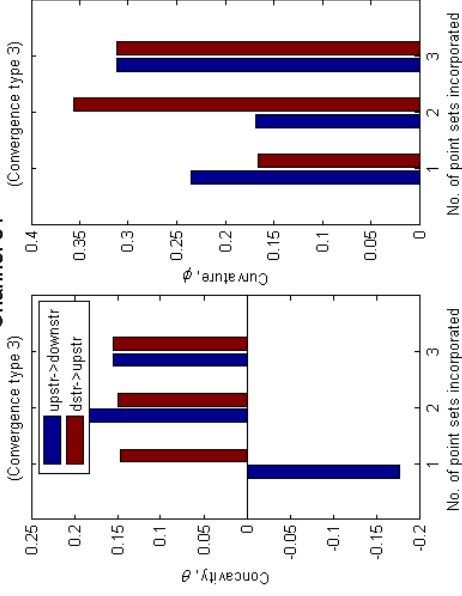
Channel 29



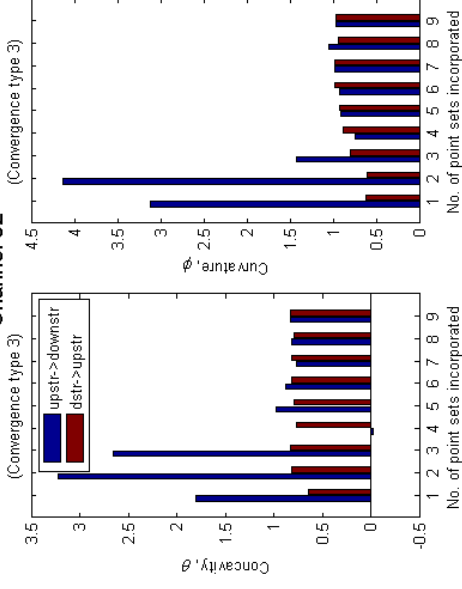
Channel 30



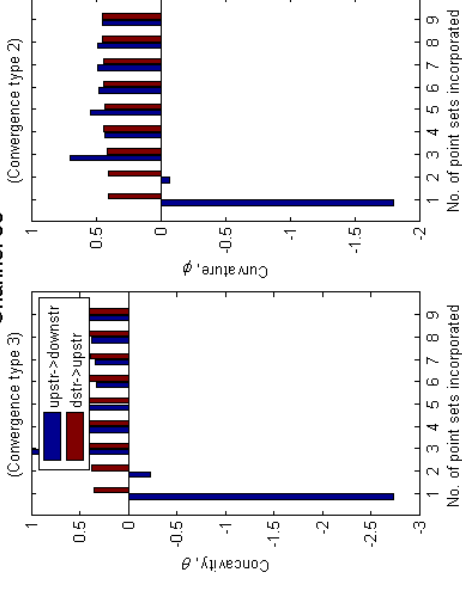
Channel 31



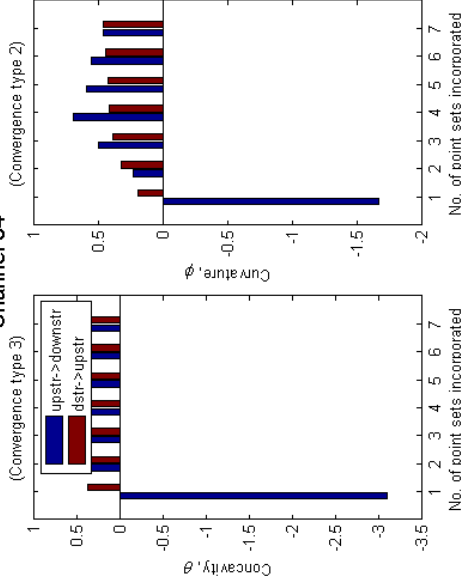
Channel 32



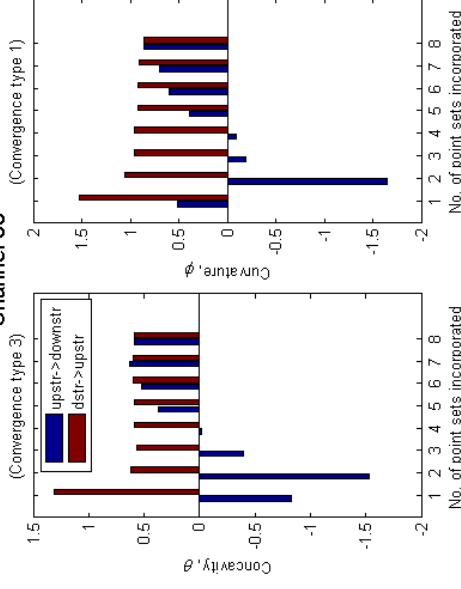
Channel 33



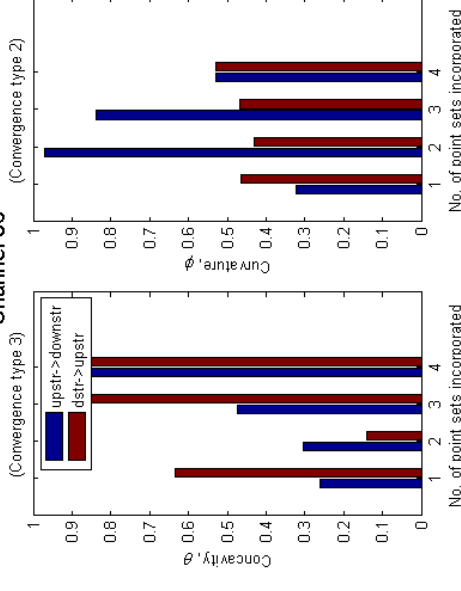
Channel 34



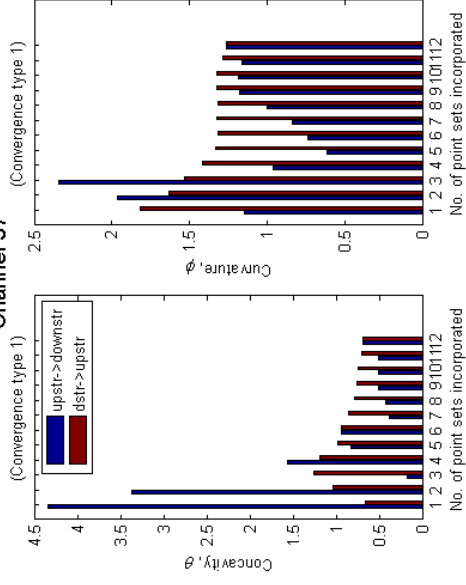
Channel 35



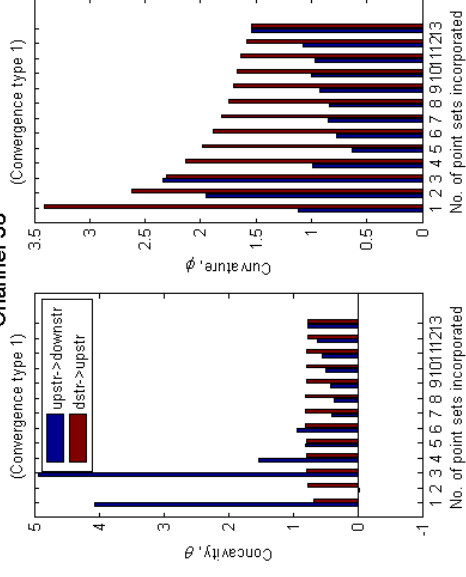
Channel 36



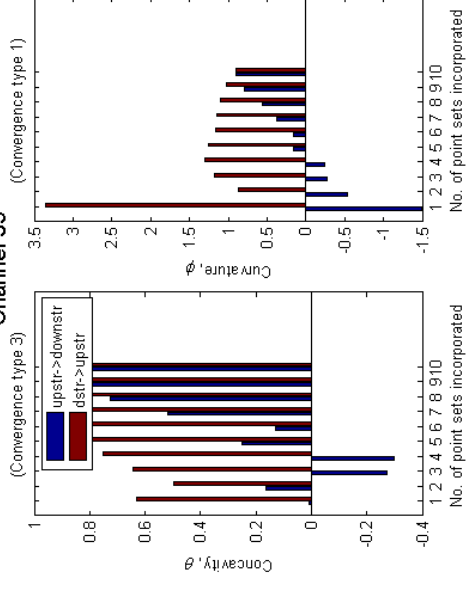
Channel 37



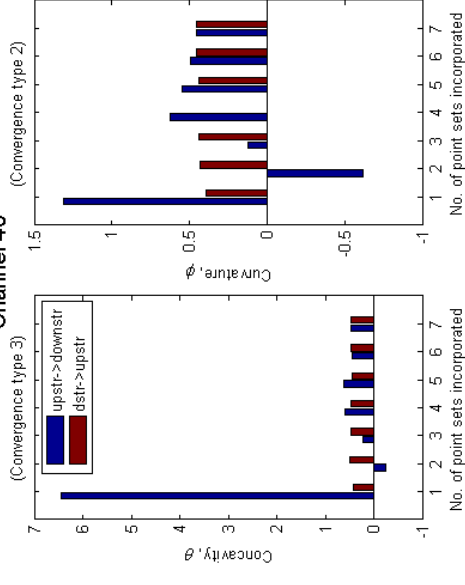
Channel 38



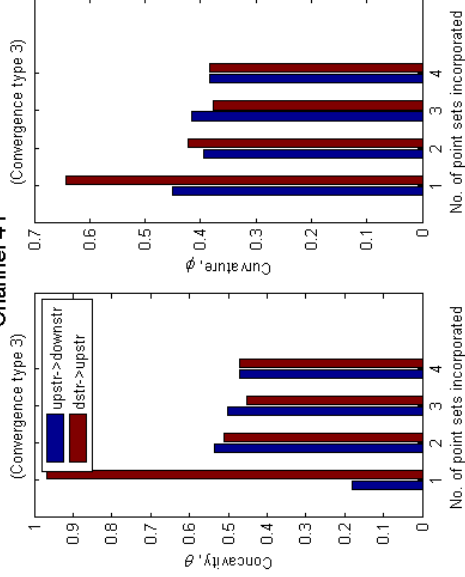
Channel 39



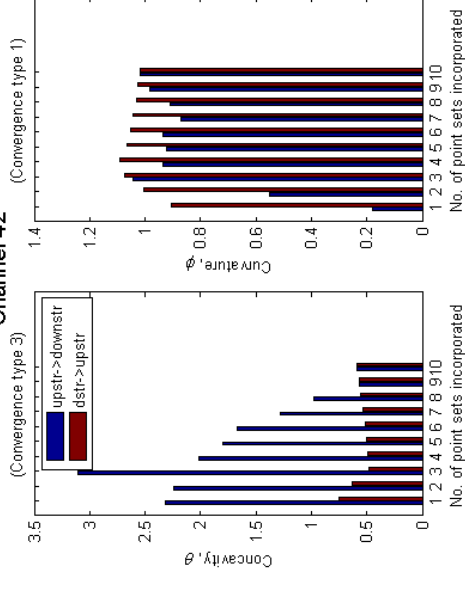
Channel 40



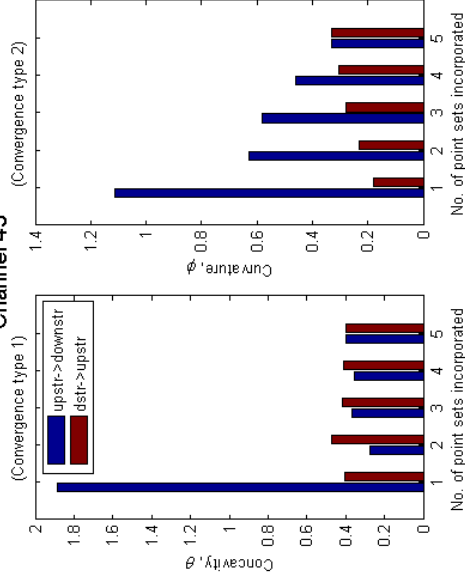
Channel 41



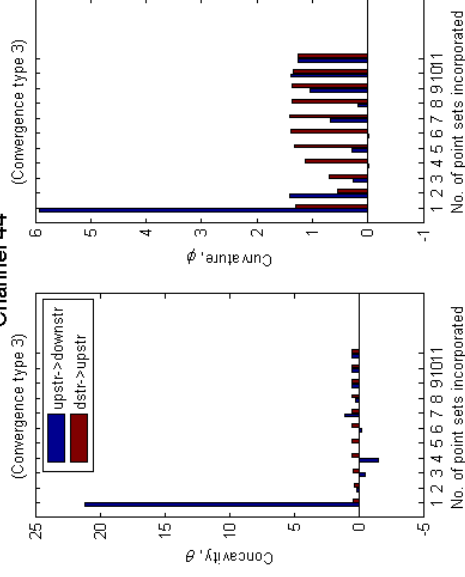
Channel 42



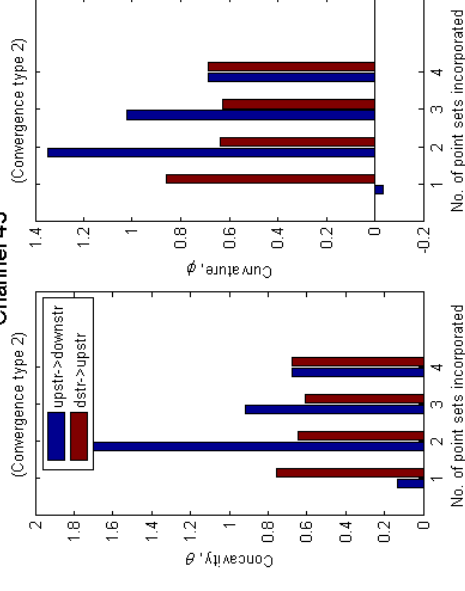
Channel 43



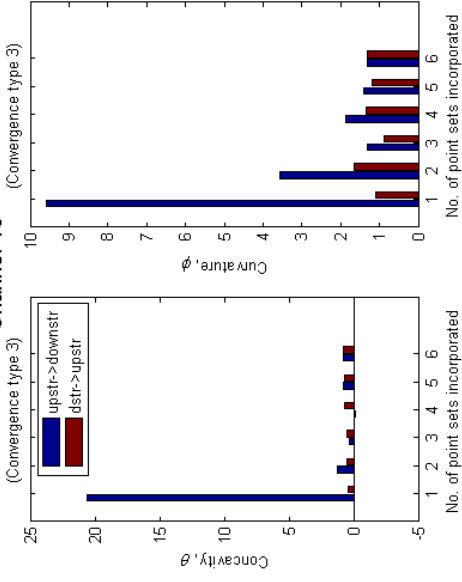
Channel 44



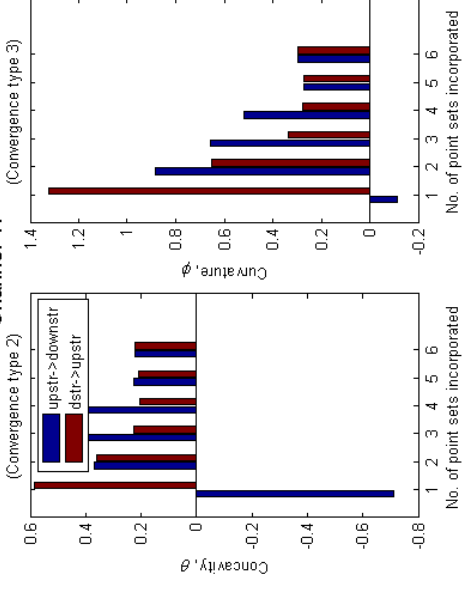
Channel 45



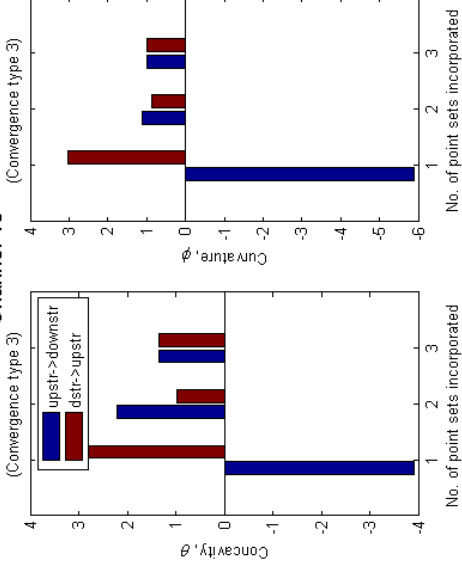
Channel 46



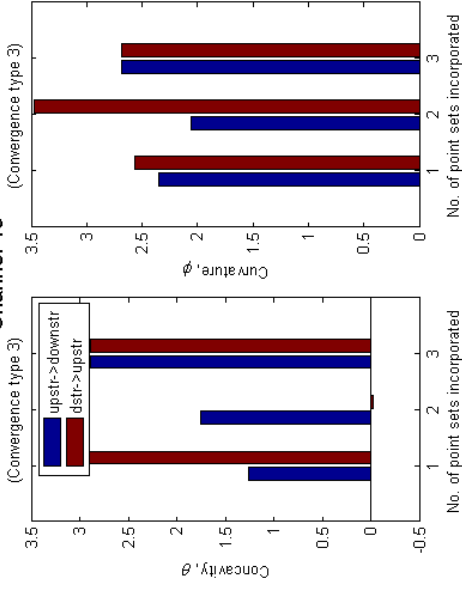
Channel 47



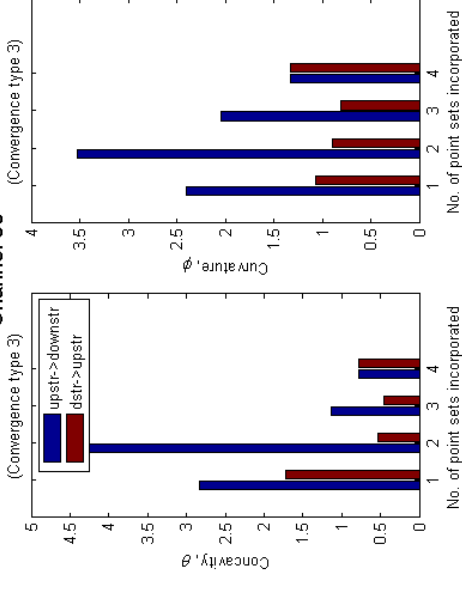
Channel 48



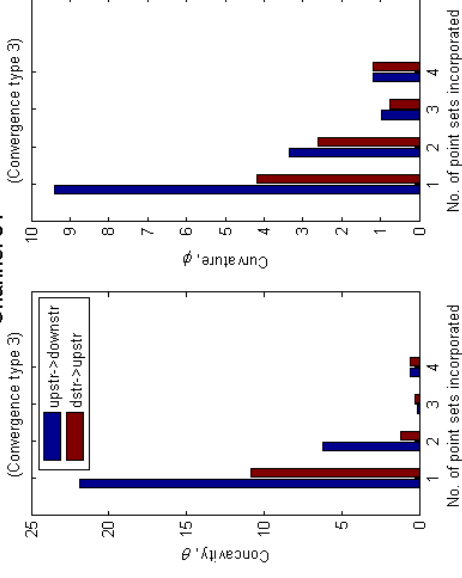
Channel 49



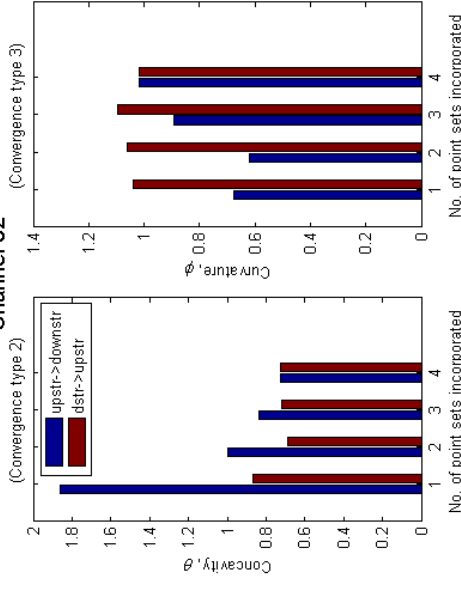
Channel 50



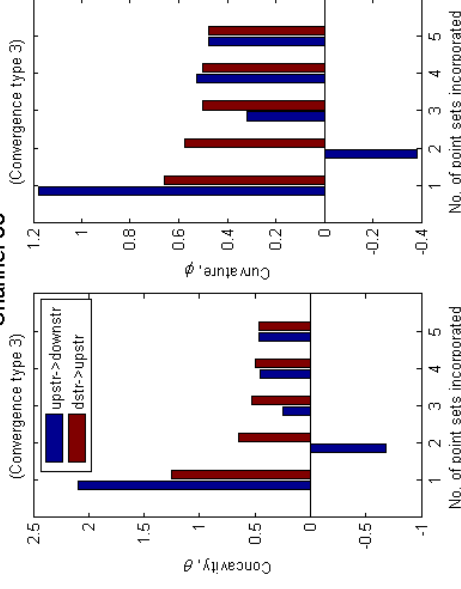
Channel 51



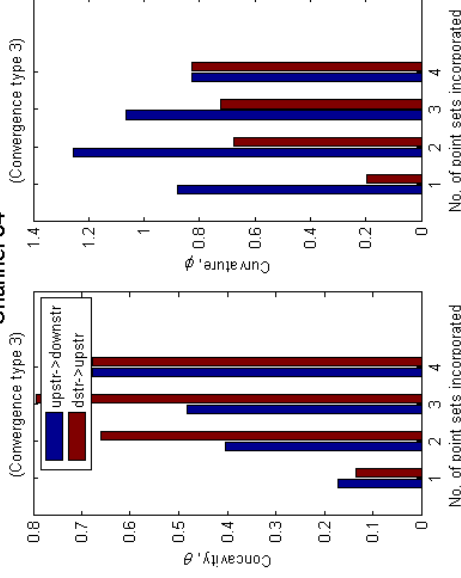
Channel 52



Channel 53

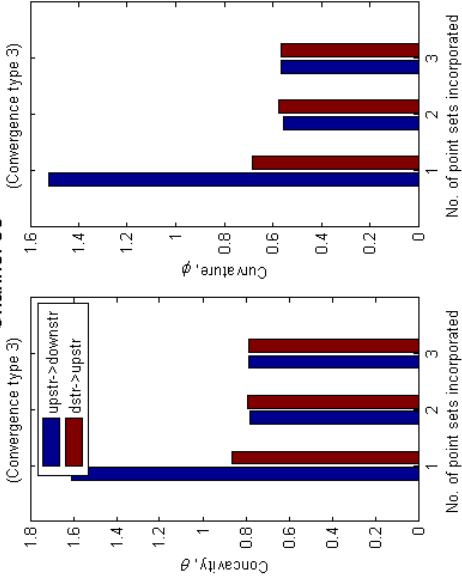


Channel 54

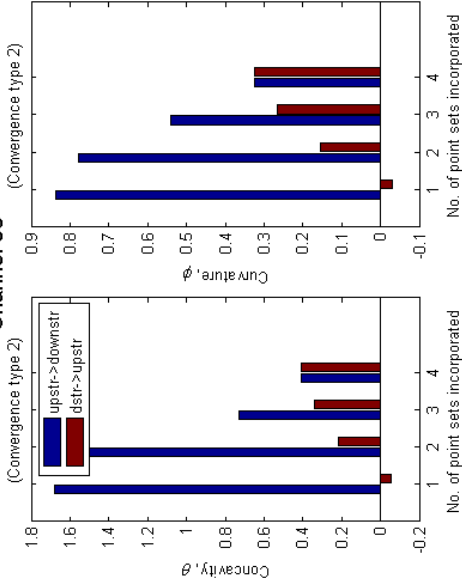




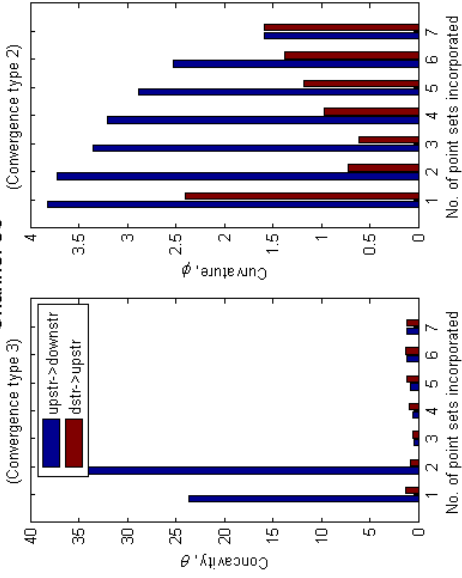
Channel 55



Channel 58



Channel 56



Channel 57

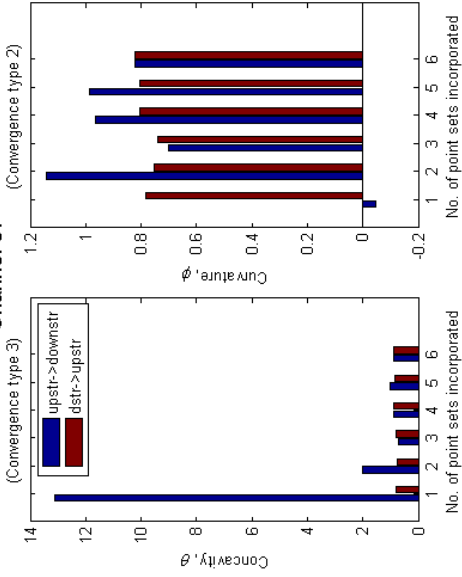


TABLE S1. DATA EXTRACTED FROM DEM FOR REACHES DOWNSTREAM OF KNICKZONES

| Channel number | Area upstream of knickzone, $A_{pc}$ ( $m^2$ ) | Total area, $A_{tot}$ ( $m^2$ ) | Downstream distance of knickzone, $x_{pc}$ (m) | Total channel length, $x_{tot}$ (m) | $A_{pc}/A_{tot}$ | $x_{pc}/x_{tot}$ | $k_\theta$ | $\theta$ | Error on $\theta$ | $k_\phi$ | $\phi$ | Error on $\phi$ |
|----------------|--|---------------------------------|--|-------------------------------------|------------------|------------------|------------|----------|-------------------|----------|--------|-----------------|
| 1              | 6.60E+07                                       | 7.44E+07                        | 15749  | 18633                               | 0.887            | 0.845            | 7.04E+42   | 5.57     | 0.76              | 6.64E+13 | 3.48   | 0.52            |
| 2              | 3.26E+06                                       | 3.32E+07                        | 779  | 7451                                | 0.098            | 0.105            | 4.93E+01   | 0.34     | 0.07              | 4.66E+00 | 0.40   | 0.08            |
| 3              | 1.99E+06                                       | 3.73E+07                        | 695  | 8804                                | 0.053            | 0.079            | 4.11E+01   | 0.33     | 0.02              | 4.16E+00 | 0.38   | 0.03            |
| 4              | 7.17E+07                                       | 1.19E+08                        | 13852  | 20710                               | 0.600            | 0.669            | 2.68E+13   | 1.80     | 0.11              | 1.45E+09 | 2.40   | 0.17            |
| 5              | 2.88E+06                                       | 1.02E+07                        | 878  | 3947                                | 0.283            | 0.223            | 2.00E+02   | 0.44     | 0.07              | 5.46E+00 | 0.44   | 0.05            |
| 6              | 2.94E+06                                       | 9.07E+06                        | 607  | 3036                                | 0.325            | 0.296            | 3.98E+02   | 0.49     | 0.08              | 5.12E+00 | 0.44   | 0.06            |
| 7              | 1.41E+07                                       | 1.66E+08                        | 4478   | 15142                               | 0.085            | 0.296            | 5.76E+03   | 0.60     | 0.05              | 3.01E+04 | 1.36   | 0.13            |
| 8              | 5.33E+07                                       | 1.65E+08                        | 10767  | 19692                               | 0.322            | 0.547            | 1.44E+05   | 0.76     | 0.12              | 5.11E+04 | 1.36   | 0.22            |
| 9              | 2.05E+07                                       | 1.65E+08                        | 5503   | 16546                               | 0.124            | 0.333            | 3.32E+02   | 0.43     | 0.03              | 3.58E+03 | 1.11   | 0.08            |
| 10             | 3.06E+06                                       | 2.71E+07                        | 1556   | 6024                                | 0.113            | 0.258            | 1.37E+02   | 0.39     | 0.07              | 1.81E+02 | 0.82   | 0.11            |
| 11             | 4.63E+07                                       | 2.72E+08                        | 11423  | 24730                               | 0.170            | 0.462            | 5.09E+03   | 0.59     | 0.04              | 1.72E+05 | 1.50   | 0.10            |
| 12             | 5.01E+07                                       | 2.71E+08                        | 13600  | 23642                               | 0.185            | 0.575            | 5.13E+03   | 0.59     | 0.03              | 3.19E+07 | 2.01   | 0.11            |
| 13             | 6.51E+06                                       | 5.30E+07                        | 2846   | 12300                               | 0.123            | 0.231            | 5.26E+03   | 0.62     | 0.03              | 5.86E+02 | 0.96   | 0.04            |
| 14             | 3.20E+06                                       | 1.49E+07                        | 683  | 4668                                | 0.215            | 0.146            | 6.30E+02   | 0.52     | 0.04              | 6.62E+00 | 0.47   | 0.03            |
| 15             | 3.86E+07                                       | 1.18E+08                        | 13411  | 20417                               | 0.327            | 0.657            | 1.03E+06   | 0.88     | 0.09              | 6.41E+08 | 2.33   | 0.25            |
| 16             | 1.63E+08                                       | 1.83E+08                        | 22297  | 30193                               | 0.891            | 0.738            | 7.02E+30   | 3.88     | 0.53              | 2.98E+06 | 1.73   | 0.22            |
| 17             | 2.77E+06                                       | 2.75E+07                        | 913  | 8629                                | 0.101            | 0.106            | 9.61E+04   | 0.83     | 0.04              | 6.29E+01 | 0.74   | 0.05            |
| 18             | 4.98E+06                                       | 2.75E+07                        | 1442   | 7324                                | 0.181            | 0.197            | 3.24E+01   | 0.36     | 0.05              | 3.31E+00 | 0.44   | 0.07            |
| 19             | 4.67E+06                                       | 1.65E+08                        | 2894   | 14724                               | 0.028            | 0.197            | 5.60E+02   | 0.49     | 0.05              | 3.32E+02 | 0.88   | 0.10            |
| 20             | 1.12E+08                                       | 1.65E+08                        | 17836  | 23187                               | 0.676            | 0.769            | 3.48E+11   | 1.55     | 0.14              | 6.61E+12 | 3.22   | 0.17            |
| 21             | 5.73E+06                                       | 4.00E+07                        | 1538   | 11648                               | 0.143            | 0.132            | 3.31E+05   | 0.88     | 0.13              | 2.31E+02 | 0.87   | 0.03            |
| 22             | 2.91E+07                                       | 7.28E+07                        | 8501   | 21593                               | 0.399            | 0.394            | 1.31E+08   | 1.19     | 0.05              | 3.30E+04 | 1.33   | 0.05            |
| 23             | 7.74E+07                                       | 1.08E+08                        | 10854  | 21138                               | 0.503            | 0.513            | 1.90E+13   | 1.85     | 0.13              | 7.04E+06 | 1.89   | 0.13            |
| 24             | 3.35E+07                                       | 8.67E+07                        | 9525   | 21821                               | 0.386            | 0.437            | 1.06E+07   | 1.03     | 0.05              | 3.48E+04 | 1.32   | 0.04            |
| 25             | 1.08E+07                                       | 8.84E+07                        | 5503   | 20265                               | 0.122            | 0.272            | 2.08E+04   | 0.70     | 0.03              | 1.68E+03 | 1.05   | 0.03            |
| 26             | 2.62E+06                                       | 1.82E+07                        | 949  | 11309                               | 0.144            | 0.084            | 4.43E+02   | 0.53     | 0.04              | 6.12E+00 | 0.49   | 0.03            |
| 27             | 4.96E+06                                       | 5.13E+07                        | 1152   | 13624                               | 0.097            | 0.085            | 3.47E+02   | 0.48     | 0.02              | 6.98E+00 | 0.49   | 0.02            |
| 28             | 3.04E+06                                       | 3.40E+07                        | 576  | 11451                               | 0.089            | 0.050            | 4.04E+01   | 0.36     | 0.02              | 1.72E+00 | 0.34   | 0.02            |
| 29             | 1.25E+07                                       | 7.12E+07                        | 5503   | 19999                               | 0.176            | 0.275            | 7.10E+03   | 0.64     | 0.04              | 2.03E+02 | 0.81   | 0.05            |
| 30             | 2.00E+07                                       | 1.17E+08                        | 6831   | 22921                               | 0.171            | 0.298            | 5.87E+04   | 0.75     | 0.03              | 4.36E+03 | 1.14   | 0.03            |
| 31             | 6.73E+06                                       | 4.19E+07                        | 3188   | 7780                                | 0.161            | 0.410            | 1.83E+00   | 0.15     | 0.03              | 1.93E+00 | 0.31   | 0.06            |
| 32             | 1.78E+07                                       | 6.96E+07                        | 4858   | 17457                               | 0.255            | 0.278            | 1.92E+05   | 0.83     | 0.03              | 7.18E+02 | 0.97   | 0.03            |
| 33             | 2.40E+06                                       | 6.37E+07                        | 646  | 13206                               | 0.038            | 0.049            | 1.02E+02   | 0.41     | 0.01              | 4.72E+00 | 0.45   | 0.01            |
| 34             | 2.45E+06                                       | 2.61E+07                        | 607  | 11613                               | 0.094            | 0.052            | 1.05E+03   | 0.56     | 0.01              | 5.47E+00 | 0.46   | 0.01            |
| 35             | 4.04E+06                                       | 5.48E+07                        | 1784   | 13624                               | 0.074            | 0.131            | 2.03E+03   | 0.59     | 0.02              | 1.78E+02 | 0.86   | 0.03            |
| 36             | 2.71E+06                                       | 2.09E+07                        | 607  | 6983                                | 0.130            | 0.087            | 9.66E+04   | 0.90     | 0.06              | 5.24E+00 | 0.53   | 0.03            |
| 37             | 1.50E+07                                       | 1.92E+08                        | 5313   | 23070                               | 0.078            | 0.230            | 1.54E+04   | 0.69     | 0.02              | 8.14E+03 | 1.26   | 0.03            |
| 38             | 1.05E+07                                       | 1.91E+08                        | 4802   | 23984                               | 0.055            | 0.200            | 5.81E+04   | 0.76     | 0.02              | 1.06E+05 | 1.54   | 0.04            |
| 39             | 3.34E+07                                       | 1.19E+08                        | 8368   | 22542                               | 0.280            | 0.371            | 1.38E+05   | 0.80     | 0.05              | 3.36E+02 | 0.90   | 0.05            |
| 40             | 3.09E+06                                       | 3.91E+07                        | 645  | 11385                               | 0.079            | 0.057            | 3.14E+02   | 0.48     | 0.02              | 5.21E+00 | 0.46   | 0.01            |
| 41             | 2.38E+06                                       | 1.30E+07                        | 607  | 6186                                | 0.183            | 0.098            | 2.01E+02   | 0.47     | 0.03              | 2.56E+00 | 0.38   | 0.02            |
| 42             | 1.01E+07                                       | 8.12E+07                        | 3545   | 17419                               | 0.124            | 0.204            | 3.09E+03   | 0.59     | 0.02              | 1.04E+03 | 1.02   | 0.02            |
| 43             | 4.39E+06                                       | 2.99E+07                        | 645  | 7623                                | 0.147            | 0.085            | 1.03E+02   | 0.40     | 0.02              | 2.34E+00 | 0.33   | 0.02            |
| 44             | 1.62E+07                                       | 2.36E+08                        | 6224   | 22119                               | 0.069            | 0.281            | 9.69E+02   | 0.51     | 0.03              | 1.18E+04 | 1.25   | 0.08            |
| 45             | 3.89E+06                                       | 2.26E+07                        | 1152   | 6777                                | 0.172            | 0.170            | 1.05E+04   | 0.67     | 0.05              | 4.62E+01 | 0.68   | 0.05            |
| 46             | 8.36E+07                                       | 1.98E+08                        | 15066  | 23632                               | 0.422            | 0.638            | 1.43E+05   | 0.76     | 0.09              | 3.90E+04 | 1.32   | 0.12            |
| 47             | 3.17E+06                                       | 4.06E+07                        | 1366   | 9863                                | 0.078            | 0.139            | 6.33E+00   | 0.22     | 0.02              | 1.93E+00 | 0.30   | 0.03            |
| 48             | 6.24E+07                                       | 7.42E+07                        | 15787  | 20531                               | 0.842            | 0.769            | 4.25E+09   | 1.35     | 0.31              | 1.73E+03 | 0.98   | 0.23            |
| 49             | 4.27E+07                                       | 5.36E+07                        | 15104  | 19274                               | 0.797            | 0.784            | 1.67E+21   | 2.89     | 0.30              | 2.22E+10 | 2.68   | 0.25            |
| 50             | 1.97E+07                                       | 4.14E+07                        | 7780   | 13890                               | 0.476            | 0.560            | 7.30E+04   | 0.77     | 0.09              | 2.52E+04 | 1.32   | 0.13            |
| 51             | 1.04E+08                                       | 1.66E+08                        | 14914  | 21441                               | 0.627            | 0.696            | 2.49E+03   | 0.55     | 0.15              | 8.21E+03 | 1.18   | 0.24            |
| 52             | 4.64E+06                                       | 2.05E+07                        | 2391   | 8349                                | 0.226            | 0.286            | 2.46E+04   | 0.72     | 0.03              | 1.04E+03 | 1.02   | 0.04            |
| 53             | 3.06E+06                                       | 2.36E+07                        | 607  | 8349                                | 0.129            | 0.073            | 1.56E+02   | 0.46     | 0.03              | 4.61E+00 | 0.48   | 0.03            |
| 54             | 5.51E+06                                       | 3.18E+07                        | 2353   | 8652                                | 0.173            | 0.272            | 8.84E+03   | 0.68     | 0.03              | 1.50E+02 | 0.83   | 0.03            |
| 55             | 2.13E+06                                       | 7.70E+06                        | 645  | 4744                                | 0.276            | 0.136            | 2.18E+04   | 0.78     | 0.04              | 9.96E+00 | 0.57   | 0.03            |
| 56             | 2.12E+07                                       | 1.25E+08                        | 6831   | 17571                               | 0.170            | 0.389            | 3.98E+07   | 1.14     | 0.05              | 2.25E+05 | 1.58   | 0.09            |
| 57             | 3.27E+06                                       | 1.61E+07                        | 1670   | 10552                               | 0.203            | 0.158            | 1.54E+05   | 0.87     | 0.03              | 1.56E+02 | 0.82   | 0.02            |
| 58             | 3.80E+06                                       | 2.23E+07                        | 576  | 7438                                | 0.170            | 0.077            | 9.72E+01   | 0.41     | 0.03              | 1.67E+00 | 0.33   | 0.02            |

**Text supporting supplementary material for the  
paper: “Processes, rates and timescales of fluvial  
response in an ancient post-glacial landscape of the  
northwest Indian Himalaya”, *GSA Bulletin***

**Daniel E. J. Hobley** – Email [dan.hobley@ed.ac.uk](mailto:dan.hobley@ed.ac.uk)

**Hugh D. Sinclair**

**Patience A. Cowie**

*School of GeoSciences, University of Edinburgh, Edinburgh, Scotland EH9 3JW, UK*

This document provides additional text supporting data which was too substantial to be included concisely within the print version of the manuscript. This comprises: -

1. Details of methodology for processing of the raw DEM data.
2. Text supporting presentation of all remotely sensed stream long profiles and scaling data used to derive the data shown in Figs. 7 and 8 in the main manuscript, and associated location information (Figs. S1a,b).
3. Text supporting figures showing a comparison of channel slopes derived from the DEM versus known field measurements of slope for two catchments on the batholith (Figs. S2a,b).
4. Text supporting figures (Fig. S3) illustrating values of concavity and curvature calculated for separate segments of each stream, used to investigate whether the measured values are systematically different for the lower part of domain 2 compared to domain 3.

This follows below.

## **1. METHODOLOGY FOR ACQUISITION AND TREATMENT OF DEM**

We have taken three arc-second resolution data freely available from NASA (<ftp://e0srp01u.ecs.nasa.gov/srtm/version2/SRTM3/>), derived from the Shuttle Radar Topography Mission (SRTM). Raw data was converted to ARCinfo GRID format for processing using IMAGEGRID.aml, developed by the United States Geological Survey ([ftp://e0srp01u.ecs.nasa.gov/srtm/version2/Documentation/Notes\\_for\\_ARCInfo\\_users.pdf](ftp://e0srp01u.ecs.nasa.gov/srtm/version2/Documentation/Notes_for_ARCInfo_users.pdf)). The data used here comprises one degree by one degree squares N33E077, N33E078, N34E076, N34E077 and N34E078 (see Fig. 1). The data for this region is in fact well suited to DEM analysis, since the glaciers have widened and flattened the valley floors over much of the rivers' courses, meaning artifacts produced by the satellite's footprint catching the valley sides as well as the channel in the valley centre are much reduced. Minor holes in the data (<2% of pixels in analyzed catchments, and rarely impinging on valley bottoms) were patched by converting the whole dataset into a point dataset then using ARCinfo to interpolate back into GRID form using a cubic spline algorithm. This process provided the base DEM on which subsequent analysis was carried out.

The base DEM was first filled to remove artificial internally draining patches – the affected area comprises <1% of the total surface, almost entirely confined to regions of the Indus valley itself and not significantly changing the profiles of the tributaries. The drainage network was then predicted from a flow accumulation threshold of 200

pixels (a drainage area of approximately  $1.4 \times 10^6 \text{ m}^2$ ). This relatively high value was chosen to avoid the prediction of channels beneath the existing glaciers and recent moraine successions in the highest elevations of the catchments, and creates a channel network that agrees well with the known channel forms seen in satellite imagery. The trunk streams for each of the 70 independent basins draining southwards into the Indus were then selected, taking more than one profile per valley if a major bifurcation of the trunk stream was present, and elevation,  $z$ , upstream drainage area,  $A$ , and distance downstream,  $x$ , data extracted for each pixel along the course of each trunk stream. MATLAB was then used first to smooth out high frequency noise in the elevation data with a low-pass filter on  $z$ , then to construct a value of channel slope,  $S$ , on a reach length scale of 500 m. Both these methods act to damp local ( $< 500 \text{ m}$ ) variation in channel slope, whether an artifact of the DEM or due to fine scale river responses. This scaling is appropriate since we only sampled local slope and channel form in the field once every 300 – 500 m, and variability on a finer scale than this will not be revealed by the data. These methods and smoothing techniques correspond broadly to those chosen by Snyder et al. (2003a) and recommended by Wobus et al. (2006), though with different absolute values chosen appropriate to the coarser resolution of our DEM data.

## **2. LONG PROFILES AND SCALING PLOTS FOR ALL ANALYZED CATCHMENTS (FIGS. S1a,b)**

An altered version of Fig. 1 is presented as Fig. S1a in order to illustrate which catchments provide acceptable slope-distance (curvature) and slope-area (concavity)

regressions, as described in the Remotely Sensed Data section of the main manuscript. Those which do are colored blue. Channels are numbered consecutively as they appear along the batholith going from west to east. Note that several catchments have more than one trunk stream, and these channels are each allocated their own number. The channels in question are 2/3, 7/8/9, 11/12, 17/18, 19/20/21 and 37/38, and the associated catchments are shown in a lighter blue in the Figure. Fig. S1b illustrates the long profile ( $z$ - $x$ ) and drainage structure ( $A$ - $x$ ) of each of these channels, along with associated slope plots  $S$ - $x$  and  $S$ - $A$ , plotted on logarithmic axes. The grayscale lines show the slope scaling relations fitted to these latter two plots by the method described in the main text, and the range of values over which the fit is made. The associated equations are also shown above these figures. The file TableS1.pdf collates all of these data, and is the source for Figs. 7 and 8 in the main text.

### **3. FIELD-DEM SLOPE COMPARISONS (FIGS. S2a,b)**

Figure S2a shows plots of channel slope,  $S$ , versus distance downstream,  $x$ , for the valleys Basgo (i) and Leh (ii). DEM-derived slopes (see section 1 of this document) are shown as grey open circles and direct field measurements over 30 m intervals, every c. 500 m are shown as black closed squares. Figure S2b displays this same data as a direct comparison for each catchment. Quoted errors on the lines of best fit are 95% confidence intervals, assuming direct linear correlation. Note that neither gradient is distinguishable from 1, but that there is a tendency for the DEM values to be slightly higher. This is probably an artifact of the different scales over which the gradient is averaged (500 m vs 30 m), especially in domain 1, where slope can be



highly variable on a scale less than 500 m. This is particularly clear in Fig. S2a. For the same reason, we note that the fit for Leh is poorer, since a larger proportion of these data points come from within domain 1.

#### **4. VARIATION OF SCALING METRICS BETWEEN DOMAINS (FIG. S3)**

As noted in the main text, the data presented here does not extend across enough variation in drainage area to conclusively calculate the scaling metrics of concavity and curvature for the bottom of domain 2 and domain 3 separately. However, in order to investigate this issue further, we present here a semi-quantitative method examining the convergence towards the whole channel values as progressively larger proportions of the channel are included. We plot calculated concavity and curvature values for each channel over the first 50, 100, 150, 200, etc. points downstream of the knickzone up to the end of the whole analyzed segment, then similarly plot the data in sections 50, 100, 150, etc. points long going from the downstream end of the channel up to the knickzone. This data is then displayed graphically on the same chart, where the fits established for the first 50 points (upper- and lower-most stream sections of the channel) are displayed to the left and the fits incorporating all of the data to the right. We then examine the manner in which the data converges to the right-hand side of the graph. The measured values are clearly quite variable where fewer data points are used, but as more data is incorporated, the variability in the values tends to stabilize. We recognize three patterns in these tails as the final elements of data are incorporated: -

1. Magnitude of concavity (or curvature) becomes gradually greater as data is incorporated towards the downstream end of the channel (blue bars), and gradually smaller as data is incorporated towards the upstream end of the channel (red bars). This suggests that the scaling exponents are uniformly lower in the upstream reaches of the channel than in the downstream reaches.
2. Magnitude of concavity (or curvature) becomes gradually lesser as data is incorporated towards the downstream end of the channel (blue), and gradually greater as data is incorporated towards the upstream end of the channel (red). This suggests that the scaling exponents are uniformly greater in the upstream reaches of the channel than in downstream reaches.
3. Neither of the above is the case, with no trends in the scaling metrics, or with trends in the same direction incorporating data going both upstream and downstream in the catchment. This category also includes catchments with few points in total ( $<200$ ). We interpret this to indicate that there is no demonstrable systematic difference in concavity (or curvature) in the upstream reaches versus the downstream reaches of the channel as a whole.

The pattern we assign for the concavity and curvature of each channel is noted above each graph as 1, 2 or 3. Note that we ignore the first three data points (50-150 data points) entirely, where random noise will certainly overwhelm any signal. This method is, at best, limited, but provides at least some indication of the variability of the scaling values quoted in the main text, and also avoids having to pre-allocate domain boundaries for all of the catchments, which are not always easy to accurately fix from the satellite imagery.

We find that for both the concavity and curvature, very many channels (34 out of 58 for  $\theta$ , 27 out of 58 for  $\phi$ ) show no uniform tendency for a changing value downstream. The remainder are split between a tendency for increase and a tendency for decrease downstream for both metrics (12 type 1, 12 type 2 for  $\theta$ ; 12 type 1, 19 type 2 for  $\phi$ ). We interpret this to mean that there is no tendency for upstream reaches to have uniformly higher or lower scaling exponents to downstream reaches, including across the boundary of domain 2 into domain 3, as discussed in the main text.